



Corrosion of mild steel under an anaerobic biofilm
by Whonchee Lee

A thesis submitted in partial fulfillment of the requirements for the degree of Doctor of Philosophy in
Chemistry

Montana State University

© Copyright by Whonchee Lee (1990)

Abstract:

Corrosion of mild steel under completely anaerobic conditions in the presence of a mixed population biofilm, including sulfate-reducing bacteria (SRB), has been studied in a continuous flow system. The open channel flow reactor was continuously fed with low concentration substrate at different dilution rates which influenced biofilm accumulation. No direct correlation was observed between corrosion and SRB activity in the absence of ferrous ion. Furthermore, corrosion of mild steel in the SRB environment was mainly determined by the nature of the metal and environmental conditions such as dissolved iron. When formation of iron sulfide film on mild steel was prevented before the biofilm accumulated, the metal surface retained its scratch lines after a 21-day experiment (SRB at $2.6 \times 10^9/\text{cm}^2$). However, when iron sulfide film was formed before the accumulation of biofilm, visible localized corrosion appeared after 14 days and increased up to 21 days. Intergranular and pitting attack were found in the localized corrosion area. Inclusions (Al, Mn, and Fe) were usually found in the localized corrosion area. At high iron concentration (about 60 mg/L in the bulk water), all biogenic sulfide was precipitated and corrosion rate significantly increased. Intergranular attack was found over the entire metal surface.

The anaerobic corrosion processes of mild steel in the presence and absence of anaerobic biofilm, including sulfate-reducing bacteria, was compared. In the biotic experiment, biofilm accumulated on a chemically-formed iron sulfide film for 21 days. The abiotic experiment was designed to simulate this hydrogen sulfide environment which had similar hydrogen sulfide concentration, redox potential, and pH. There was no difference in the metal matrix at three days in the two conditions. However, corrosion propagation was different for the two cases after 3 days. Localized corrosion was found in the presence of biofilm while uniform intergranular attack was observed in the absence of biofilm.

CORROSION OF MILD STEEL UNDER AN ANAEROBIC BIOFILM

by

Whonchee Lee

A thesis submitted in partial fulfillment
of the requirements for the degree

of

Doctor of Philosophy

in

Chemistry

MONTANA STATE UNIVERSITY
Bozeman, Montana

April 1990

D378
L5165

APPROVAL

of a thesis submitted by

Whonchee Lee

This thesis has been read by each member of the thesis committee and has been found to be satisfactory regarding content, English usage, format, citations, bibliographic style, and consistency, and is ready for submission to the College of Graduate Studies.

4/5/90
Date

W. G. Charachin
Cochairperson, Graduate Committee

4/5/90
Date

Erin P. Mansueti
Cochairperson, Graduate Committee

Approved for the Major Department

4/5/90
Date

Edwin H. Abbott
Head, Major Department

Approved for the College of Graduate Studies

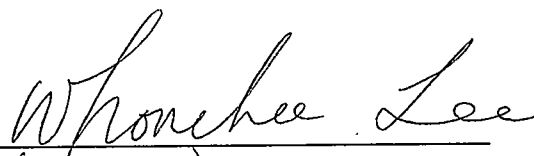
4/5/90
Date

Henry L. Parsons
Graduate Dean

STATEMENT OF PERMISSION TO USE

In presenting this thesis in partial fulfillment of the requirements for a doctoral degree at Montana State University, I agree that the Library shall make it available to borrowers under rules of the Library. I further agree that copying of this thesis is allowable only for scholarly purposes, consistent with "fair use" as prescribed in the U.S. Copyright Law. Requests for extensive copying or reproduction of this thesis should be referred to University Microfilms International, 300 North Zeeb Road, Ann Arbor, Michigan 48106, to whom I have granted "the exclusive right to reproduce and distribute copies of the dissertation in and from microfilm and the right to reproduce and distribute by abstract in any format."

Signature



Date

4/4/90

ACKNOWLEDGEMENTS

I wish to express my appreciation to the following:

Bill Characklis for providing advice, support, and research environment which made my graduate experience a particularly productive and enjoyable period of my life.

Vern Griffths, Hector Videla, Brenda Little, and Gordon Pagenkopf for their contribution to my graduate program.

Eric Grimsrud, Richard Geer, Kenneth Emerson, Edward Anacker, and Clyde Greer for serving on my thesis committee.

David Ward, Warren Jones, Anne Camper, and Dave Davis for help with my thesis.

Gordon Williams, John Rompel, Stuart Aasgaard, and Andy Blixt for technical and analytical assistance.

Diane, Wendy, Lynda, Zbigniew, Al, Dick, Frank, Ron, Paul, Ewout, Brent, Vivek, Feisal, Bill, Robert, Gabi, Bryan, Jamie, Mike for their cooperation.

The staff of Chemistry Department and Civil Engineering whom have contributed to my education.

National Science Foundation, IPA Industrial Associates, and Chemistry Department for financial support.

TABLE OF CONTENTS

	Page
LIST OF TABLES	vii
LIST OF FIGURES	x
ABSTRACT	xvi
INTRODUCTION	1
Economic Impact of Sulfate-Reducing Bacteria (SRB) ...	1
Corrosion of Mild Steel under Anaerobic Conditions in the Absence of Bacteria	1
Corrosion of Mild Steel under Anaerobic Conditions in the Presence of Bacteria	2
The Problem	4
Research goal	5
Objectives	5
Tasks	5
LITERATURE REVIEW	6
Types of SRB and Their Substrate	6
Stoichiometry and Kinetic of SRB	9
Stoichiometry of SRB	9
Kinetics of SRB	10
Mechanisms of Metal Corrosion by SRB	12
Mechanisms of H ₂ S Corrosion in the Absence of Bacteria	17
Mechanisms	18
Film Diffusion Control in Corrosion Mechanism	19
Localized Corrosion of Steel in H ₂ S Environment	20
Use of Electrochemical Techniques for Studying Microbial Corrosion	20
Open Circuit Corrosion Potential	22
Redox Potential	23
Potentiostatic Polarization	25
Pitting Potentials	25
Alternating Current Methods	27
EXPERIMENTAL	30
Experimetal Reactor	30
Media and Biofilm Growth Conditions	31
Coupon	32
Corrosion Measurements	33

TABLE OF CONTENTS (Continued)

Water Chemistry	33
Biological Analysis	34
Surface Analysis of Biofilm and Corrosion Products ...	35
RESULTS	36
Stoichiometry of a Mixed Population SRB Biofilm with Corrosion Coupons	36
Corrosion of Mild Steel at Different Substrate Loading Rate	37
Corrosion of Mild Steel with a Precoated Biofilm at Different Ferrous Ion Concentrations	49
Corrosion of Mild Steel on a Precoated Iron Sulfide Film Followed by Biofilm Accumulation	56
Anaerobic Corrosion Under Abiotic Conditions	66
DISCUSSION	73
Effect of Substrate Loading Rate on the Corrosion of Mild Steel	73
Effect of Ferrous Ion Concentration on the Corrosion of Mild Steel with a Precoated Biofilm	77
Anaerobic Corrosion Processes of Mild Steel on a Precoated Iron Sulfide Film Followed by Biofilm Accumulation	79
Anaerobic Corrosion Processes of Mild Steel in the Abiotic Conditions	84
SUMMARY	89
CONCLUSIONS	91
REFERENCES	93
APPENDIX	98

LIST OF TABLES

Table	Page
1. Growth Requirements of Selected Sulfate-Reducing Bacteria	8
2. Typical values for the maximum specific growth rate, μ_{max} , and saturation constant, k_s , for lactate-utilizing SRB in lactate, sulfate medium at temperature = 30° C	11
3. The history of cathodic depolarization theories	15
4. The ionic compositions of 1/10 strength artificial seawater	32
5. Elemental composition of AISI 1018 mild steel	32
6. Sulfate, lactate consumption and sulfide, acetate production occurred at 25 hrs resident time with medium contained no ferrous ions	44
7. Sulfate, lactate consumption and sulfide, acetate production occurred at 1.33 hr resident time with medium contained no ferrous ions	45
8. Sulfate, lactate consumption and sulfide, acetate production occurred at 1.33 hr resident time with different ferrous ions concentrations ..	49
9. Sulfate, lactate consumption and sulfide, acetate production occurred at 1.33 hr resident time with medium contained no ferrous ion but metal coupon was precoated with iron sulfide film	57
10. MPN for GAB and SRB at different time periods in bulk water and biofilm at low substrate loading rate	98
11. MPN for GAB and SRB at different time periods in bulk water and biofilm at high substrate loading rate	98

LIST OF TABLES (Continued)

Table	Page
12. MPN for GAB and SRB at different iron concentration in bulk water and biofilm at high substrate loading rate	99
13. MPN for GAB and SRB at different time periods in bulk water and biofilm when metal coupons are precoated with iron sulfide film	99
14. Water chemistry analysis in the bulk water under batch culture conditions for stoichiometric study	100
15. Anodic polarization data at different time periods with low substrate loading rate in the absence of iron	101
16. Cathodic polarization data at different time periods with low substrate loading rate in the absence of iron	102
17. Anodic polarization currents at different time periods at high substrate loading rate in the absence of iron	103
18. Cathodic polarization data at different time periods at high substrate loading rate in the absence of iron	104
19. Anodic polarization data for different ferrous ion concentrations at high substrate loading rate	105
20. Cathodic polarization data for different ion concentrations at high substrate loading rate	106
21. Anodic polarization data at different time periods on a precoated iron sulfide film at high substrate loading rate	107
22. Cathodic polarization data at different time periods on a precoated iron sulfide film at high substrate loading rate	108

LIST OF TABLES (Continued)

Table	Page
23. Anodic polarization data at different time periods in the abiotic conditions109	109
24. Cathodic polarization data at different time periods in the abiotic conditions110	110

LIST OF FIGURES

Figure	Page
1. Proposed reactions of anaerobic corrosion in the presence of SRB on an iron surface	13
2. Schematic representation of the classical mechanisms (top) and alternative mechanism (bottom) on microbial corrosion under anaerobic conditions	14
3. Model for microbial biofilm in oxygenic environment	17
4. Continuous open channel flow reactor with dimensions 1.00 m x 0.15 m x 0.30 m and with a working volume of 4.5 liters and a surface area of 0.35 m ²	30
5. Sulfide production, lactate consumption, and sulfate degradation in mixed culture containing SRB. Attached picture (x50) indicates no iron sulfide corrosion products at the end of experiment	37
6. Scanning electron micrographs of biofilm grown on a mild steel surface for 3 days, x1300, at low substrate loading rate	39
7. Scanning electron micrographs of biofilm grown on a mild steel surface for 7 days, x1300, at low substrate loading rate	39
8. Scanning electron micrographs of biofilm grown on a mild steel surface for 21 days, x1300, at low substrate loading rate	40
9. Scanning electron micrographs of biofilm accumulated on a mild steel surface for 3 days, x30, at high substrate loading rate	40
10. Scanning electron micrographs of biofilm accumulated on a mild steel surface for 7 days, x30, at high substrate loading rate	41

LIST OF FIGURES (Continued)

Figure	Page
11. Scanning electron micrographs of biofilm accumulated on a mild steel surface for 21 days, x30, at high substrate loading rate	41
12. Scanning electron micrograph of a biofilm accumulated on a mild steel surface for 21 days at high substrate loading rate. x20,000	42
13. MPN for GAB and SRB at low substrate loading rate in the bulk water at different exposure times	42
14. MPN for GAB and SRB at high substrate loading rate in the bulk water at different exposure times	43
15. MPN for GAB and SRB at low substrate loading rate in the biofilm at different exposure times	43
16. MPN for GAB and SRB at high substrate loading rate in the biofilm at different exposure times	44
17. Scanning electron micrograph of a mild steel surface after biofilm has been removed at 21 days. x700	46
18. X-ray dot map indicating the elemental distribution of iron, sulfur, and phosphorous on the top of biofilm and the cross section of biofilm and metal surface	46
19. Cathodic depolarization curves of mild steel at low substrate loading rate at different exposure times	47
20. Cathodic polarization curves of mild steel at high substrate loading rate at different exposure times	47

LIST OF FIGURES (Continued)

Figure	Page
21. Anodic polarization curves of mild steel at low substrate loading rate at different exposure times. Pitting potential becomes more noble (40mv) during 21 days experiment	48
22. Anodic polarization curves of mild steel at high substrate loading rate at different exposure times. Pitting potential becomes more noble (150mv) during 21 days experiment	48
23. Most probable number (MPN) for GAB and SRB in the bulk water at different ferrous ion concentration	50
24. Most probable number (MPN) for GAB and SRB in the biofilm at different ferrous ion concentration	50
25. Accumulation of iron sulfide on a precoated biofilm at 1 mg/L ferrous ion concentrations. x50	52
26. Accumulation of iron sulfide on a precoated biofilm at 10 mg/L ferrous ion concentrations. x50	52
27. Accumulation of iron sulfide on a precoated biofilm at 60 mg/L ferrous ion concentrations. x50	53
28. Scanning electron micrograph of biofilm when the media contain 60 mg/L ferrous ion concentration. x4,000	53
29. X-ray dot map indicating the elemental distribution of iron, sulfur, and phosphor on the top and cross section of biofilm and metal substratum	54
30. Cathodic polarization curves of mild steel on a precoated biofilm followed by step increase in ferrous ion concentrations	54

LIST OF FIGURES (Continued)

Figure	Page
31. Anodic polarization curves of mild steel on a pre-coated biofilm followed by step increase in ferrous ion concentrations	55
32. Nyquist plots for mild steel on a pre-coated biofilm at different ferrous ion concentrations	55
33. Scanning electron micrograph of a mild steel surface indicating the non-protective iron sulfide film and intergranular attack over the entire metal surface. x550	56
34. Most probable number (MPN) for GAB and SRB in the bulk water at different exposure time.	57
35. Most probable number (MPN) for GAB and SRB in the biofilm at different exposure time.	58
36. Macroscopic photographs of the mild steel coupons after biofilm and iron sulfide film have been removed at 3 days. x 50	60
37. Macroscopic photographs of the mild steel coupons after biofilm and iron sulfide film have been removed at 7 days. x50	60
38. Macroscopic photographs of the mild steel coupons after biofilm and iron sulfide film have been removed at 14 days. x50	61
39. Macroscopic photographs of the mild steel coupons after biofilm and iron sulfide film have been removed at 21 days. x50	61
40. Scanning electron micrograph of a mild steel surface after biofilm and iron sulfide film have been removed at 3 days. x2,800	62
41. Scanning electron micrograph of a mild steel surface after biofilm and iron sulfide film have been removed at 7 days. x2,300	62

LIST OF FIGURES (Continued)

Figure	Page
42. Scanning electron micrograph of a mild steel surface in the localized corrosion area where spherical deposits were found at 21 days. x 100	63
43. Scanning electron micrograph of a detached iron sulfide film just above the localized corrosion area where spherical deposits also found. x100 ...	63
44. Intergranular and pitting attack were found in the localized corrosion area at higher magnification. The grain boundary triple point also found in that area. x1,200	64
45. The circular deposition were iron sulfide crystal and bacteria. x 5,300	64
46. Scanning electron micrograph of a cross section of iron sulfide film and biofilm. x 10,000	65
47. Anodic polarization curves of mild steel on a precoated iron sulfide film followed by biofilm accumulation at different exposed times	65
48. Cathodic polarization curves of mild steel on a precoated iron sulfide film followed by biofilm accumulation at different exposed times	66
49. Weight loss vs. time curve in the abiotic conditions	68
50. Open circuit corrosion potential vs. time curves in abiotic experimental conditions. Two curves indicate the scattering of 24 coupons	68
51. Cathodic polarization curves in the abiotic conditions at different exposed times	69
52. Anodic polarization curves in the abiotic conditions at different exposed times	69
53. Scanning electron micrograph of iron sulfide film on mild steel in the abiotic conditions at 3 days. x50	70

LIST OF FIGURES (Continued)

Figure	Page
54. Scanning electron micrograph of a mild steel surface after iron sulfide film was removed in the abiotic conditions at 3 days. x 2,800	70
55. Scanning electron micrograph of iron sulfide film on mild steel in the abiotic conditions at 7 days. x50	71
56. Scanning electron micrograph of a mild steel surface after iron sulfide film was removed in the abiotic conditiond at 7 days. x 2,800	71
57. Scanning electron micrograph of iron sulfide film on mild steel in the abiotic conditions at 21 days. x50	72
58. Scanning electron micrograph of a mild steel surface after iron sulfide film was removed in the abiotic conditions at 21 days. x 750	72
59. Cathodic polarization curves of a mild steel before and after biofilm has been removed	76
60. Cathodic polarization curves of a mild steel with and without 1.5% agar	77
61. Anaerobic corrosion process of mild steel on a precoated iron sulfide film followed by biofilm accumulation up to 21 days	83
62. Anaerobic corrosion process of a mild steel in the abiotic conditions up to 21 days	86
63. Cathodic polarization curves of a mild steel with and without noncoherent iron sulfide precipitation under abiotic conditions	87
64. Anodic polarization curves for mild steel with and without noncoherent iron sulfide precipitates under abiotic conditions	87
65. Mass and electron transfer through the loose iron sulfide film	88

ABSTRACT

Corrosion of mild steel under completely anaerobic conditions in the presence of a mixed population biofilm, including sulfate-reducing bacteria (SRB), has been studied in a continuous flow system. The open channel flow reactor was continuously fed with low concentration substrate at different dilution rates which influenced biofilm accumulation. No direct correlation was observed between corrosion and SRB activity in the absence of ferrous ion. Furthermore, corrosion of mild steel in the SRB environment was mainly determined by the nature of the metal and environmental conditions such as dissolved iron. When formation of iron sulfide film on mild steel was prevented before the biofilm accumulated, the metal surface retained its scratch lines after a 21-day experiment (SRB at $2.6 \times 10^9/\text{cm}^2$). However, when iron sulfide film was formed before the accumulation of biofilm, visible localized corrosion appeared after 14 days and increased up to 21 days. Intergranular and pitting attack were found in the localized corrosion area. Inclusions (Al, Mn, and Fe) were usually found in the localized corrosion area. At high iron concentration (about 60 mg/L in the bulk water), all biogenic sulfide was precipitated and corrosion rate significantly increased. Intergranular attack was found over the entire metal surface.

The anaerobic corrosion processes of mild steel in the presence and absence of anaerobic biofilm, including sulfate-reducing bacteria, was compared. In the biotic experiment, biofilm accumulated on a chemically-formed iron sulfide film for 21 days. The abiotic experiment was designed to simulate this hydrogen sulfide environment which had similar hydrogen sulfide concentration, redox potential, and pH. There was no difference in the metal matrix at three days in the two conditions. However, corrosion propagation was different for the two cases after 3 days. Localized corrosion was found in the presence of biofilm while uniform intergranular attack was observed in the absence of biofilm.

INTRODUCTION

Economic Impact of Sulfate-Reducing
Bacteria (SRB).

The corrosion of iron and steel in the form of storage tanks, pipelines, pumps, and other systems by SRB is a serious problem faced by many industries including the petroleum industry. These bacteria also cause a decrease in the permeability of the fine pores of underground reservoirs, impeding the secondary recovery of petroleum by water injection. Recently, SRB have been suspected of contributing to failure of certain enhanced (tertiary) oil-recovery operations. Thus, almost every aspect of oil recovery can be hindered by SRB. SRB also are suspected to cause problems in pulp and paper industry, nuclear power plants, and other chemical industries. The cost related to SRB-mediated corrosion is estimated to be 1 to 2 billion dollars per year.

Corrosion of Mild Steel Under Anaerobic
Conditions in the Absence of Bacteria

Thermodynamically and abiotically, there is very little, if any, corrosion of steel in the absence of oxygen under neutral or alkaline conditions. However, anaerobic corrosion may occur in the presence of sulfide due to cathodic depolarization ($2 \text{H}_2\text{S} + 2 \text{e}^- \rightarrow 2 \text{HS}^- + \text{H}_2$). The attack

occurs by dissolved sulfide as well as iron sulfide (Smith et al, 1975). Iron sulfide causes cathodic depolarization by decreasing the hydrogen overpotential.

The anaerobic corrosion process of mild steel has been studied in a saturated hydrogen sulfide solution (Tewari et al, 1979; Shoesmith et al, 1980). Initially, a solid-state reaction produces a layer of mackinawite, which readily cracks and spalls from the metal surface and results in a loose iron sulfide precipitate. The corrosion rate is mainly controlled by the stability of the iron sulfide film in the initial stage. The saturated hydrogen sulfide (approximately 3150 mg/L hydrogen sulfide) represents an extreme condition unlikely to exist in a natural environment containing SRB. The levels of hydrogen sulfide released by the anaerobic decay of a marine fouling deposit (Edyvean et al, 1985) is about 5 to 150 mg/L. Therefore a more realistic assessment of the corrosion effects of hydrogen sulfide induced by fouling deposits on the corrosion behavior can be obtained by testing at low levels of hydrogen sulfide.

Corrosion of Mild Steel Under Anaerobic Conditions in the Presence of Bacteria

Biotic production of sulfide may lead to corrosion of mild steel in anaerobic environments. For example, chemostat (planktonic cells) investigations indicate that microbial sulfide production leads to cathodic depolarization primarily due to the iron sulfide reaction. Booth et al. (1966, 1967)

reported that no correlation exists between hydrogenase activity and corrosion rate when experiments were undertaken in semi-continuous and continuous culture in low or high concentration ferrous medium. Low rates of corrosion were observed in low level iron medium due to the formation of a protective iron sulfide film. However when these films ruptured, very high rates of corrosion occurred. In field investigations, Starkey (1985) also reported that only slight corrosion of a completely buried steel pipe was detected in anaerobic mud supporting an active community of SRB.

Von Wolzogen Kühr and van der Vlugt (1934) proposed the cathodic depolarization theory for microbial (SRB) corrosion based on batch (closed) reactor investigations. They suggested that hydrogenase catalyzed the hydrogen reduction reaction on the iron surface. King and Miller (1973) supported the hydrogenase theory but proposed that the cathodic depolarization occurred on the iron sulfide instead of the iron surface. Costello (1974) reports that Desulfovibrio desulfuricans, in a batch reactor, produces H_2S which directly depolarizes the cathode. In summary, H_2S corrosion is under kinetic control and the iron sulfide film seems to play an important role in the anaerobic corrosion process both in biotic and abiotic systems. There is evidence for cathodic depolarization as an important mechanism in the anaerobic corrosion of iron and mild steel. However, the exact mechanism, including the role of hydrogenase and reaction site

of hydrogen reduction, is not definitively understood.

Most microbial corrosion in nature and in technological systems occurs in association with microbial aggregates or biofilms. Hamilton (1985) has developed a qualitative biofilm model of anaerobic microbial corrosion where the growth of biofilm SRB requires that the appropriate physicochemical conditions be supplied by other facultative and anaerobic organisms within the biofilm. To address the anaerobic microbial corrosion problems in natural environments, the activities and behavior of biofilm or sessile SRB, not planktonic SRB, must be considered.

There is very little quantitative information available related to the rate and extent of microbial sulfide production in biofilms. Nielsen (1987) reports from a continuous flow SRB biofilm reactor that sulfate diffusion in the biofilm is rate-limiting for SRB biofilm activity.

The Problem

The relation between SRB activity and corrosion rate of mild steel is still not well established despite decades of research. Progress in microbial corrosion research has been limited by at least two factors: 1) avoidance of experimental methods which simulate biofilm processes in continuous systems and 2) analytical techniques which can be used in a biofilm systems and while providing adequate characterization of the corroding metal surface.

Research Goal

The goal of this research was to obtain a fundamental understanding of corrosion of mild steel under an anaerobic biofilm. To accomplish this goal, the following objectives and tasks were established.

Objectives

1. Determine the effects of anaerobic biofilms on the corrosion behavior of mild steel.
2. Determine the impacts of environmental parameters on the corrosion behavior of mild steel in the presence of an anaerobic biofilm.

Tasks

1. Determine the effect of substrate loading rate on the corrosion of mild steel in the absence of ferrous iron and relate SRB biofilm activity with the cathodic depolarization reaction.
2. Assess the influence of suspended iron sulfide on the corrosion of mild steel in the presence of a mixed SRB biofilm.
3. Evaluate the effect of the iron sulfide film on the corrosion of mild steel in the presence of a mixed SRB biofilm.
4. Assess the influence of low concentrations of hydrogen sulfide on the corrosion behavior of mild steel in the absence of bacteria.

LITERATURE REVIEW

Types of SRB and Their Substrates

The most common cell morphologies of SRB are curved and oval to rod-shaped; their diameters usually range from 0.5 to 2 μm . Many SRB are actively motile by flagella. Other forms are spheres and long multicellular filaments. Several types of SRB tend to grow in clumps or cell aggregates and stick to surfaces.

Nutritionally, SRB may be divided into two major groups. Species of the first group carry out an incomplete oxidation of organic substrates with acetate as an end product. Species of the second group oxidize organic substrate, including acetate, completely to CO_2 .

Most incompletely oxidizing SRB may grow rather fast under optimum conditions and reach doubling times of about 10 hours. The best-studied representatives are Desulfovibrio species that can be easily isolated from nearly every aquatic sediment (Postgate, 1984). For most, lactate is an excellent substrate that is oxidized to acetate and CO_2 .

The completely oxidizing SRB grow relatively slowly, with optimum doubling times seldom shorter than 15 hours. The nutritionally specialized Desulfobacter species prefer acetate as substrate, the quantitatively most important organic

fermentation product; higher fatty acids are not used. Other completely oxidizing SRB are nutritionally more versatile; they may oxidize propionate, higher fatty acids, lactate, alcohol; and even aromatic organic acids. Some of the completely oxidizing SRB can use H_2 as electron donor and synthesize cell material from CO_2 as the sole carbon source. The growth requirements and growth rates of selected SRB are given in Table 1.

Table 1. Growth requirements of selected sulfate-reducing bacteria

Species	Electron Donor			Doubling Time, HR.	Growth Range	Temp. °C Optimum	Growth pH		Other Requirements
	Acetate	Propionate	Butyrate				Range	Optimum	
Incomplete Oxidation									
<i>Desulfobulbus propionicus</i>	No	Yes	No	appx. 10	10-43	39 (28-39)	6.0-8.6	7.2	p-aminobenzoic acid
<i>Desulfovibrio sapovorans</i>	No	No	Yes	NR	15-38	34 (30-36)	6.5-9.3	7.7	NR
Complete Oxidation									
<i>Desulfobacter postgatei</i>	Yes	No	No	15-20	10-37	32	6.2-8.5	7.3	salt-0.7%, p-aminobenzoic acid and biotin
<i>Desulfotomaculum acetoxidans</i>	Yes	No	Yes	12-24 (15-30)	20-40	35	6.6-7.6	7.1	vitamins
<i>Desulfococcus multivorans</i>	Yes	Yes	Yes	appx. 24	NR	35	NR	NR	NR
<i>Desulfosarcina variabilis</i>	Yes	Yes	Yes	NR	15-38	33 (38-33)	6.7-9.0	7.4	salt-1.5%, p-aminobenzoic acid and biotin
<i>Desulfonema limicola</i>	Yes	Yes	Yes	30-100	15-36	29 (30)	6.5-8.8	7.6	salt-1.5%, surface, biotin
<i>Desulfonema magnum</i>	Yes	Yes	Yes	30-100	15-37	32	6.6-7.5	7.0	salt-2%, surface, biotin, aminobenzoic acid, vitamin B ₁₂
<i>Desulfovibrio baarsii</i>	Yes	Yes	Yes	NR	20-43	35-39	6.5-8.2	7.3	NR
Mixed culture	Yes	NR	NR	32	NR	NR	NR	NR	NR

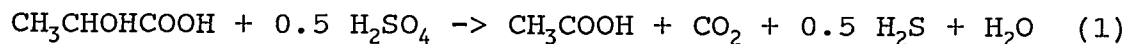
Stoichiometry and Kinetics of SRB

There are two aspects of the microbial reaction of science and engineering interest; stoichiometry and kinetics. Stoichiometry provides what changes will occur and to what extent. Kinetics describes how fast the change will occur.

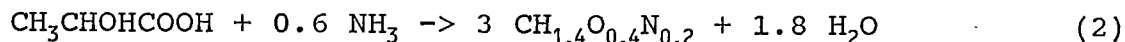
Stoichiometry of SRB

Dissimilating sulfate reduction can be represented by a pair of chemical equations that describe the oxidation of an organic carbon source and the synthesis of bacterial cells. For example, in the case that lactate is an electron donor and energy source, stoichiometric equations of sulfate reduction are described as following:

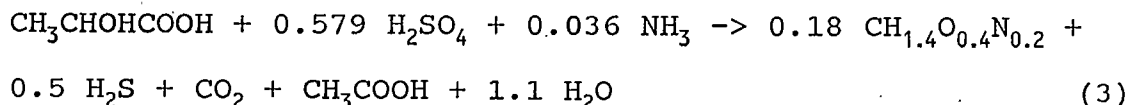
Energy with lactate



Synthesis with lactate



Overall stoichiometry



Overall stoichiometric equation was balanced using the experimental data concerning biomass yield and carbon dioxide production of D. desulfuricans culture determined by Traore et al (1982). D'Alessandro et al (1974) reported very similar stoichiometry of sulfate reduction by D. vulgaris. In both cases, lactate and sulfate were consumed in stoichiometric ratio of 2 : 1.

Kinetics of SRB

Bacterial cells reproduce by binary fission. For a given set of environmental conditions (e.g., temperature and pH) the rate of reproduction due to binary fission depends on the concentration of nutrient which are available for growth. If all required nutrients are supplied in excess except one, the growth limiting nutrients, the rate of cellular reproduction can be empirically related to the concentration of the limiting nutrient. The equation most widely used to describe this relation was originally proposed by Monod (1949) to describe the growth of Escherichia coli on glucose. The Monod equation is written as follows:

$$\mu = \frac{\mu_{\max} S}{k_s + S} \quad (4)$$

where

- μ = cellular specific growth rate (t^{-1})
- μ_{\max} = maximum cellular specific growth rate (t^{-1})
- s = concentration of the limiting nutrients, commonly referred to as the substrate ($M_s L^{-3}$)
- k_s = saturation coefficient, numerically equal to the substrate concentration at $\mu = 1/2 \mu_{\max}$ ($M_s L^{-3}$)

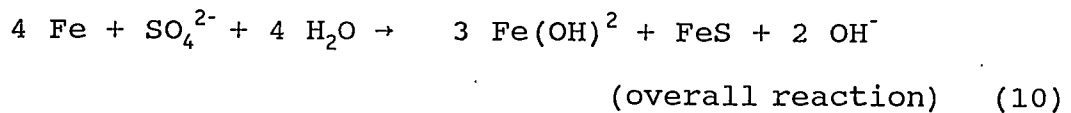
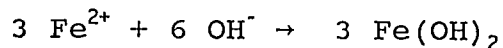
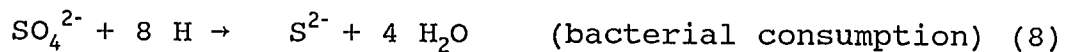
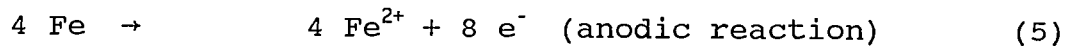
A number of information in terms of μ_{\max} and k_s for SRB are given in Table 2.

Table 2. Typical values for the maximum specific growth rate, μ_{\max} , and the saturation constant, k_s , for lactate-utilizing SRB in lactate, sulfate medium at temperature = 30 ° C.

Bacterial species	μ_{\max} (h^{-1})	k_s (mg/L)	pH	Reference
<u>D. desulfuricans</u>	0.041	-	6.5	Cork et al (1979)
<u>D. desulfurucans</u>	0.360	-	7.4	Cappenberg (1975)
<u>D. desulfuricans</u>	0.104	-	-	Traore (1982)
<u>D. vulgaris</u>	0.011	0.461	7.2	Ivgvorsen (1984)
<u>D. sapovorans</u>	0.007	0.700	7.2	
<u>D. salexigens</u>	0.021	7.363	7.2	

Mechanisms of Metal Corrosion by SRB

Anaerobic bacteria, particularly sulfate reducers, have been the most studied microorganisms in biological corrosion investigations. The early work of Von Wolzogen Kühr and van der Vlugt (1934) suggested the following electrochemical reactions:



The overall process was described as "depolarization" based on the theory that these bacteria remove hydrogen that accumulates on the iron surface. The electron removal as a result of hydrogen utilization results in cathodic depolarization forcing more iron to be dissolved at the anode. The direct removal of hydrogen from the surface is equivalent to lowering the activation energy for hydrogen removal by providing a "depolarization" reaction (Figure 1). The enzyme, hydrogenase, synthesized by many species of Desulfovibrio, may be involved in this specific depolarization process. Booth et al. (1962) using polarization techniques and weight loss

measurements versus hydrogenase activity have provided additional evidence to substantiate this theory based on batch culture experiments. However, Booth et al (1966, 1967) further proved that this relationship does not exist in low and high ferrous iron medium in semi-continuous or continuous culture experiments. Low rates of corrosion were observed in low iron concentration medium due to the formation of a protective iron sulfide film. However when these films ruptured, very high rates of corrosion occurred. Mara and Williams (1972) observed the same trend and concluded that film breakdown resulted from sulphidation of the primary corrosion product mackinawite, FeS_{1-x} to greigite Fe_3S_4 , resulting in an increase in product volume.

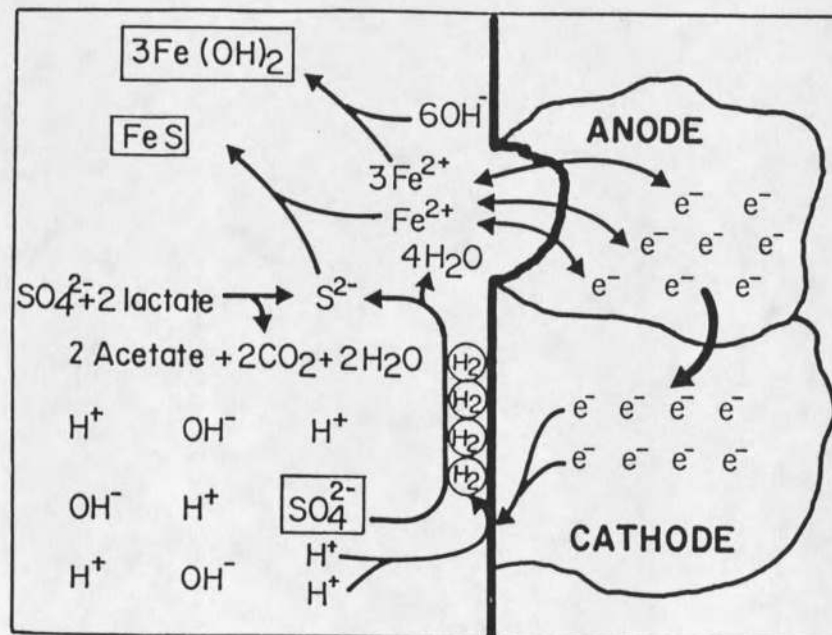


Figure 1. Proposed reaction of anaerobic corrosion in the presence of SRB on an iron surface.

Miller and Tiller (1970) have proposed cathodic "depolarization" induced by microbially produced FeS as a corrosion mechanism. King and Miller (1973) demonstrated that weight loss of steel as proportional to the concentration of ferrous sulfide and the stoichiometry of the particular ferrous sulfide minerals. They concluded that accelerated corrosion of mild steel in the presence of SRB was due principally to the formation of iron sulfide. Because iron sulfide is not a permanent cathodic depolarizer, sustained corrosion rates were found to be dependent on the removal of the bound hydrogen by the action of bacterial hydrogenase. The comparison of the two mechanisms is shown in Figure 2.

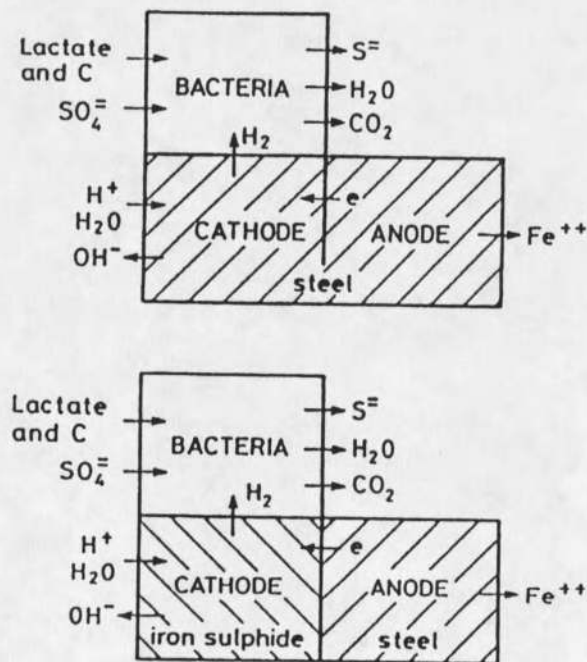


Figure 2. Schematic representation of the classical mechanism (top) and alternative mechanism (bottom) of microbial corrosion under anaerobic conditions (after Miller & King).

Costello (1974) proposed that dissolved H_2S produced by SRB is responsible for the cathodic depolarization. Further evidence was provided by Togano et al (1975) who demonstrated that the corrosion rate was proportional to the concentration of H_2S produced by SRB, and it was suggested that H_2S accelerated both anodic and cathodic reactions. The cathodic depolarization theories are summarized in Table 3.

Table 3. The history of cathodic depolarization theories.

Yr	Experimen- ter	Type of Bacteria	Type of Culture	Medium	Depol- arizer	Mater- ial	Experi- mental period
'34	Von Wolzo- gen Kuhr	D.desul- furicans	batch	wet soil	hydro- genase	iron	/
'62	Booth and Tiller	D.sale- xigens	batch	rich*	hydro- genase	mild steel	11 days
'68	Booth et al.	SRB	Semi & contin.	rich*	FeS	mild steel	60 weeks
'72	Mara and Milliams	D.vul- garis	contin.	rich*	FeS	mild steel	10 weeks
'73	King and Miller	D.desul- furicans	batch	rich*	hydro- genase & FeS	/	/
'74	Costello	SRB	batch	rich*	H_2S	mild steel	8 days

* rich means the media has carbon between 1000 to 2000 mg/L.

The impact of oxygen on obligate anaerobic SRB was examined by Hardy and Brown (1984) using a synthetic seawater

medium and a Desulfovibrio strain. Corrosion rates were determined by weight-loss measurements and by electrical resistance. Corrosion rates were low under totally anaerobic conditions, but increased with the addition of oxygen. Successive aeration-deaeration caused shifts in the corrosion rate: high rates were observed during periods of aeration. The attack was confined to areas beneath tubercles that consisted of loosely adherent material as opposed to the hard, tightly adherent films on uncorroded metal. The authors concluded that the presence of tubercles fixed the anode and forced the cathodic reaction to occur on the adherent sulfide film.

The situation in which aerobic and anaerobic conditions co-exist on metal surfaces can be achieved through the colonization of metal by aerobic micro- or macro- organisms, where due to their metabolic activities a rapid depletion of oxygen occurs. Hamilton (1985) has developed a qualitative biofilm model of anaerobic microbial corrosion where the growth of biofilm SRB requires that the appropriate physicochemical conditions be supplied by other facultative and anaerobic organisms within the biofilm (Figure 3). This anaerobic area then becomes the anode where the corrosion will take place, while the aerated region will provide the balancing cathodic reaction. Corrosion due to such oxygen concentration cells is quite common in industrial cooling water systems and heat exchangers.

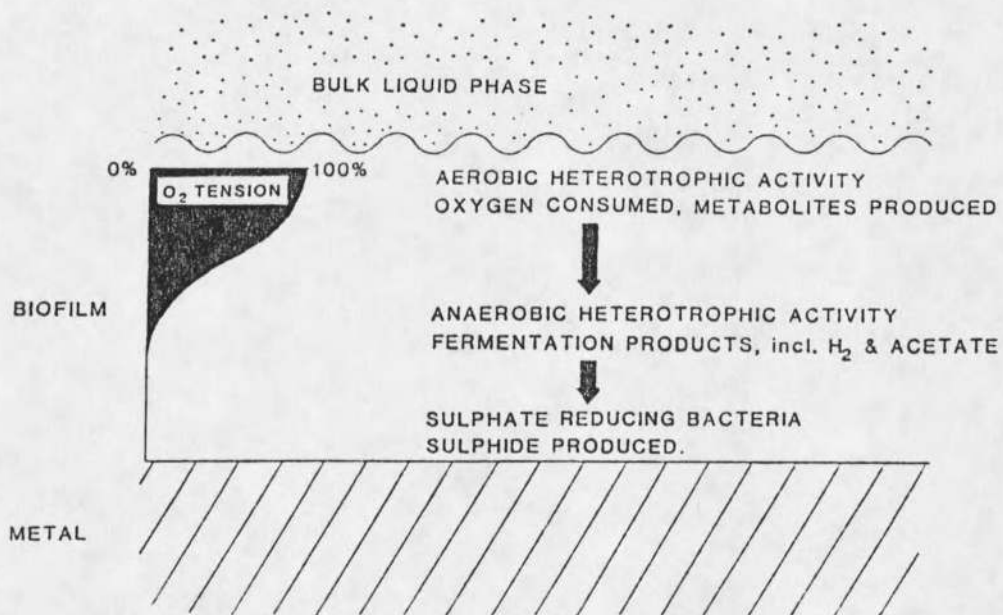


Figure 3. Model for microbial biofilm in oxygenic environment.

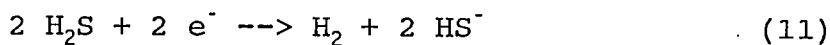
Mechanisms of H₂S Corrosion in the Absence of Bacteria

An iron sulfide film forms on the metal surface during corrosion of iron by hydrogen sulfide (Meyer et al, 1958). Surface analysis demonstrates that the type of film is dependent on pH, temperature, and hydrogen sulfide concentrations. The combined presence of CO₂ and H₂S often alters the type of film produced. Sardisco et al (1963) and Sardisco and Pitts (1965) found that iron corroding in a wet H₂S-CO₂ atmosphere at low H₂S partial pressure follows a seemingly parabolic rate expression, while at high H₂S partial pressure, distinction between linear and parabolic rate laws become impossible. Authors suggest that hydrogen sulfide pressure must affect the structure or permeability of the iron

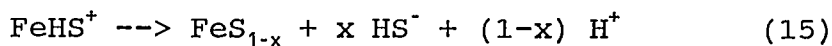
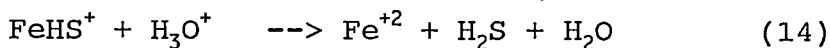
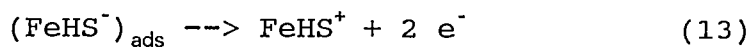
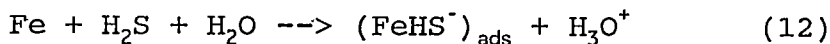
sulfide film. A number of authors have investigated the corrosion of iron by hydrogen sulfide as a function of pH (Sardisco et al, 1965; Gutzeit, 1968; Hutchison et al, 1961). All results indicate that the corrosion rate decreases with increasing pH between 4 and 7.

Mechanisms

In acid H₂S environment, the overall cathodic reaction has been suggested to be the following (Bolmer, 1965):



This reaction was found to be limited by H₂S diffusion and H₂ overpotential. It was suggested by the author that at regions beyond the diffusion current, the reduction of HS⁻ or H₂O was responsible for increased cathodic current. Iofa, Batrakov, and Ba (1965) proposed the following anodic dissolution mechanism in H₂SO₄ containing Na₂S at 25 °C:



In this mechanism, Fe is first converted to a catalyst

(FeHS^-) adsorbed on the iron surface, which then transforms to the hydrosulfide ion (FeHS^+). Subsequent to reaction (13), the species FeSH^+ may be hydrolyzed to yield a dissolved species (eg.14), or it may be incorporated directly into a growing layer of mackinawite (eg.15).

Film Diffusion Control in Corrosion Mechanism

Hausler et al (1972) demonstrated that the behavior of the iron sulfide film and its growth kinetics are principally controlled by environmental parameters such as pH and H_2S concentrations. At pH 4, they suggested that the rate-controlling film can reach a critical thickness. If the iron sulfide film grows beyond that thickness, the film breaks up and any additional thickness no longer affects corrosion rate. At pH 7, low rate of corrosion occurs due to formation of a coherent iron sulfide film. Shoesmith et al (1980) also showed the importance of pH in controlling the film properties under saturated hydrogen sulfide solutions. At pH 4, initially a solid-state reaction produces a layer of mackinawite, which readily cracks and spalls from the metal surface. This layer is replaced by a second solid-state growth mackinawite layer, which cracks again. Significant passivation was observed only at pH 7, when the initial mackinawite base layer remained virtually intact. Tewari et al (1979) concluded that corrosion of iron in saturated H_2S solution is governed by the dissolution rate of mackinawite. This dissolution is controlled by the chemical reaction between mackinawite and

H⁺ and by the transport of the complexed FeSH⁺ from the metal surface to the bulk. The developed noncoherent iron sulfide may accelerate corrosion by decreasing hydrogen overpotential but is limited by concentration-diffusion polarization (Booth et al, 1968 and Martin et al, 1981).

Localized Corrosion of Steel in the H₂S Environment

In addition to general corrosion, depending on sulfide level and pH, steel may undergo pitting corrosion. Gupta (1981) demonstrated that pitting corrosion of carbon steel was predominant at a medium sulfide level of 150 to 300 mg/L at pH 6 through 14. Brown (1970) proposed that localized corrosion is initiated and propagated due to the local acidity. The acidity is caused by hydrolysis of one or more corrosion products of the metal or alloy, and the acidity persists because of the restricted mass transfer between the corrosion cell and bulk environment caused by the porous corrosion products. Sulfide inclusions such as (Mn,Fe)S in the steel can also act as sources of pit nucleation (Smialowska, 1972):

Use of Electrochemical Techniques for Studying Microbial Corrosion

Microorganisms influence corrosion by changing the electrochemical conditions at the metal surface. Theoretically, these changes may have many effects ranging from the induction of localized corrosion to a change in the

rate of corrosion, to corrosion inhibition. In every case, however, the process of corrosion is electrochemical and electrochemical techniques can generally be applied in the investigation of corrosion under both aerobic and anaerobic conditions.

Recently, a greater recognition of the complexity of the microbial corrosion process has developed. Microbial corrosion is rarely linked to a unique mechanism or to a single species of microorganisms. In the present state of knowledge, it is widely accepted that the growth of different microbial species within adherent biofilms facilitate the development of structured consortia that enhance the microbial effects on corrosion. Therefore, interpretation of electrochemical data from systems in which complex biofilm, consisting of microorganisms and their extracellular polymeric substances (EPS), must also consider the water chemistry in the biofilm.

Electrochemical methods have been used in complex electrolytes, such as microbiological culture media, where the type and properties of passive films are not fully known. The presence of high concentrations of aggressive anions and pitting inhibitors in these solutions make interpretation of the experimental results difficult. Microbial colonization of passive metals can drastically change the metal resistance to breakdown by locally changing the type and concentration of anions, pH, oxygen, paints and inhibitors. These changes may

result in significant modifications in the electrochemical behavior of the metal and in the electrochemical parameters used in laboratory experiments.

In many cases, laboratory studies have been made without considering the presence of different passive films on the metal before microbial colonization. The presence of a complex layer of corrosion products, cells and EPS may drastically modify the results of conventional electrochemical techniques. Some techniques must be used with special care at a biologically conditioned metal/solution interface, where classical electrochemical parameters are not always valid. However, the use of appropriate electrochemical methods coupled with a careful characterization of the microbiological components can lead to a better understanding of the corrosion mechanisms.

Open Circuit Corrosion Potential

The potential of a corroding metal can be measured by determining the voltage difference between that metal immersed in a corrosive medium and an appropriate reference electrode such as the saturated calomel electrode (SCE). The magnitude and sign of the corrosion potential are functions of the metal composition, as well as the composition, temperature and hydrodynamics of the electrolyte. The open circuit potential is measured using a potentiometer, or a high impedance digital voltmeter or electrometer. These instruments are capable of accurately measuring small voltages without drawing enough

current to polarize the reference electrode.

Because of its simplicity, measurement of the corrosion potential has been used in microbial studies for many years. The progress of open circuit potential has been used to assess the electrochemical behavior of steel specimens immersed in batch cultures of SRB (Hadley, 1943; Wanklyn and Spruit, 1952; Horvath, 1960). The initial potential decay observed in these media was attributed to cathodic depolarization of the steel electrode (Hadley) or to enhancement of the anodic process (Wanklyn and Spruit). Some years later, in similar experiments, Horvath attributed the steady-state corrosion potential after the initial drop to the formation of a semiprotective film of iron sulfide. Early use of open-circuit potential for studying in SRB corrosion were limited by the lack of complementary measurements. However, a plot of potential vs. time was useful for detecting the initiation of accelerated attack due to bacteria.

Redox Potential

The oxidation-reduction (or redox) potential is useful for predicting whether or not a metal will corrode in a given environment. Redox potential is the potential associated with the oxidation and reduction of hydrogen or oxygen in a corrosive environment and is a function of the oxygen concentration, temperature, and pH. At a given temperature and pH, the redox potential of any natural aqueous environment becomes more negative (or active) with decreasing dissolved

oxygen concentration. This type of redox potential measurement has been used frequently in microbiology to assess the suitability of a given environment for growth of SRB, SRB require an environment with a very active (negative) redox potential.

When measuring the redox potential, the concurrent measurement of pH is necessary because the experimental values have to be referred to a standard pH. Strictly speaking, the redox potential is only defined for an electrochemical reaction under equilibrium (zero current flow) conditions, and it must be measured by special electrochemical techniques under carefully controlled equilibrium conditions. Such equilibrium conditions are not usually encountered in living systems, such as within the microbiological films of interest here. Nevertheless, steady-state conditions do occur in microbial cultures and films, and the redox potential measured under these conditions can provide useful information on the redox characteristics of that environment and any environmental changes resulting from bacterial metabolism. Generally, a noble (positive) redox potential value for a given environment indicates conditions favorable for corrosion. If a noble redox potential occurs together with a noble corrosion potential and an active (negative) pitting potential for a particular alloy, it does indicate that the environment is very aggressive for that alloy.

Potentiostatic Polarization

The current-potential (Evans) diagram is a graphical method for demonstrating the relationship between corrosion rate and the polarization of anodic and cathodic reactions in which both reactions are presented as linear E-i curves that converge and intersect. This intersection point corresponds to the corrosion potential and the corrosion current density. The corrosion current density cannot be measured directly since the current involved is one that flows between numerous microscopic anodic and cathodic sites on the surface of the corroding metal. A convenient practice is to employ a potentiostat in conjunction with a reference electrode to polarize the specimen first in the active (or cathodic) direction and then in the noble (or anodic) direction. In this procedure, the specimen is initially made to act as a cathode in the electrochemical cell and the potential-current density curve is measured over several hundred millivolts active to the open circuit corrosion potential, varying the applied potential in discrete steps (25 mV every 5 minutes is common). At the corrosion potential, the applied potential is zero, and the measured cathodic current density approaches zero.

Pitting Potentials

Microorganisms often stimulate localized forms of corrosive attack, such as pitting, depending on the passive film formed on the metal or alloy. Thus, different methods for determining characteristic pitting potential values can be

useful in defining the tendency of microorganisms to accelerate pitting in a given metal/solution system. "Pitting potential", as used in the literature, is a non-specific term related to the onset of pitting corrosion. The numerical value obtained for the "pitting potential" depends strongly on the experimental technique used to measure it. Strictly speaking, the value measured by each of these techniques should be called by a different name. As an example, the "critical pitting potential," E_{cpp} , is usually defined as the most noble potential at which the passive current density remains stable and pits do not nucleate (on a crevice-free surface). E_{cpp} is measured potentiostatically in the laboratory under carefully controlled conditions. If measured carefully, E_{cpp} is independent of the geometry of the specimen and the test apparatus. The "breakdown potential," E_p , is defined as the potential at which the anodic polarization curve shows a marked increase in current, leading to breakdown of the passive film and pit initiation. E_p is usually measured by potentiodynamic polarization sweep techniques and depends on both the sweep rate and experimental geometry.

Several laboratory studies (de Mele et al., 1979; Salvarezza et al., 1979; Salvarezza and Videla, 1980; Videla, 1986a; Gaylarde and Videla, 1987) indicate that the presence of certain microorganisms decreases (makes less noble) the E_p values of several metals and alloys. In one study (Salvarezza and Videla, 1980), SRB and sulfide in artificial sea water

resulted in equivalent E_p values of 100-200 mV more active than in sea water alone. These experimental results suggest that, since planktonic SRB behave in a similar manner to chemically added sulfide, the action of anaerobic bacteria on the corrosion of mild steel is a consequence of metabolic sulfide production. In addition, the breakdown of passivity was accomplished more easily in deaerated solutions where lower levels of sulfides were needed.

Alternating Current Methods

In recent years, electrochemical impedance techniques have been used for measuring the polarization resistance and other characteristics of a corroding metal surface. Problems of accuracy and reproducibility frequently encountered in the application of direct current methods have led to an increasing use of electrochemical impedance spectroscopy (ECIS). The rapid development of commercially available instrumentation allows one to take measurements over a wide range of frequencies from 10^{-3} to above 10^3 Hz.

Direct current techniques assess the overall corrosion process occurring at a metal surface but treat the metal/solution interface as if it were a pure resistor. The ECIS technique measures not only the resistive, but also the capacitive and inductive components of the overall interfacial impedance. Thus, ECIS is particularly useful in the presence of non-conducting and semi-conducting surface films such as organic paints and many metal oxide films. The organic and

microbiological films that adsorb to all surfaces immersed in natural aqueous environments are also non-conducting, so ECIS techniques are potentially useful in their presence. Some caution is required in data interpretation, however, because the adsorbed organic and biological films tend to provide patchy, rather than continuous surface coverage.

ECIS techniques are also able to distinguish between electrochemical reactions based on their relaxation times. A given electrochemical reaction will only respond to an alternating current signal whose period is longer than the characteristic time for the rate limiting step for that reaction to occur across the interface. The evaluation of the impedance spectrum of an electrode over a wide range of frequencies can then be used to distinguish among the various processes taking place at the interface between the metal and the electrolyte or between the metal and a film or coating.

ECIS techniques in microbial corrosion research should be used with caution: a) The interpretation of ECIS data depends largely on the development of equivalent electrical circuits for modeling of the solid/electrolyte interface. These equivalent circuits are difficult to formulate for complex interfaces involving partial coverage by microbial films. b) The combination of microbial film and corrosion products often encountered in microbial corrosion causes the impedance to become very high at low frequencies, thus requiring extrapolation. c) Microbial films are not stable

like paint films or even metal oxide films. Rather, microbial films are dynamic entities, within which changes are continually occurring as a result of metabolism. Such changes can cause short-term fluctuations in the electrochemistry at the metal/film interface, causing localized attack under the film that is not easily detected. d) The period of these fluctuations can be shorter than the time necessary to gather ECIS data when using a full frequency sweep, meaning that not all frequencies of the applied signal are responding to the same electrochemical conditions (Lee, 1986). e) In addition, it must be emphasized that the continuous changes occurring at the metal solution interface due to biofilm formation and detachment, and microbial activity within the biofilm, cannot be adequately interpreted through equivalent electrical circuits.

EXPERIMENTAL

Experimental Reactor

All experiments were conducted in a continuous open channel flow reactor with dimensions 1.00 m x 0.15 m x 0.30 m and containing a working volume of 4.5 liters and a surface area of 3.5 m² (Figure 4).

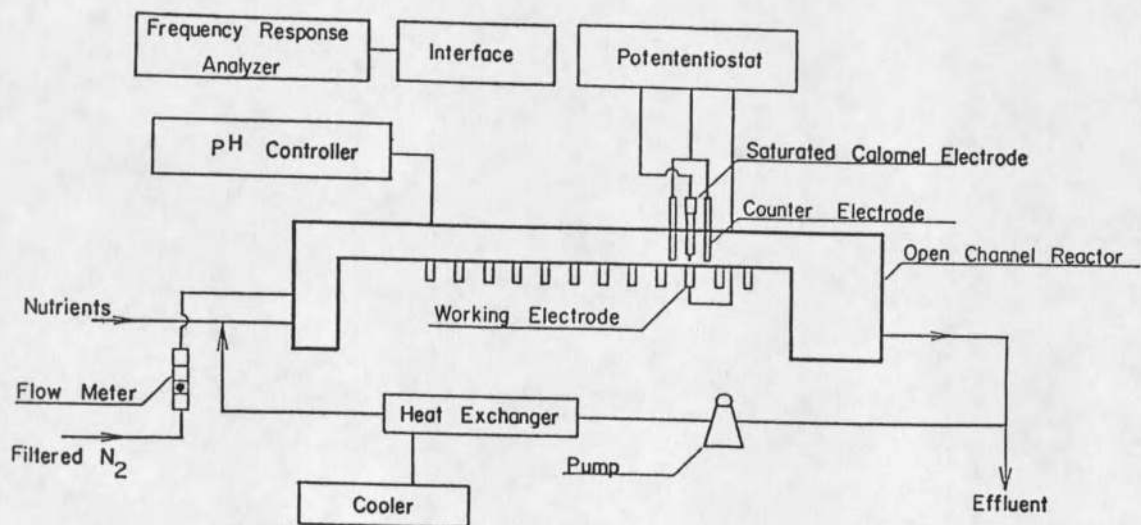


Figure 4. Continuous open channel flow reactor with dimensions 1.00 m x 0.15 m x 0.30 m and with a working volume of 4.5 liters and a surface area of 0.35 m².

The reactor has a recirculation loop to provide sufficient mixing and a flow velocity of approximately 0.3 m/s. The whole experimental system is sparged with nitrogen to minimize air permeation. The purge gas was first passed through hot copper filings to remove traces of oxygen. The reactor contains twenty-four (24) corrosion coupons which are connected to a potentiostat.

Media and Biofilm Growth Conditions

Bacteria were grown in 1/10 strength artificial seawater, 200 mg/L lactate acid, 50 mg/L yeast extract, 50 mg/L NH_4Cl , and 5 mg/L Na_2HPO_4 . The ionic composition of 1/10 strength artificial seawater is listed in Table 4. Ferrous iron was absent in the media except for selected experiments. The pH was controlled at 8 with 0.1 N NaOH and 0.1 N HCl. The stock solution of both NaOH and HCl were flushed with nitrogen and reduced by adding 0.013% Na_2SO_3 . Temperature was controlled at 30° C by a heat exchanger and cooler. Desulfovibrio desulfuricans (ATCC 5575) was inoculated into the open channel flow reactor which, for the first week, was operated as a batch reactor until surface colonization occurred. Thereafter, substrate was continuously fed to the reactor. The experiment was not conducted aseptically in order to simulate natural marine environments in which the SRB grow.

Table 4. The ionic compositions of 1/10 artificial seawater.

ION		PPM @ 3.4%
Chloride	[Cl ⁻]	1,878.8
Sodium	[Na ⁺]	1,042.4
Sulfate	[SO ₄ ⁼]	257.7
Magnesium	[Mg ⁺⁺]	126.5
Calcium	[Ca ⁺⁺]	39.8
Potassium	[K ⁺]	37.1
Bicarbonate	[HCO ₃ ⁻]	14.5
Borate	[BO ₃ ⁼]	2.8
Phosphate	[PO ₄ ⁼]	0.14
TOTAL		3,399.74ppm

Coupons

Disks of AISI 1018 mild steel (Metal Samples, Inc., Mumford, AL.) 15.9 mm in diameter were cast in acrylic resin to minimize crevice corrosion. The coupons were polished with grit paper (120, 200, 320, 400, 600) followed by ultrasonic cleaning in 100% alcohol for 1 minute and dried in air at room temperature. The elemental composition of AISI 1018 mild steel are presented in Table 5.

Table 5. Elemental composition of AISI 1018 mild steel

Element	C	P	S	Mn	Fe
%	0.20	0.01	0.014	0.76	Balance

Corrosion Measurements

Corrosion potential, polarization, AC impedance, and weight loss were measured in the open channel flow reactor periodically for up to 21 days. DC measurements were made using a Princeton Applied Research Corporation (PARC) 273 Potentiostat/Galvanostat and AC measurements using a Solartron 1250 Frequency Response Analyzer through a Solartron 1186 Electrical Interface.

The potential of the working electrode was measured against a saturated calomel electrode (SCE). Two graphite rods were used as counter electrodes. Cathodic polarization measurements were performed from E_{corr} to 400 mV in the cathodic direction at a scan rate 0.2 mV/s. Pitting potential measurements were performed beginning at -800 mV in the anodic direction with the same scan rate as cathodic polarization. AC impedance measurements curve made using a sine wave voltage with an amplitude of 7.5 mV at frequencies between 2 mHz and 10 KHz. Ten frequencies were examined per decade. At the end of each experiment, coupons were removed from the reactor and cleaned in an ultrasonic bath with an inhibited acid solution for 30 seconds prior to the weight loss measurement.

Water Chemistry

Desulfovibrio desulfuricans uses lactate as a carbon and energy source and oxidizes it to acetate coupled with the reduction of sulphate to sulfide. As a consequence, the

chemical analysis of the reactor fluid included lactate, acetate, sulfate, total dissolved sulfide, and redox potential. Samples were taken from both influent and effluent to complete material balances.

Lactate was determined by an enzymatic method (Boehringer Mannheim GmbH). Acetate was measured with a Varian 3700 gas chromatograph. Sulfate concentration was determined using the barium chloride turbidimetric method (Standard Method, 1971). Total dissolved sulfide was determined by adding zinc acetate to precipitate sulfide followed by use of methylene blue method (Cline, 1969). The redox potential was determined by measuring the potential of a platinum electrode using the PARC 273 Potentiostat/Galvanostat against a saturated calomel electrode.

Biological Analysis

SRB numbers in the biofilm were determined by the five (5) tube multiple dilution MPN method using Postgate B broth. A metal coupon containing a biofilm was removed from the reactor and transferred to an anaerobic tent in which the biofilm was removed by brushing into 30 ml of sterile 1/10 artificial seawater and homogenized to disperse the biofilm. A dilution series to 10^{-10} is prepared from 1 ml suspended biofilm using the normal procedure. SRB number in the bulk water phase were determined by the same MPN method for a 1 ml sample.

Numbers of GAB both in the biofilm and bulk water were determined by the same procedure as that for SRB but used fluid thioglycollate medium.

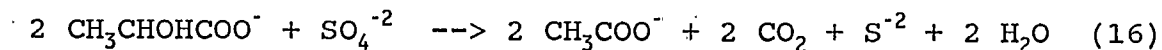
Surface Analysis of Biofilm and
Corrosion Products

A biofilm sample was transferred anaerobically to the anaerobic tent and fixed for 8 hours in 2% glutaraldehyde diluted with filter-sterilized artificial seawater. Then, it was dehydrated in a graded series of alcohol (15 minutes in alcohol 30% - 95%, and 30 mins. in 100%) washes. The sample was then dried using a Balzers CPD-020 critical point dryer for scanning electron microscopy (SEM). Finally, the sample was coated with Au-Pd alloy and examined with a ISI-40 scanning electron microscope. Composition of the corrosion products was analyzed with the SEM and a Princeton Gamma-Tech System 4 Energy-dispersive X-ray Spectrometer (EDS).

RESULTS

Stoichiometry of a Mixed Population SRB
Biofilm with Corrosion Coupon

Stoichiometric determinations were conducted in batch conditions after biofilm had accumulated in the open channel flow reactor. The exhaustion of lactate corresponded to plateau values for sulfate reduction and sulfide production (Figure 5). The decrease in sulfide concentration was due to the continuous purge of nitrogen in the reactor. Both sulfate reduction and sulfide production agreed with the theoretical calculations based on the stoichiometry of lactate oxidation:



The stoichiometric ratios provide strong evidence that SRB dominated the biofilm under the experimental conditions.

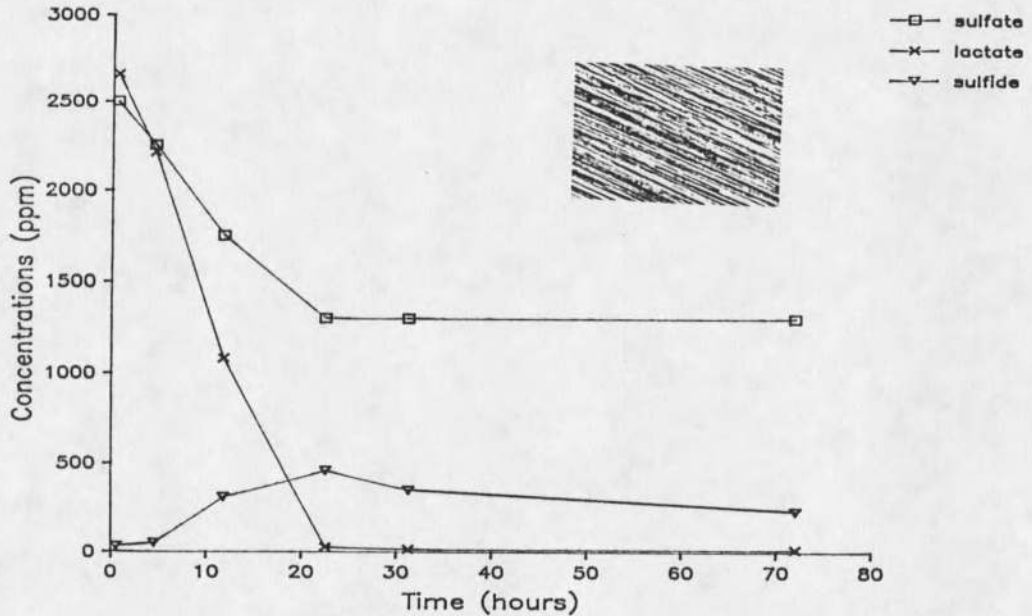


Figure 5. Sulfide production, lactate consumption, and sulfate degradation in mixed culture containing SRB. Attached picture (x50) indicates no iron sulfide corrosion products at the end of experiment.

Corrosion of Mild Steel at Different Substrate Loading Rates

Biofilm accumulation was strongly dependent on substrate loading rate. At constant substrate concentration, there was enough residence time (25 hours) for the organisms to grow in the bulk liquid at low dilution rate (0.04 h^{-1}) and resulted in a thin biofilm. It appears that bulk liquid cells compete effectively with biofilm for substrate. However, there was not enough time for organisms to grow in the bulk liquid at high dilution rate (0.75 h^{-1}) which resulted in a thick biofilm. The formation of iron sulfide precipitates on the mild steel surface was deliberately prevented before the

biofilm accumulation to reduce the interference of iron sulfide with the cathodic depolarization reaction. Dissolved sulfide in the bulk liquid and hydrogen sulfide in the gas phase were flushed away after some initial biofilm had accumulated in the open channel flow reactor. Then, corrosion experiments were initiated by insertion of clean metal coupons into the reactor followed by normal substrate input. The continuous flow experiments were conducted for 21 days.

Biofilm accumulation was a function of substrate loading rate (Figures 6 to 11). Biofilm thickness reached about 1000 μm at the high substrate loading rate while accumulating to only about 5 μm at the low substrate loading rate after 21 days. At the high loading rate, the biofilm was mainly composed of cells with a small amount of extracellular polymeric substances (EPS) (Figure 12). Much higher SRB populations were found both in the bulk liquid (Figures 13 to 14) and biofilm (Figures 15 to 16) at the high substrate loading rate. The high numbers in the bulk liquid were a result of detachment from the biofilm. The GAB numbers in the bulk water decrease as the substrate loading rate increases. Chemical analysis of the bulk water showed similar concentration of sulfide and acetate and redox potential for the two loading rates. However, there was residual lactate in the high substrate loading rate experiment (Tables 6 and 7).

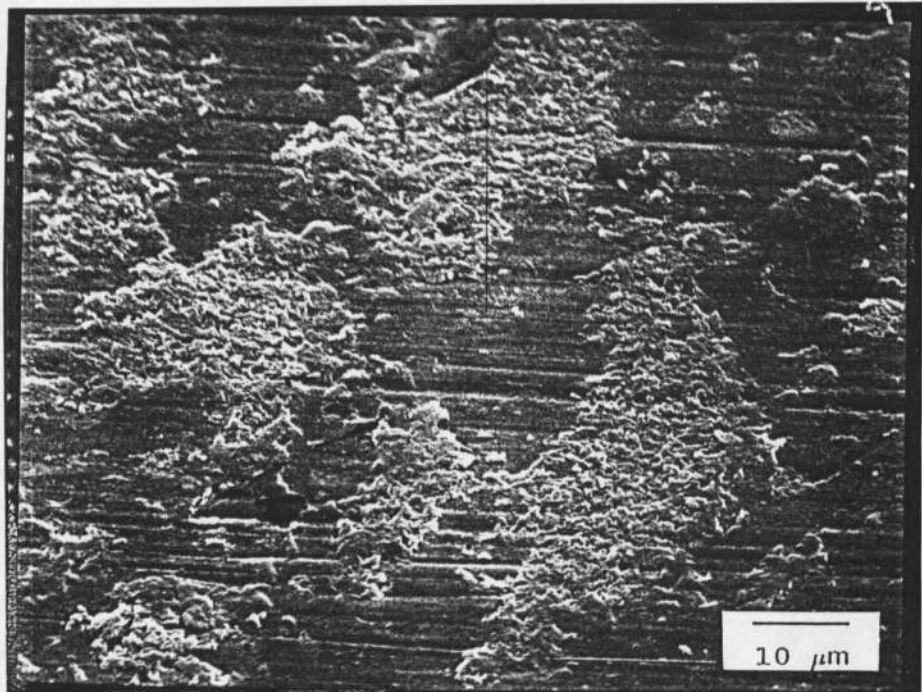


Figure 6. Scanning electron micrographs of biofilm grown on a mild steel surface for 3 days, x1300, at low substrate loading rate.

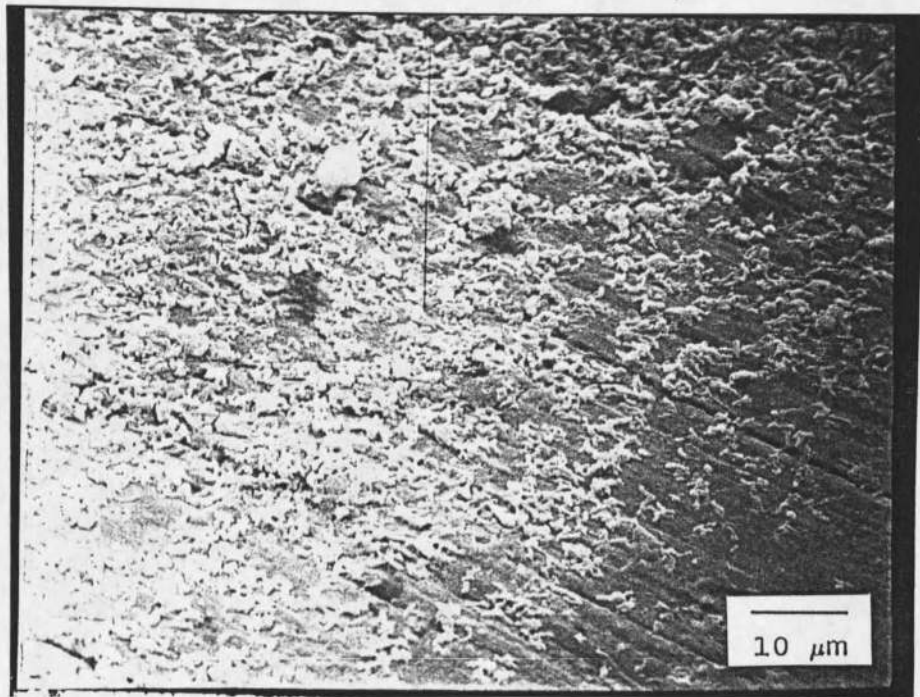


Figure 7. Scanning electron micrographs of biofilm grown on a mild steel surface for 7 days, x1300, at low substrate loading rate.

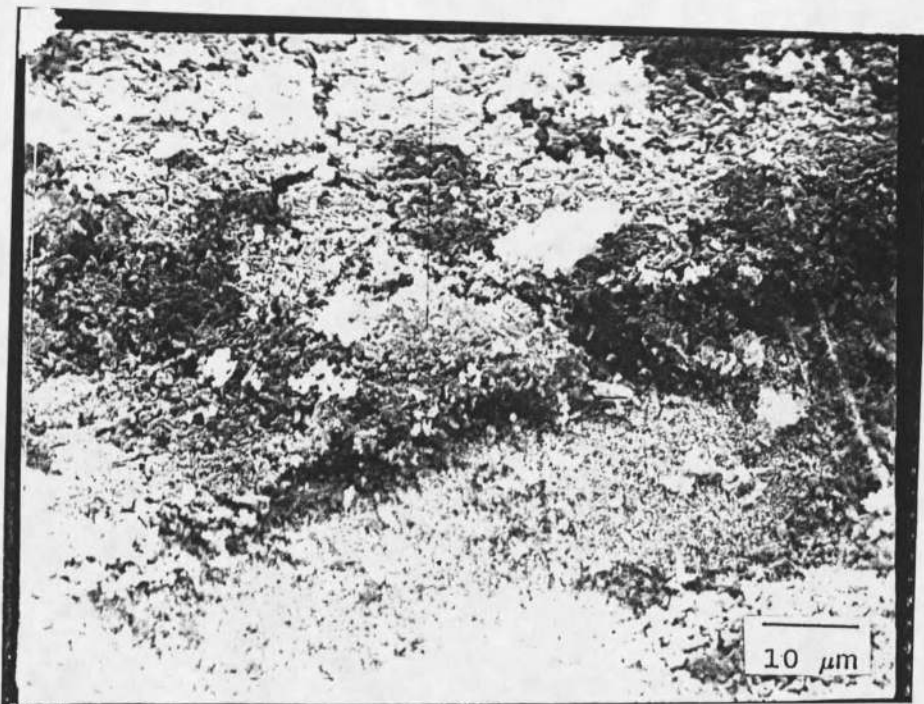


Figure 8. Scanning electron micrographs of biofilm grown on a mild steel surface for 21 days, x1300 at low substrate loading rate.

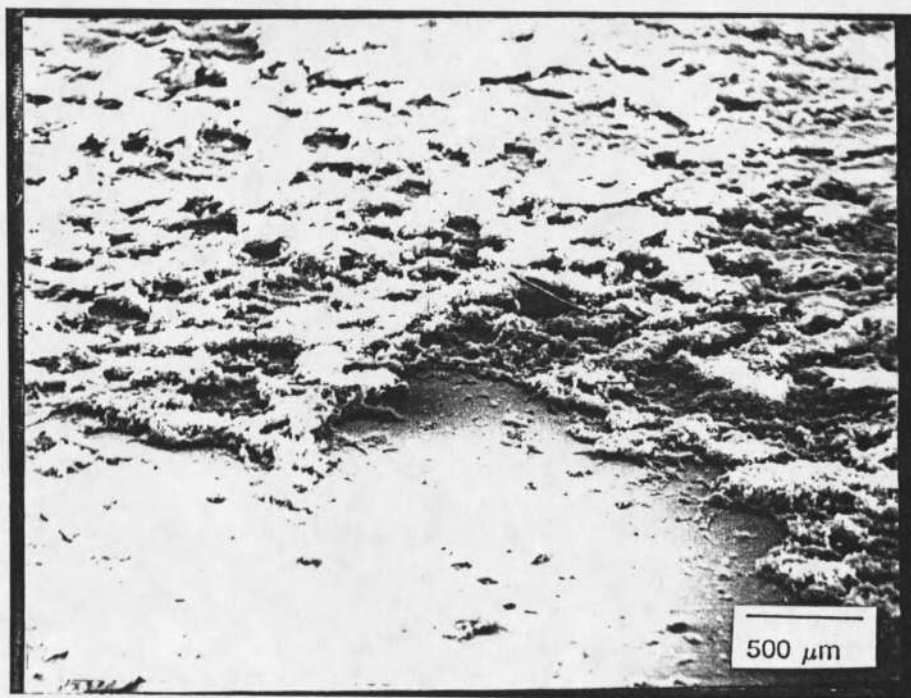


Figure 9. Scanning electron micrographs of biofilm accumulated on a mild steel surface for 3 days, x30, at high substrate loading rate.

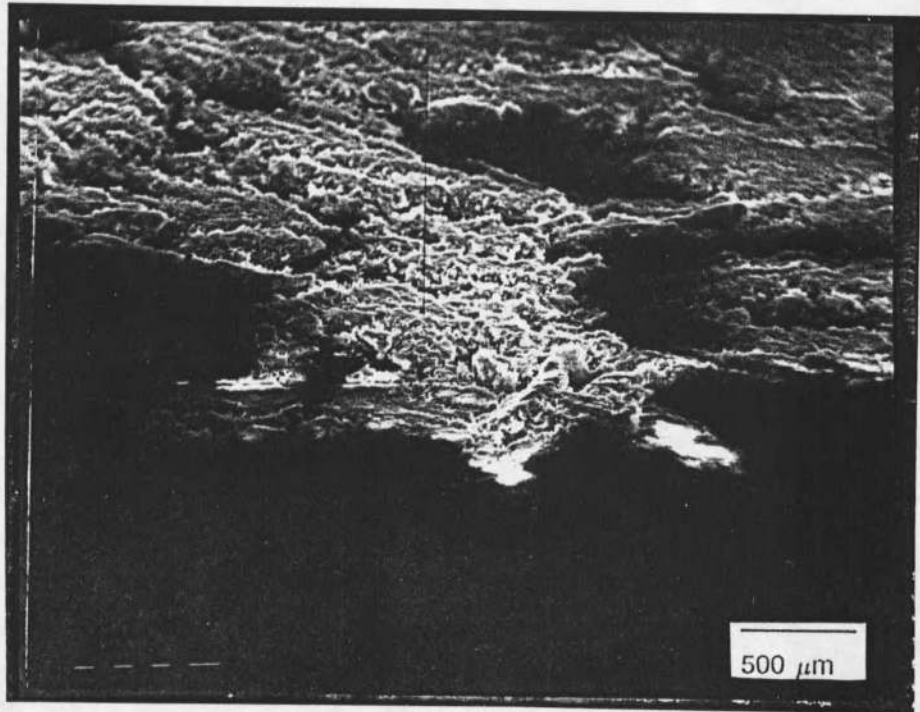


Figure 10. Scanning electron micrographs of biofilm accumulated on a mild steel surface for 7 days, x30, at high substrate loading rate.

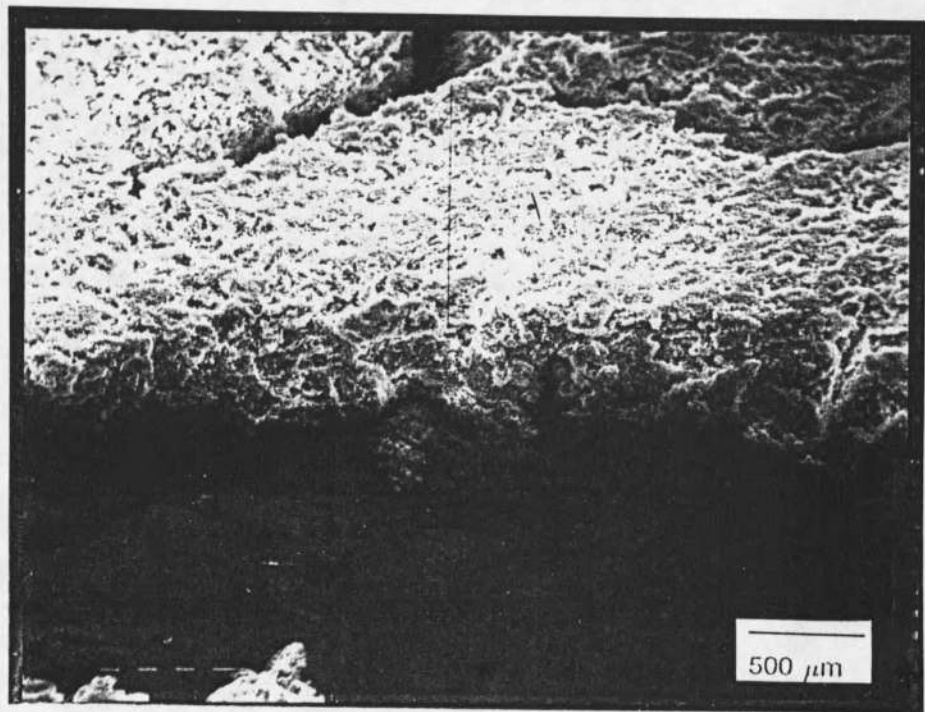


Figure 11. Scanning electron micrographs of biofilm accumulated on a mild steel surface for 21 days, x30, at high substrate loading rate.

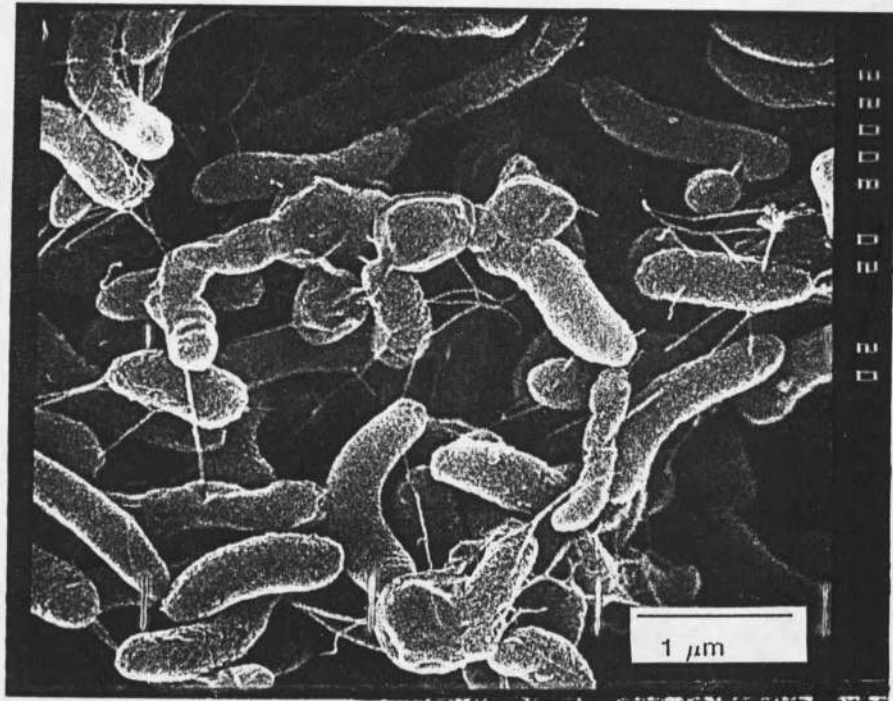


Figure 12. Scanning electron micrograph of a biofilm accumulated on a mild steel surface for 21 days at high substrate loading rate. x20,000

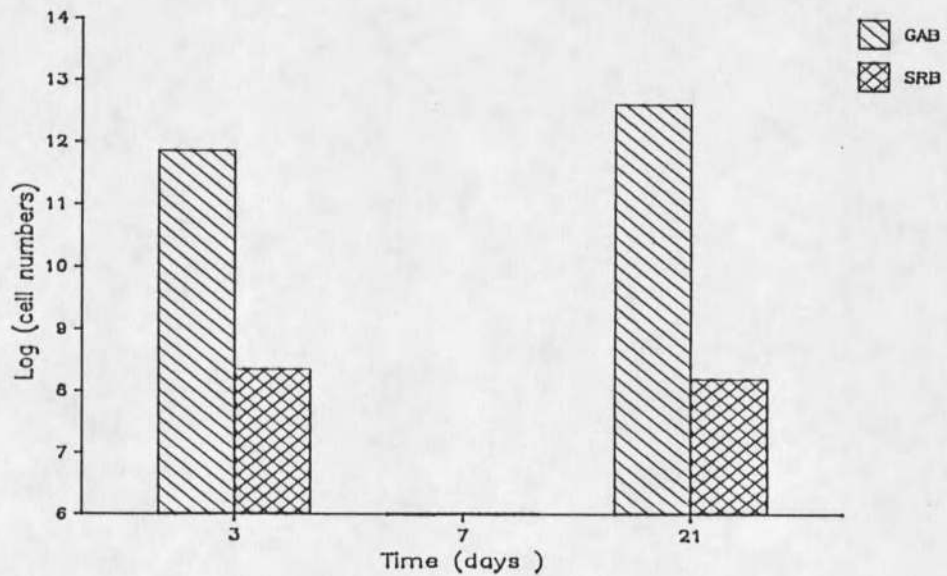


Figure 13. MPN for GAB and SRB at low substrate loading rate in the bulk water at different exposure times.

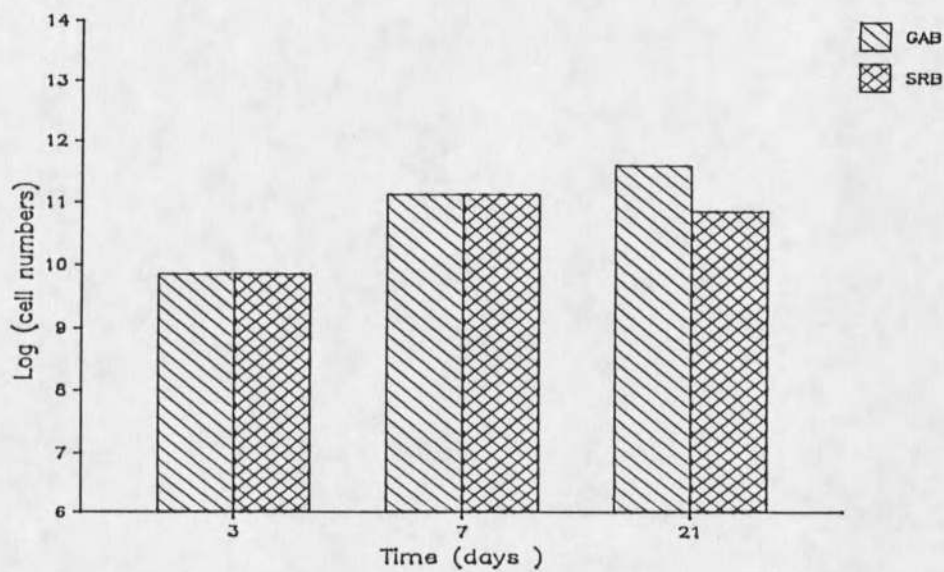


Figure 14. MPN for GAB and SRB at high substrate loading rate in the bulk water at different exposure times.

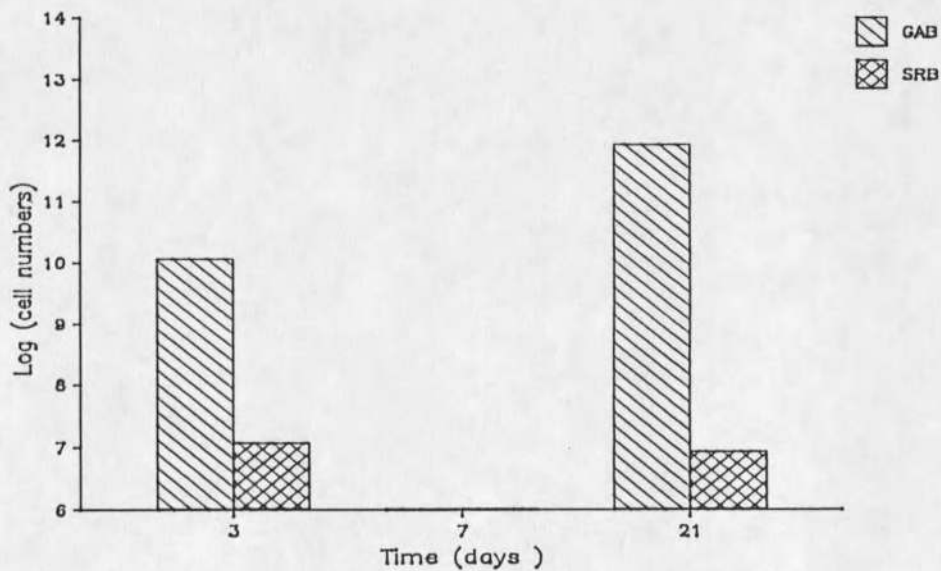


Figure 15. MPN for GAB and SRB at low substrate loading rate in the biofilm at different exposure times.

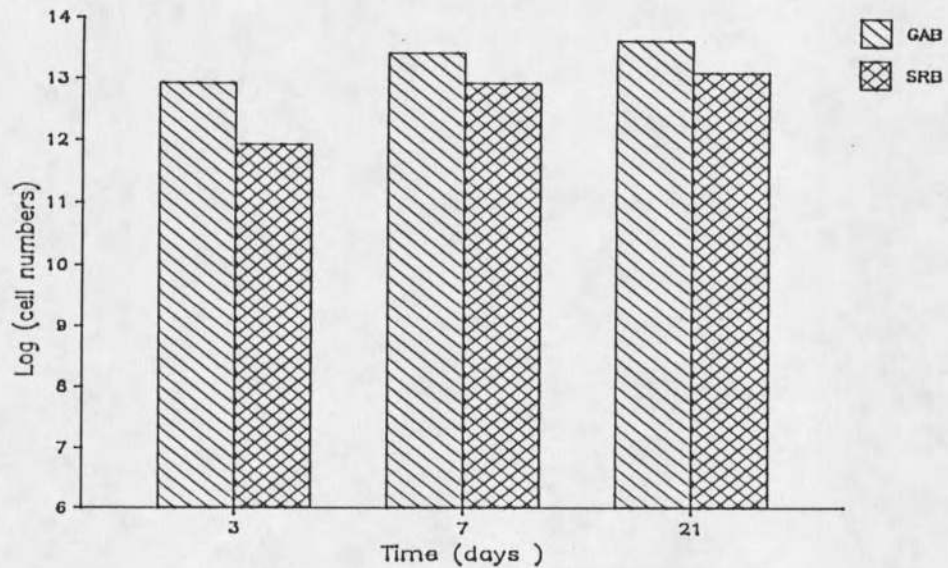


Figure 16. MPN for GAB and SRB at high substrate loading rate in the biofilm at different exposure times.

Table 6. Sulfate, lactate consumption and sulfide acetate production occurred at 25 hrs resident time with medium contained no ferrous ions.

chemicals time	sulfate consumed	lactate consumed	sulfide produced	acetate produced	redox potential
3 days	125 ppm	182 ppm	-	-	-.495V
7 days	115 ppm	202 ppm	-	-	-
21 days	120 ppm	230 ppm	58 ppm	50 ppm	-.465V

Table 7. Sulfate, lactate consumption and sulfide, acetate production occurred at 1.33 hr resident time with medium contained no ferrous ions.

chemicals time	sulfate consumed	lactate consumed	sulfide produced	acetate produced	redox potential
3 days	90 ppm	110 ppm	46 ppm	40 ppm	-.440V
7 days	120 ppm	120 ppm	46 ppm	43 ppm	-.420V
21 days	100 ppm	127 ppm	47 ppm	41 ppm	-.483V

There was no detectable difference in weight loss due to change in loading rate. The scratch lines on the coupon can be seen after 21 days under the biofilm and no iron sulfide film formed (Figure 17). An X-ray dot map (Figure 18) indicated no iron in the biofilm. No cathodic depolarization occurred either at low (Figure 19) or high (Figure 20) substrate loading rate in the absence of ferrous iron. The pitting potential becomes more noble as the biofilm become thicker both at low (40 mV, Figure 21) and high (150 mV, Figure 22) substrate loading rates. There was no pitting or localized corrosion observed on the metal surface under open circuit conditions after 21 days.

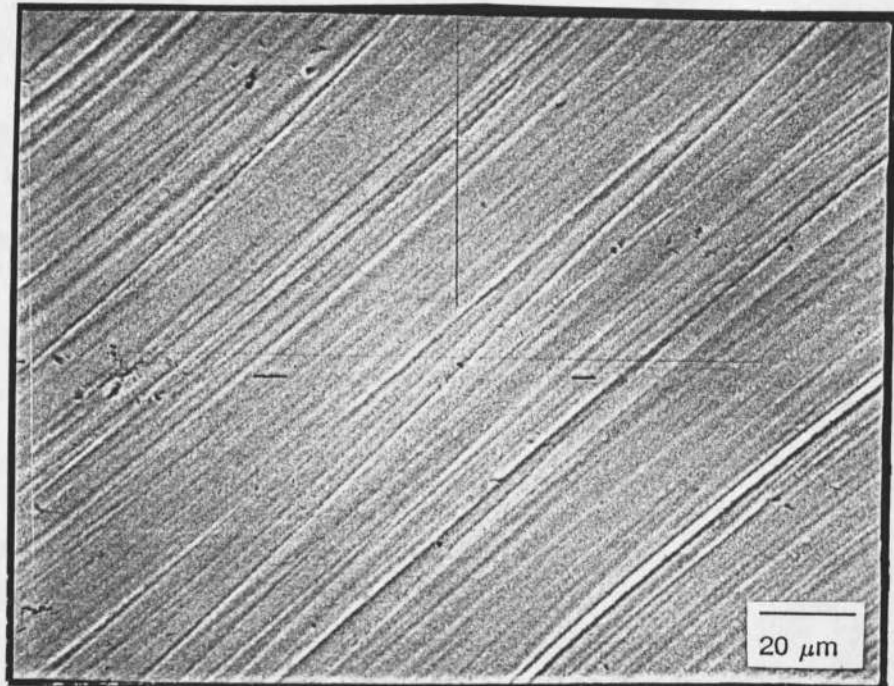
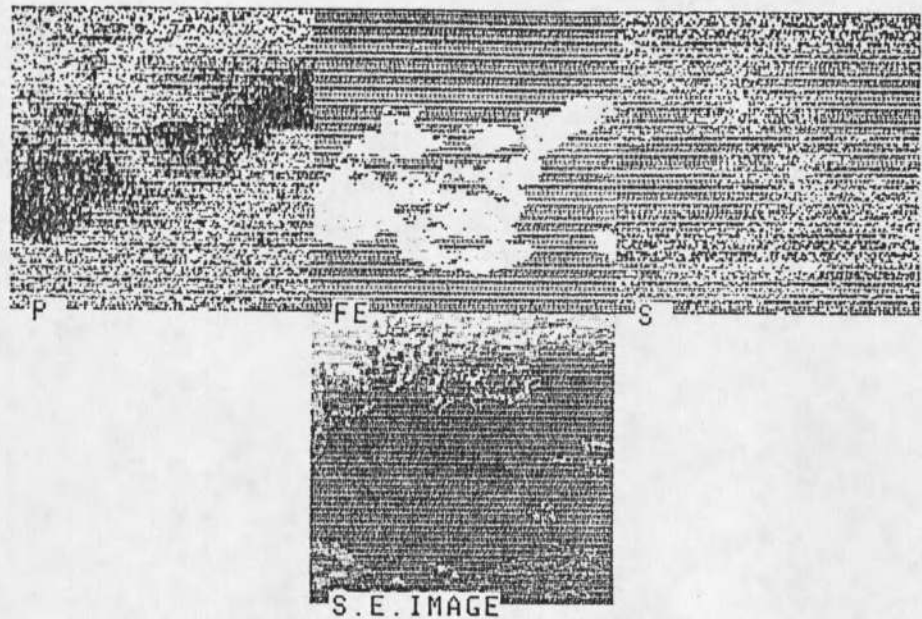


Figure 17. Scanning electron micrograph of a mild steel surface after biofilm has been removed at 21 days. x700



SPECIMEN SRB21

100X MAGNIFICATION

Figure 18. X-ray dot map indicating the elemental distribution of iron, sulfur, and phosphorous on the top of biofilm and the cross section of biofilm and metal surface.

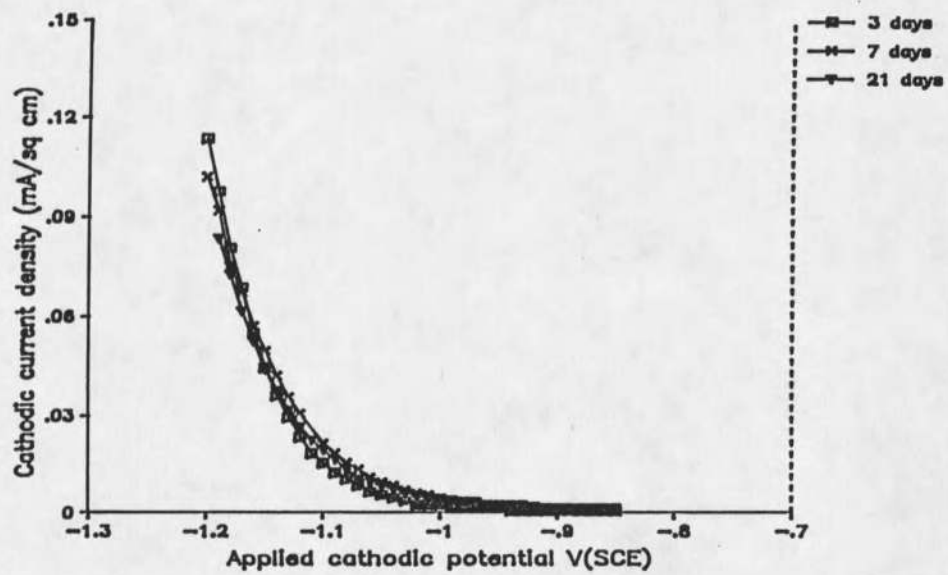


Figure 19. Cathodic depolarization curves of mild steel at low substrate loading rate at different exposure times.

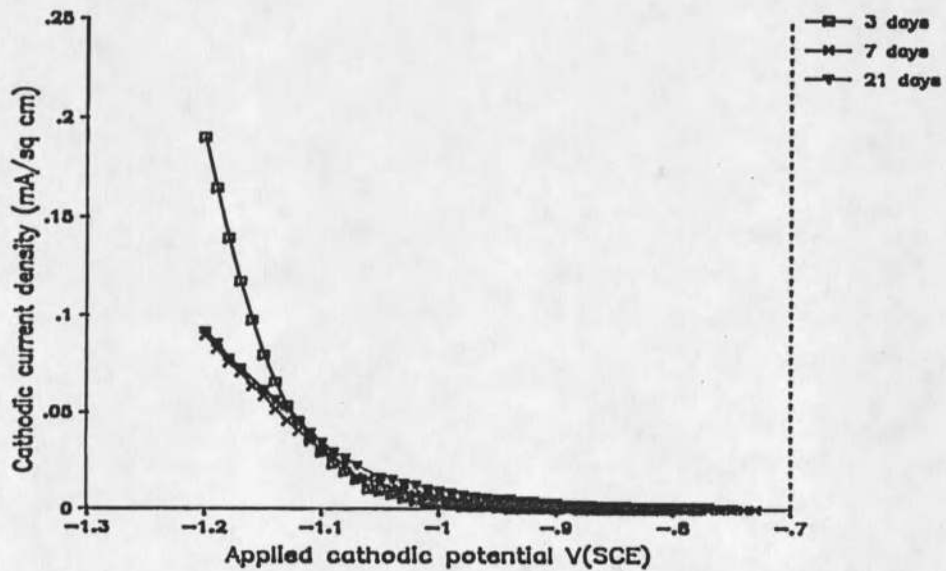


Figure 20. Cathodic polarization curves of mild steel at high substrate loading rate at different exposure times.

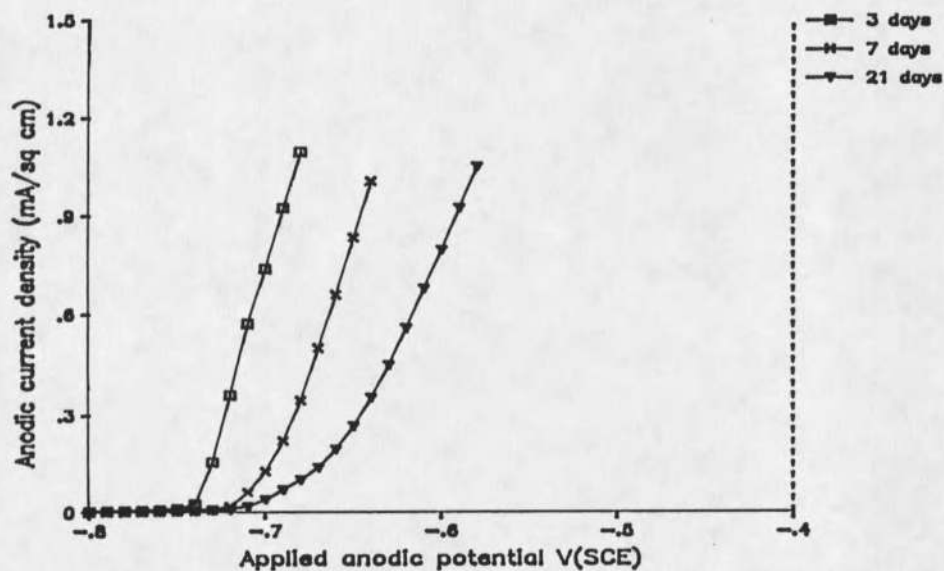


Figure 21. Anodic polarization curves of mild steel at low substrate loading rate at different exposure times. Pitting potential becomes more noble (40mv) during 21 days experiment.

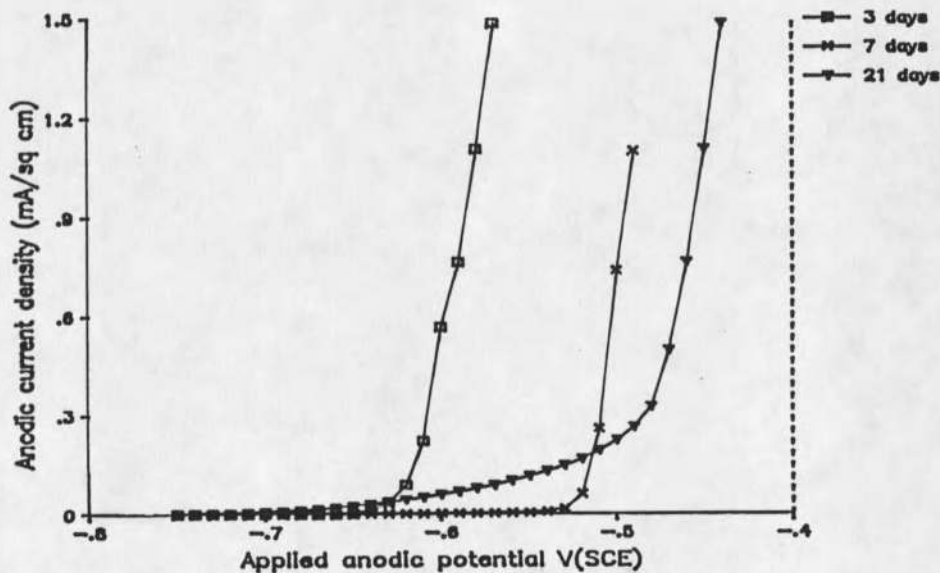


Figure 22. Anodic polarization curves of mild steel at high substrate loading rate at different exposure times. Pitting potential becomes more noble (150mv) during 21 days experiment.

Corrosion of Mild Steel with a Precoated Biofilm
at Different Ferrous Ions Concentration

The mild steel coupons were precoated with biofilm at a high substrate loading rate for one week in the absence of ferrous ions followed by weekly step increases in ferrous ion to 1, 10, and 60 mg/L.

There were higher populations of SRB and general anaerobic bacteria (GAB) in the biofilm than that in the bulk water during the experiment (Figures 23 to 24). The total dissolved sulfide concentration decreased in the bulk water as ferrous ion concentration increased in the influent and reached zero when ferrous ion concentration was 60 mg/L. There was residual lactate during the experiment (Table 8)

Table 8. Sulfate, lactate consumption and sulfide, acetate production occurred at 1.33 hr resident time with different ferrous ions concentrations.

chemicals time	sulfate consumed	lactate consumed	sulfide produced	acetate produced	redox potential
7 days	65 ppm	70 ppm	50 ppm	30 ppm	-.450V
14 days	90 ppm	98 ppm	50 ppm	35 ppm	-.450V
21 days	83 ppm	71 ppm	40 ppm*	25 ppm	-.440V
28 days	85 ppm	84 ppm	0 ppm*	-	-

* Sulfide ions in the bulk water were precipitated with ferrous ions and cannot be detected accurately.

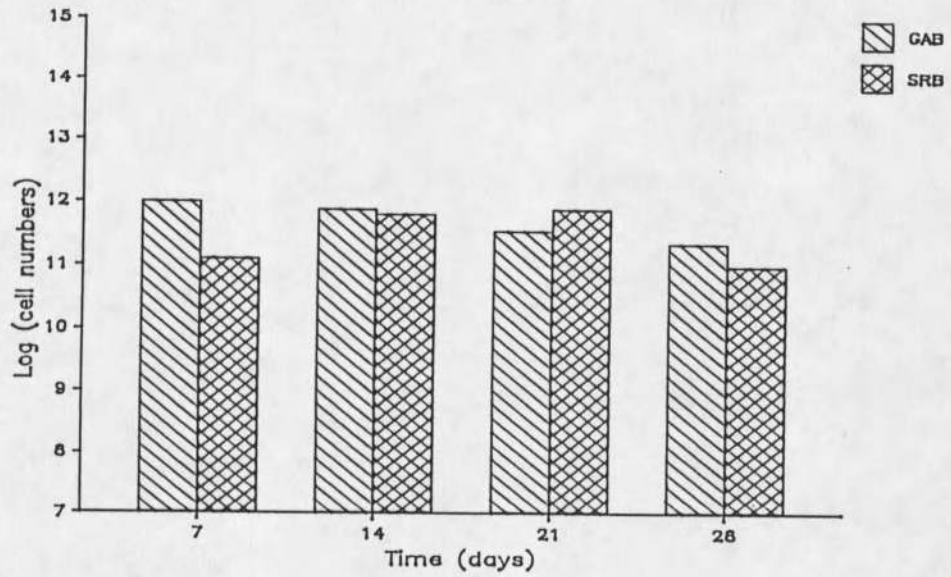


Figure 23. Most probable number (MPN) for GAB and SRB in the bulk water at different ferrous ion concentrations.

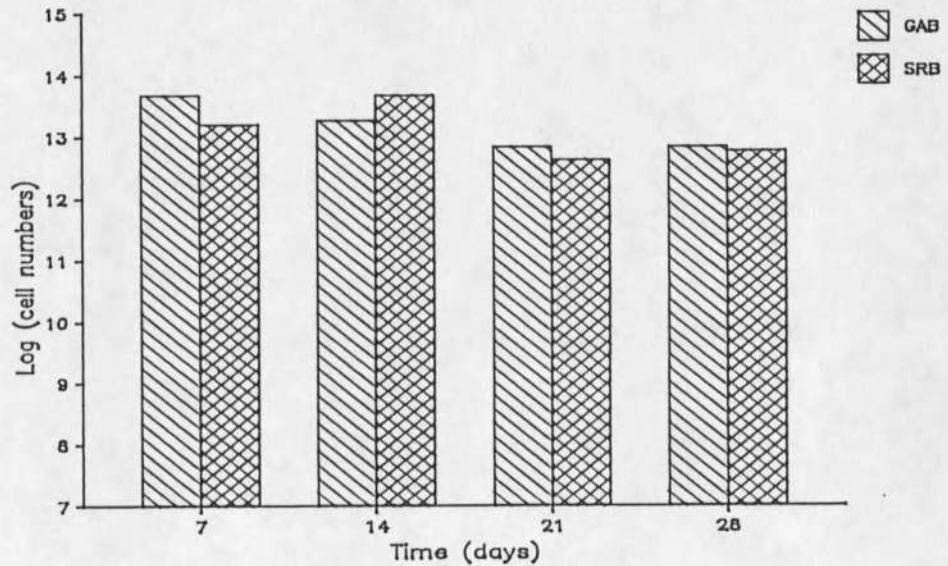


Figure 24. Most probable number (MPN) for GAB and SRB in the biofilm at different ferrous ion concentrations.

The accumulation of iron sulfide in the biofilm at different ferrous ion concentrations is illustrated in Figures 25 to 27. Very little corrosion occurred at zero or low ferrous ion concentration (0, 1 and 10 mg/L). Some iron sulfide particles accumulated in the biofilm but no direct contact occurred between iron sulfide particles and the mild steel surface. However, iron-rich media (60 mg/L which is enough to precipitate all the biogenic sulfide) caused large amounts of precipitation of iron sulfide (Figure 28). An X-ray dot map showed the iron sulfide particles penetrate through the biofilm and contact the metal surface (Figure 29). Cathodic (Figure 30) and anodic (Figure 31) currents increased dramatically as ferrous ions increased from 10 to 60 mg/L. Nyquist plots indicated that corrosion rate was much higher at 60 mg/L Fe^{+2} than at 10 Fe^{+2} . The charge transfer resistance (R_{ct} , the diameter of the semicircle, which is inversely proportional to the corrosion rate) decreased dramatically as ferrous iron concentration increased from 10 mg/L Fe^{+2} to 60 mg/L Fe^{+2} (Figure 32). There was no coherent sulfide film formed under the biofilm in the iron rich media. Uniformly intergranular attack was observed over the entire metal surface after precipitated iron sulfide and biofilm was removed (Figure 33).

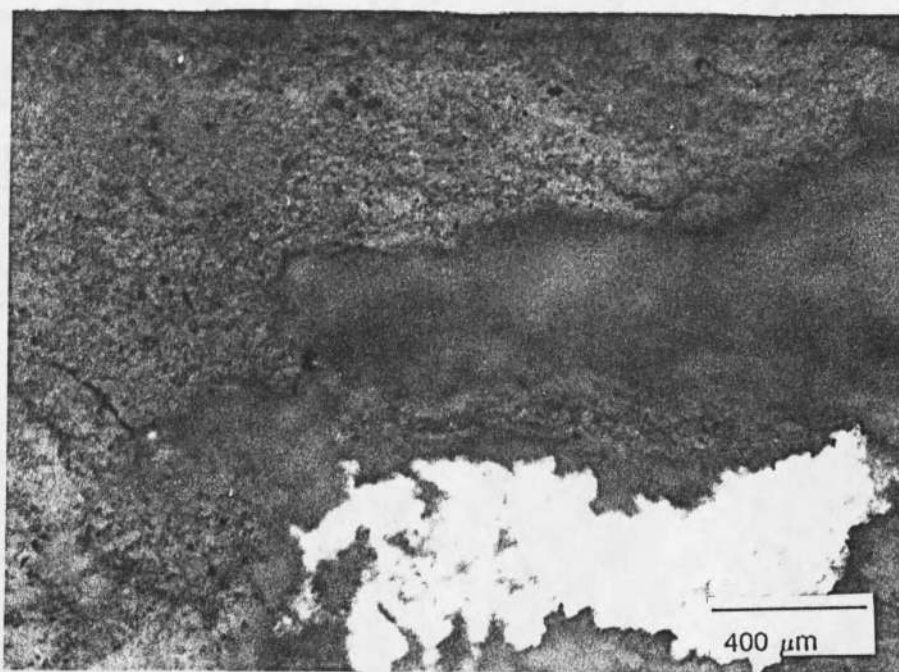


Figure 25. Accumulation of iron sulfide on a precoated biofilm at 1 mg/L ferrous ion concentration. x50

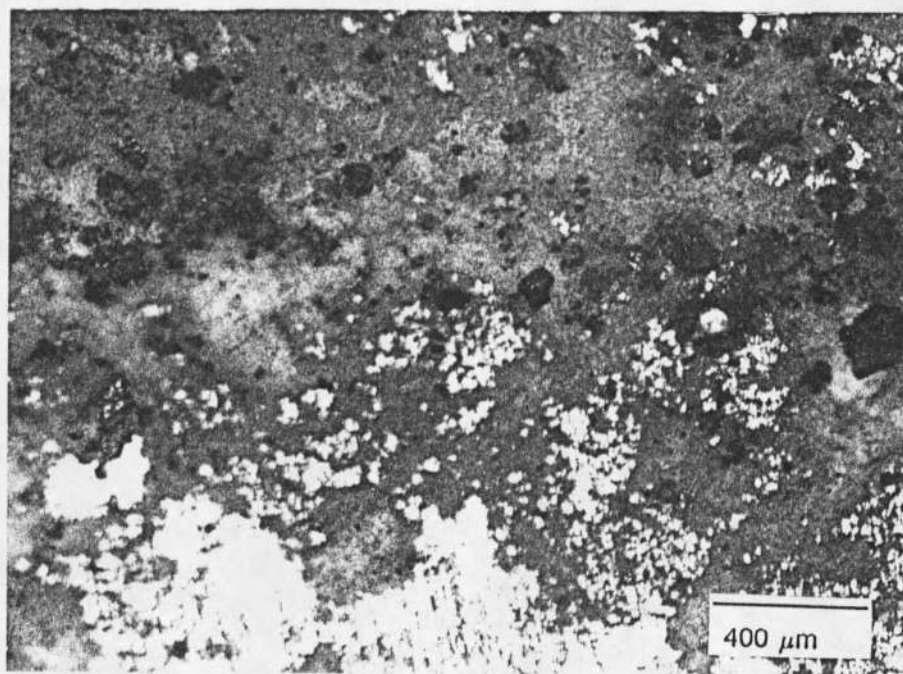


Figure 26. Accumulation of iron sulfide on a precoated biofilm at 10 mg/L ferrous ion concentrations. x50

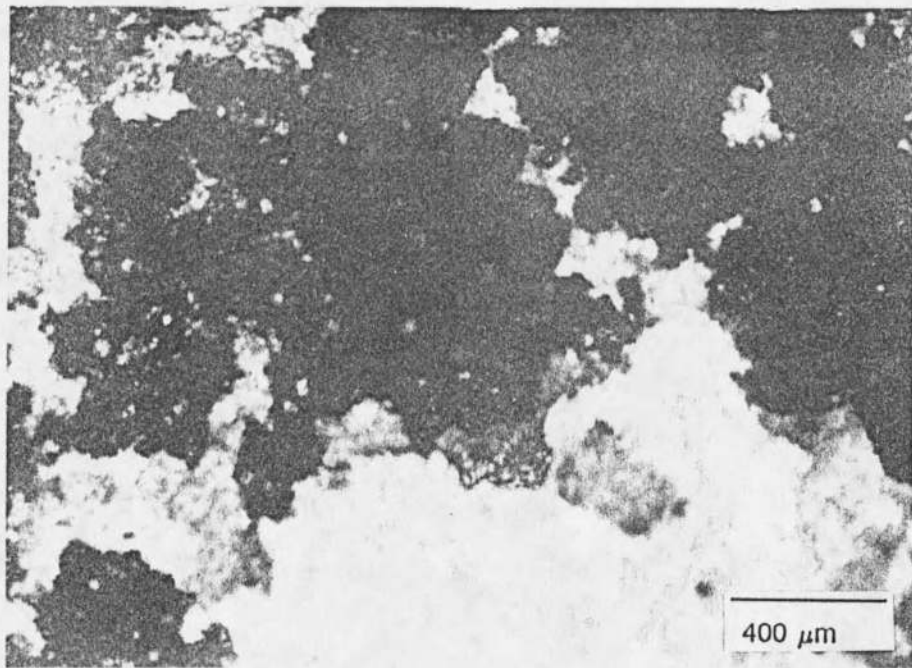


Figure 27. Accumulation of iron sulfide on a precoated biofilm at 60 mg/L ferrous ion concentrations. x50

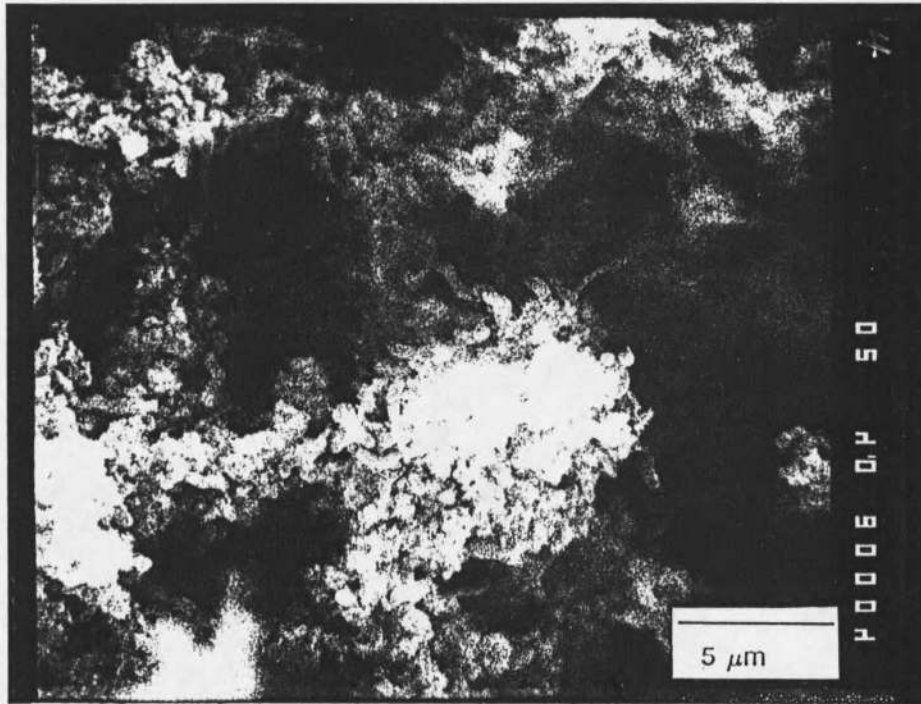
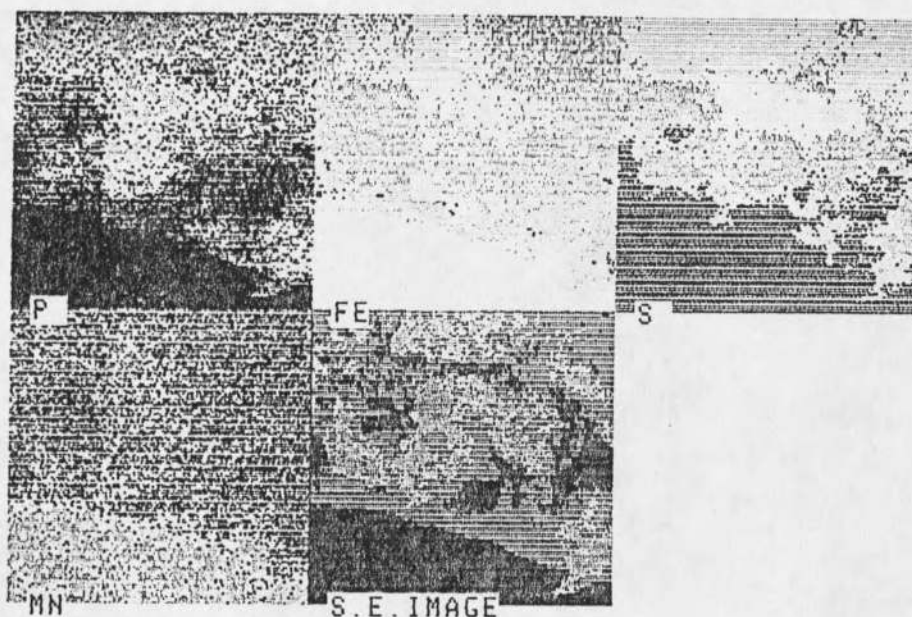


Figure 28. Scanning electron micrograph of biofilm when the media contain 60 mg/L ferrous ion concentration. x4,000



SPECIMEN SRB B10 MAGNIFICATION 100X

Figure 29. X-ray dot map indicating the elemental distribution of iron, sulfur, and phosphorus on the top of biofilm and metal substratum.

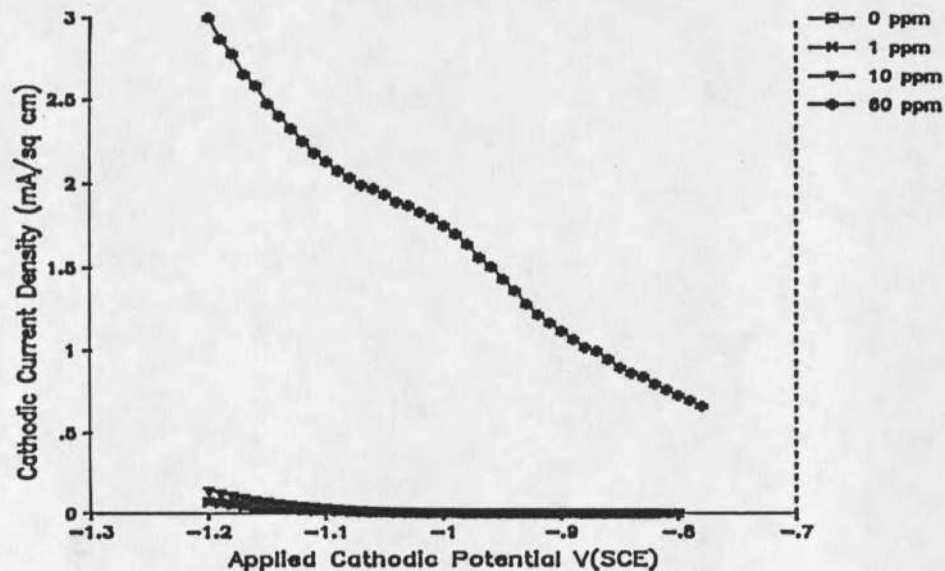


Figure 30. Cathodic polarization curves of mild steel on a pre-coated biofilm followed by step increase in ferrous ion concentrations.

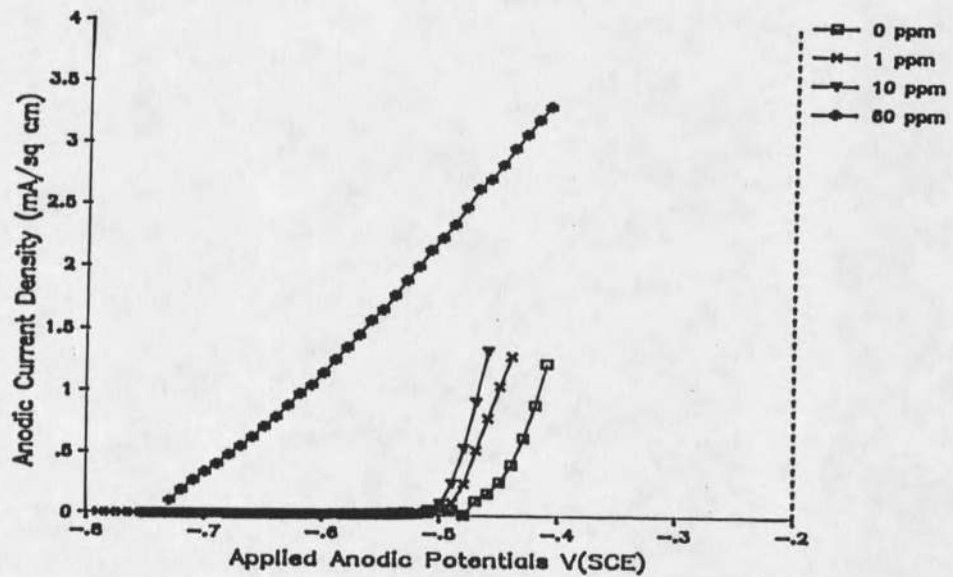


Figure 31. Anodic polarization curves of mild steel on a precoated biofilm followed by step increase in ferrous ion concentrations.

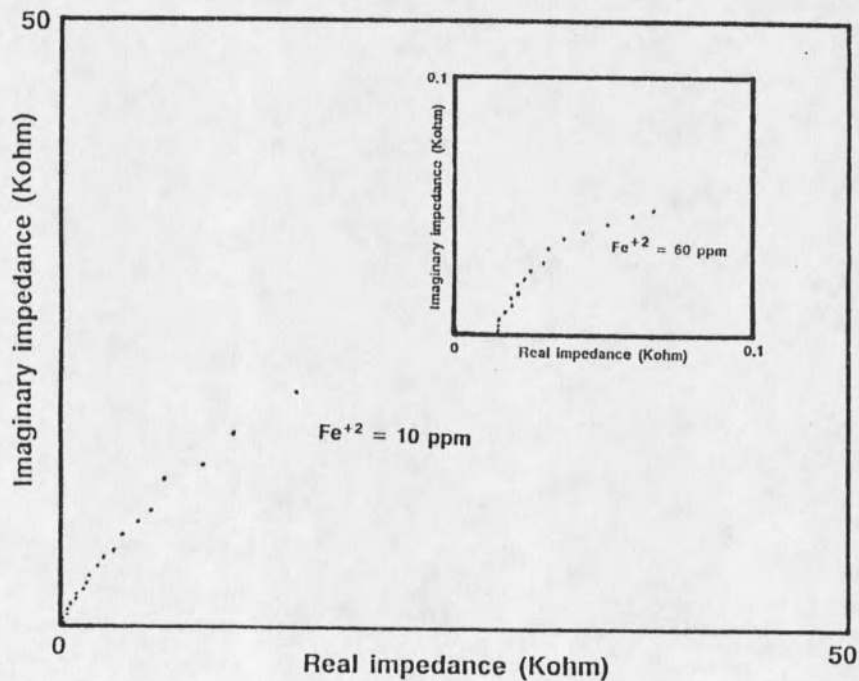


Figure 32. Nyquist plots for mild steel on a precoated biofilm at different ferrous ion concentrations.

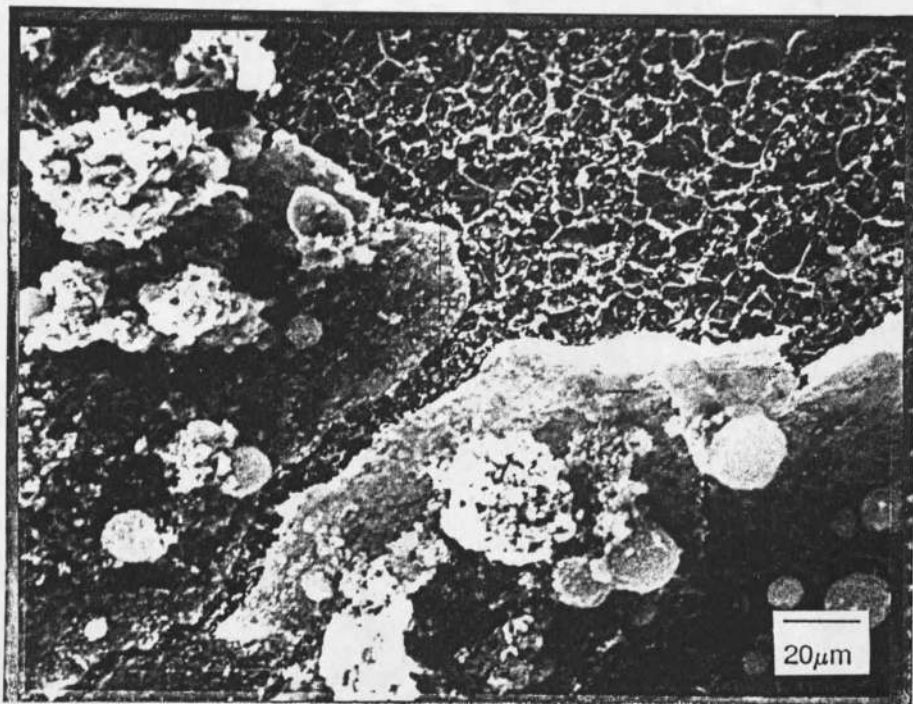


Figure 33. Scanning electron micrograph of a mild steel surface indicating the non-protective iron sulfide film and intergranular attack over the entire metal surface. x550

Corrosion of Mild Steel on a Precoated Iron Sulfide Film Followed by Biofilm Accumulation

The steel surface was precoated with a layer of iron sulfide film followed by biofilm accumulation at the high substrate loading rate. The precoating procedure consisted of flushing the mild steel coupons with 30 mg/L sulfide solution ($\text{Na}_2\text{S}\cdot 9\text{H}_2\text{O}$) under anaerobic conditions at $\text{pH} = 8$ for one day.

Biological analysis showed there were higher populations of SRB and general anaerobic bacteria (GAB) in the biofilm than that in the bulk water (Figures 34 to 35). Chemical analysis showed the total dissolved sulfide concentration in bulk water was between 30 and 40 mg/L after 21 days (Table 9).

Table 9. Sulfate, lactate consumption and sulfide, acetate production occurred at 1.33 hr resident time with medium contained no ferrous ion but metal coupon was precoated with iron sulfide film.

chemicals time	sulfate consumed	lactate consumed	sulfide produced	acetate produced	redox potential
3 days	65 ppm	78 ppm	30 ppm	-	-.440V
7 days	80 ppm	83 ppm	30 ppm	-	-.440V
21 days	90 ppm	83 ppm	40 ppm	25 ppm	-.450V

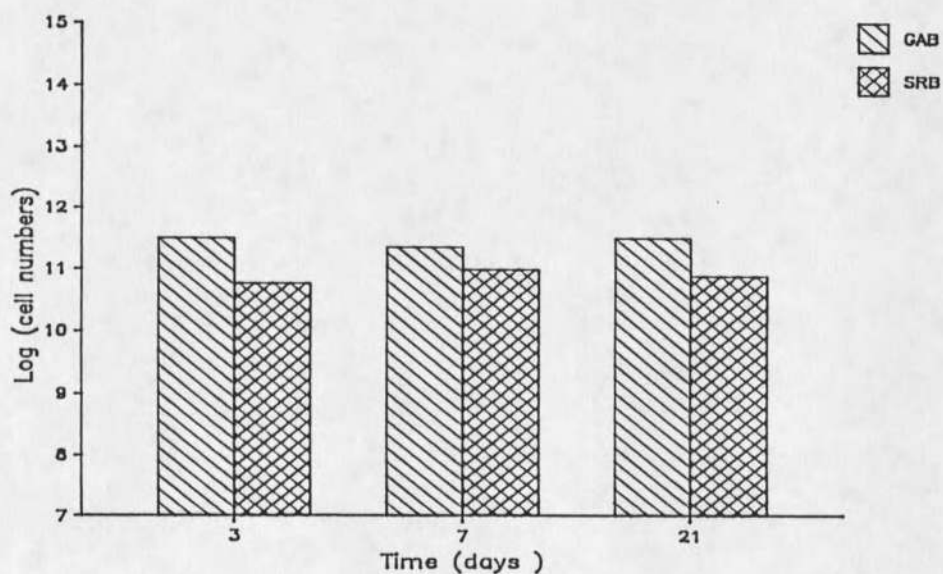


Figure 34. Most probable number (MPN) for GAB and SRB in the bulk water at different exposure time.

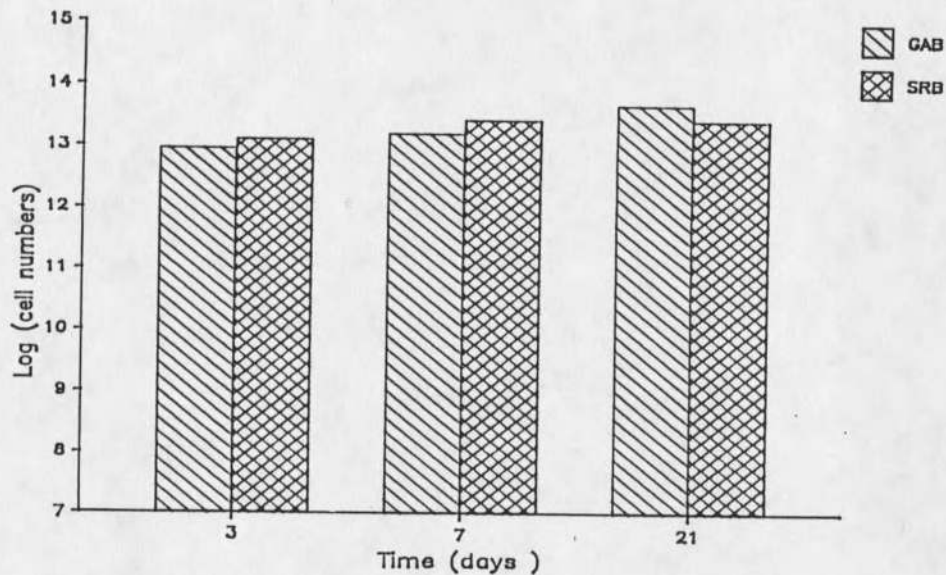


Figure 35. Most probable number (MPN) for GAB and SRB in the biofilm at different exposure time.

Localized corrosion was observed when biofilm developed on a precoated coupon. The progression of localized corrosion under open circuit conditions is presented in Figures 36 to 39. Microscopic examination indicated inclusions and micropits in the metal after iron sulfide film was removed at 3 days (Figure 40). More micropits were found at 7 days (Figure 41). Visible localized corrosion appeared after 14 days and increased rapidly through 21 days. A series of scanning electron micrographs illustrate the whole structure from the metal to the biofilm after 21 days. The localized corrosion area contained spherical deposits (Figure 42). The iron sulfide film cracked and detached just above the localized corrosion area (Figure 43). Intergranular and pitting attack

were found in the grain boundary triple points, and inclusions (Al, Mn, and Fe) were usually found in this area (Figure 44). The spherical deposits consisted of iron sulfide crystals and bacteria (Figure 45). The cross section of iron sulfide film and biofilm was illustrated in Figure 46. The metal surface retained its polish scratch marks underneath the coherent iron sulfide film at the end of experiment. Pitting potential shifted to more active value (150 mV) as experiment proceeded (Figure 47), which was consistent with the macroscopic picture after biofilm and iron sulfide were removed. Cathodic polarization measurements (Figure 48) indicated that the electrode was slightly polarized as the experiment proceeded suggesting that most of the metal surface remained passive except in the localized corrosion area. There was no suspended iron sulfide in the bulk water after 21 days.

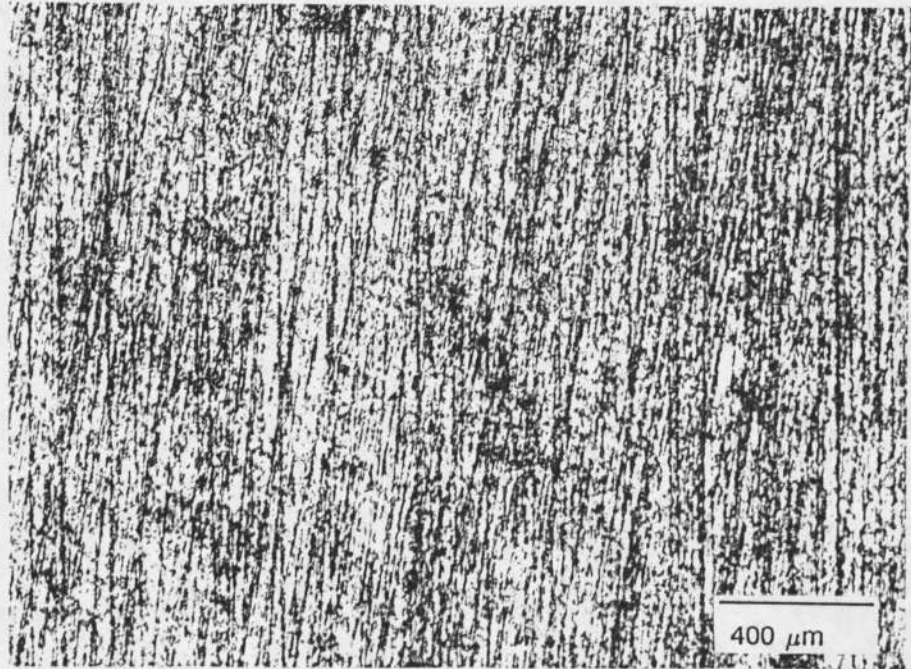


Figure 36. Macroscopic photographs of the mild steel coupons after biofilm and iron sulfide film have been removed at 3 days. x50

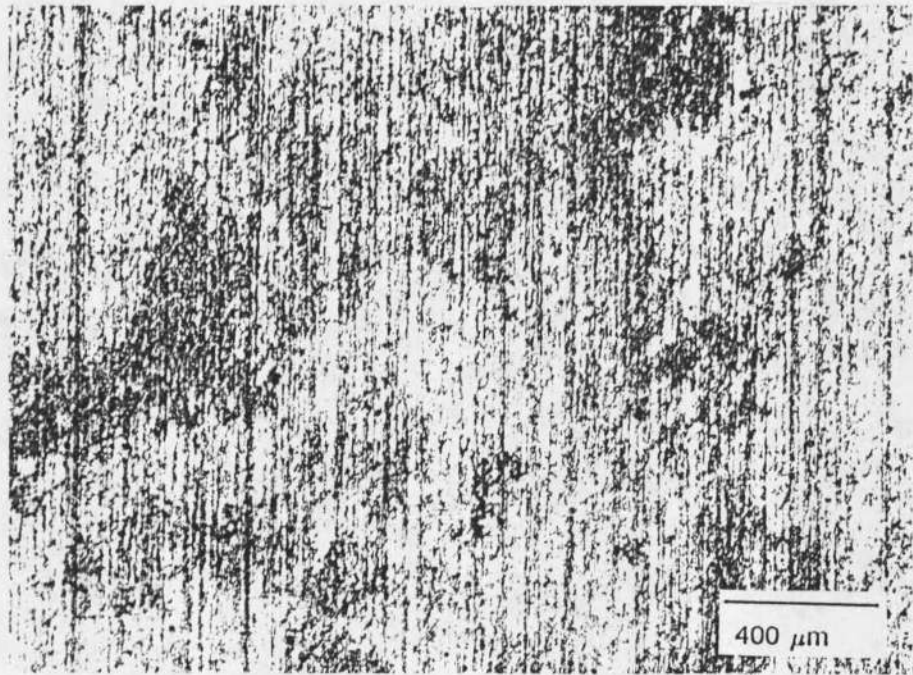


Figure 37. Macroscopic photographs of the mild steel coupons after biofilm and iron sulfide film have been removed at 7 days. x50

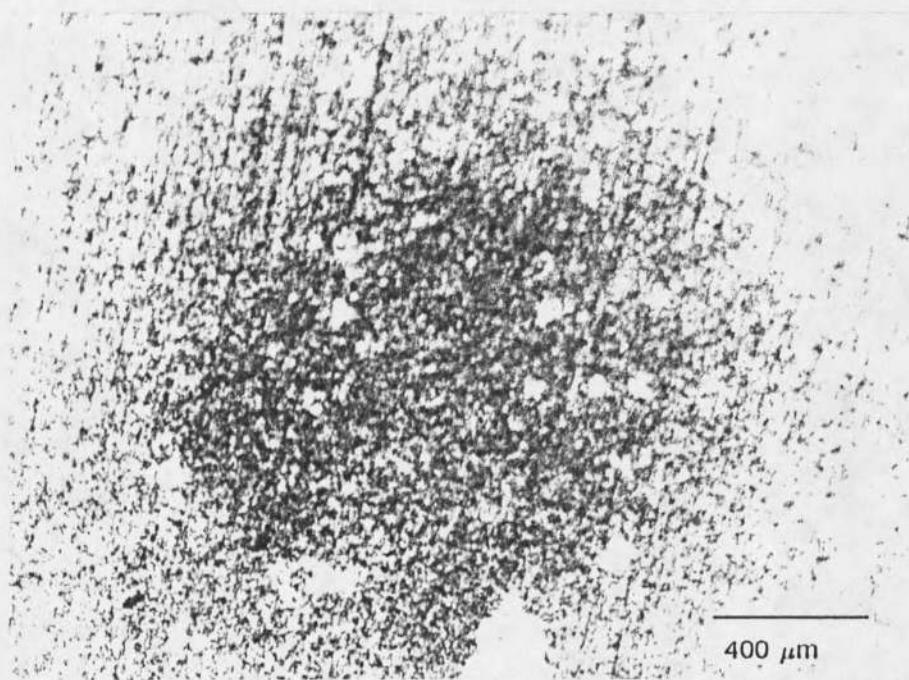


Figure 38. Macroscopic photographs of the mild steel coupons after biofilm and iron sulfide film have been removed at 14 days. x50

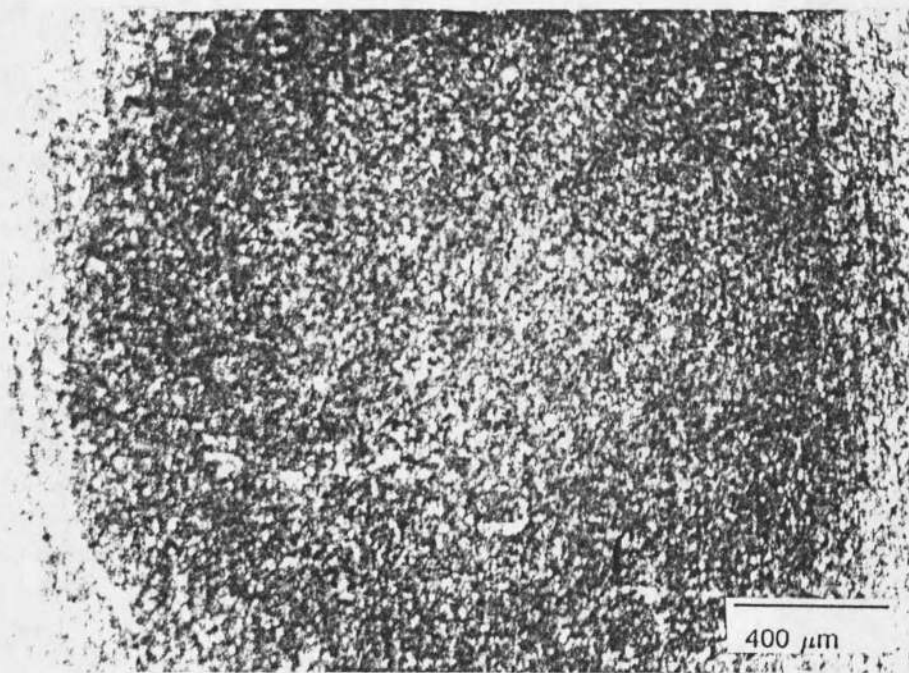


Figure 39. Macroscopic photographs of the mild steel coupons after biofilm and iron sulfide film have been removed at 21 days. x50

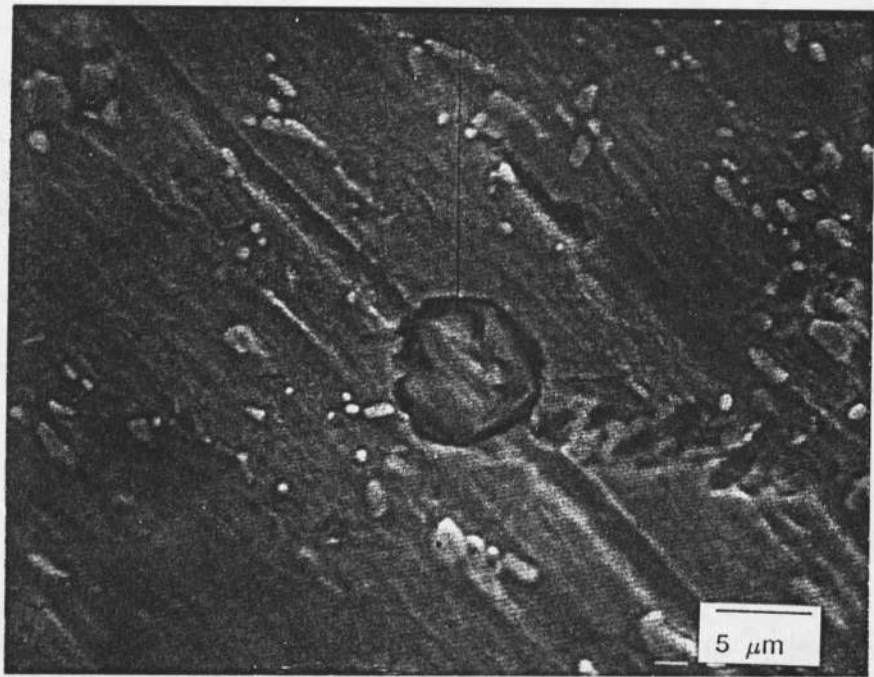


Figure 40. Scanning electron micrograph of a mild steel surface after biofilm and iron sulfide film have been removed at 3 days. x2,800

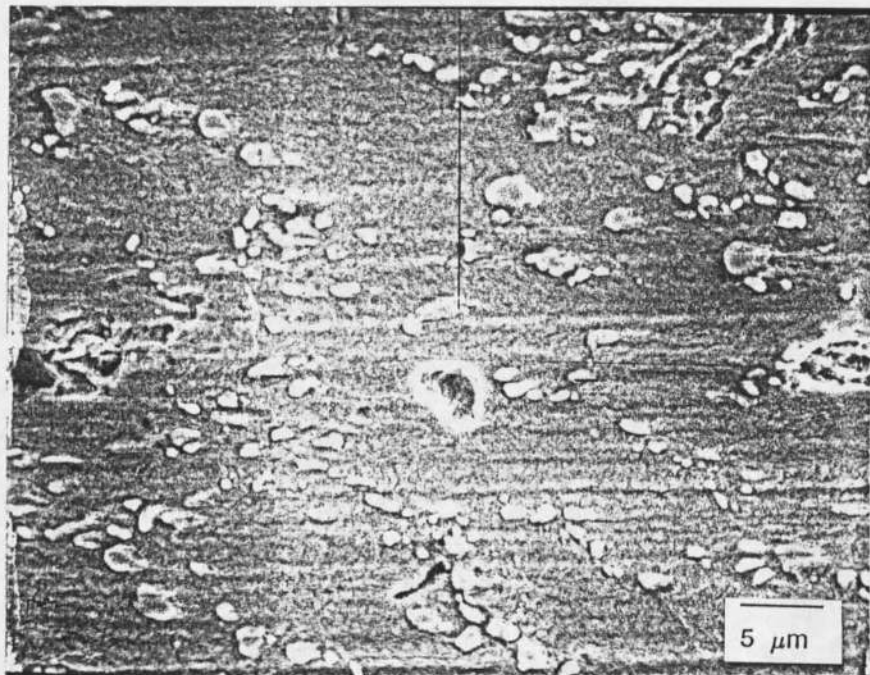


Figure 41. Scanning electron micrograph of a mild steel surface after biofilm and iron sulfide film have been removed at 7 days. x2,300

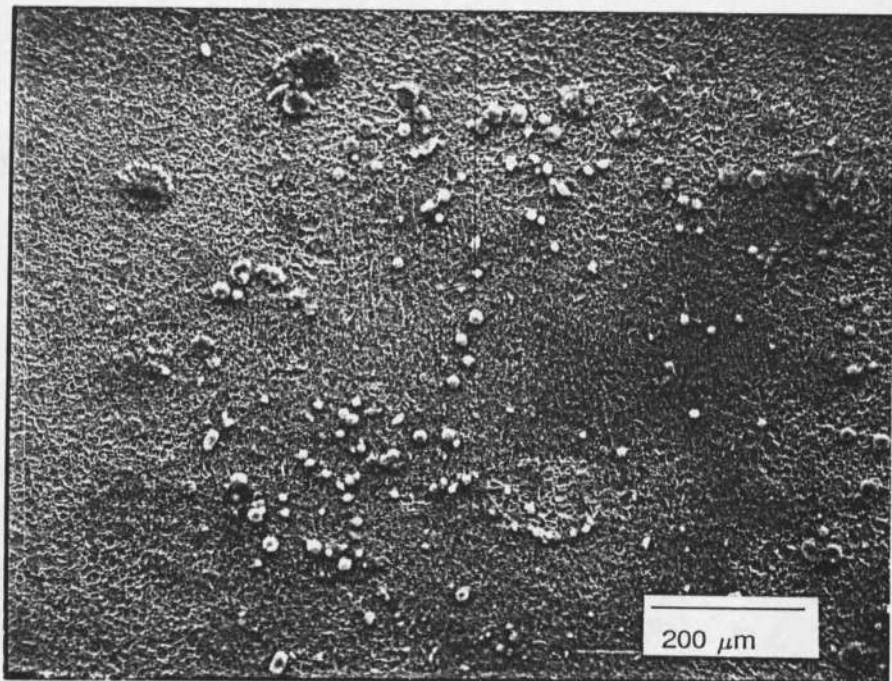


Figure 42. Scanning electron micrograph of a mild steel surface in the localized corrosion area where spherical deposits were found at 21 days. x 100

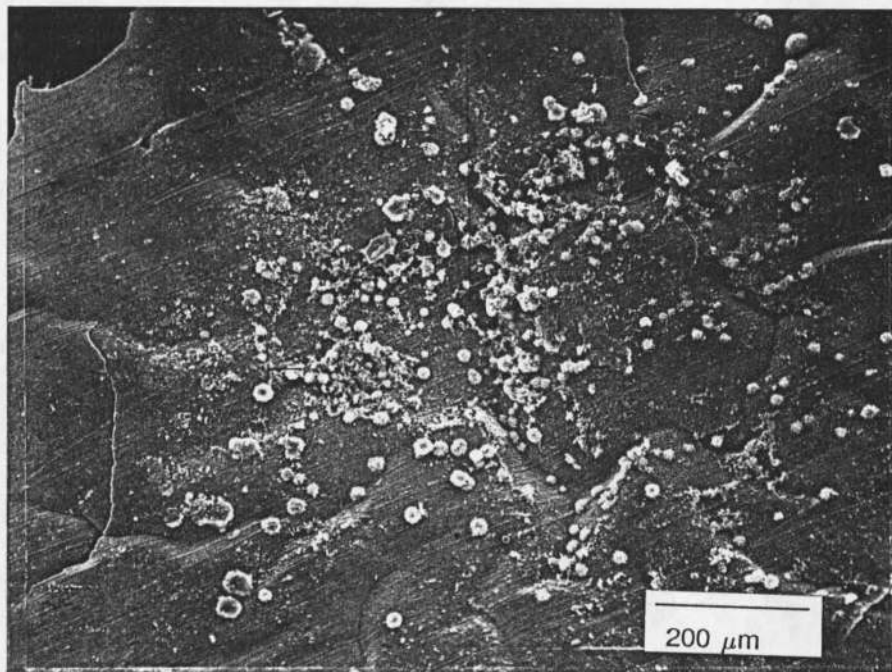


Figure 43. Scanning electron micrograph of a detached iron sulfide film just above the localized corrosion area where spherical deposits also found. x100

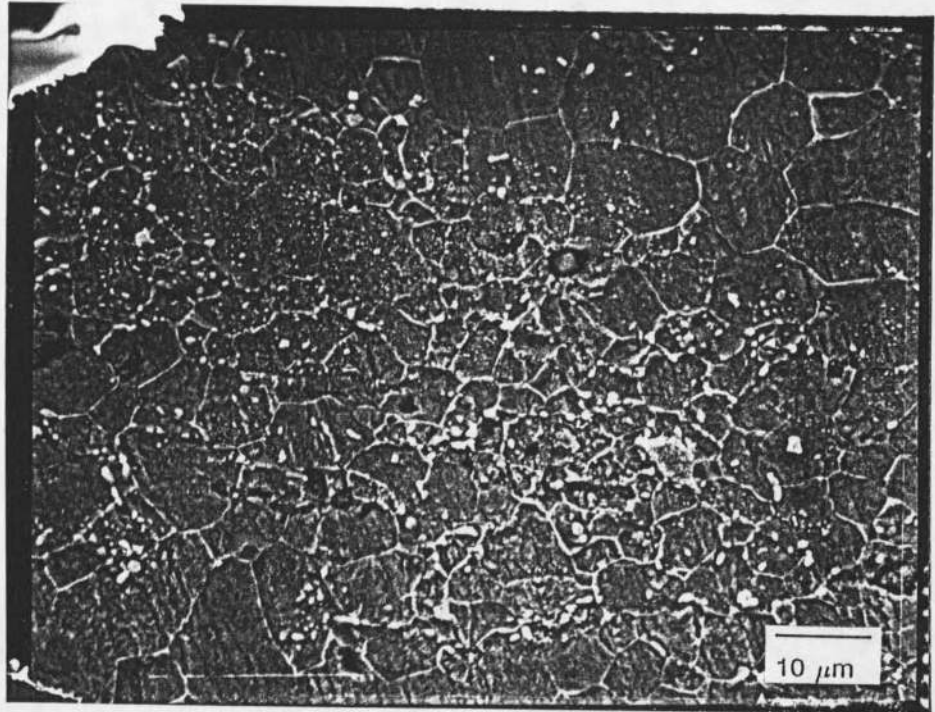


Figure 44. Intergranular and pitting attack were found in the localized corrosion area at higher magnification. The grain boundary triple point also found in that area. x1,200

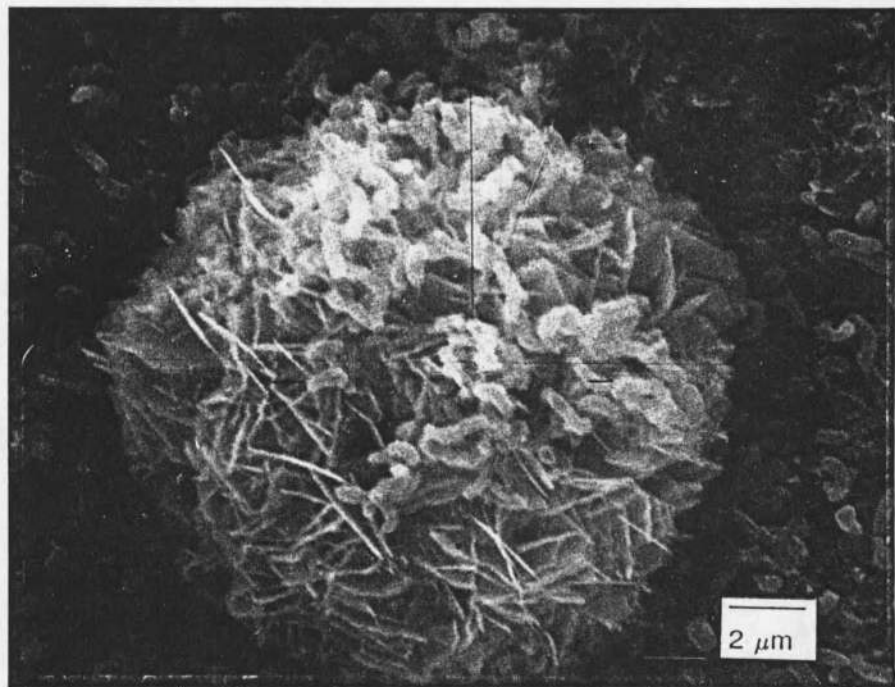


Figure 45. The circular deposition were iron sulfide crystal and bacteria. x 5,300

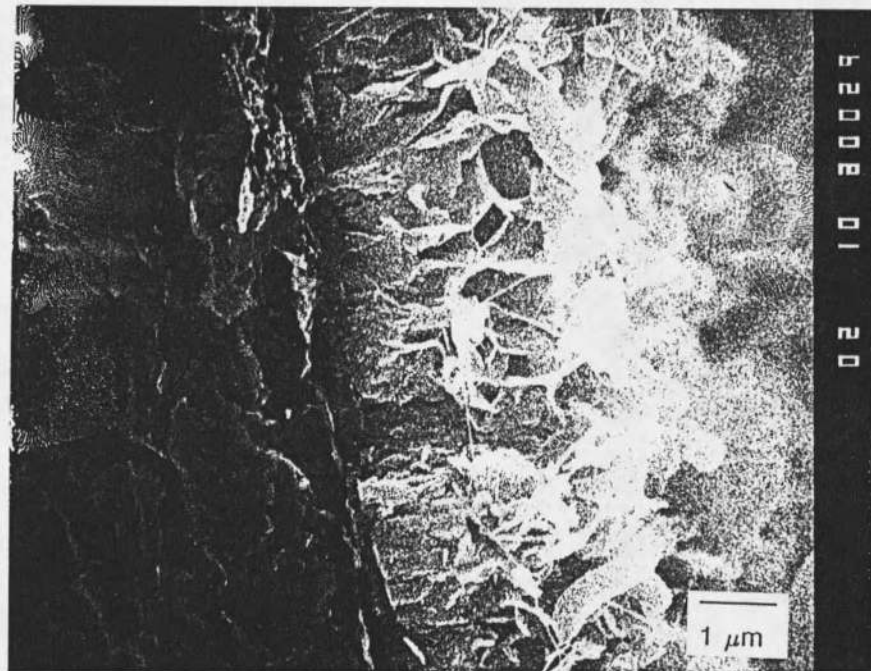


Figure 46. Scanning electron micrograph of a cross section of iron sulfide film and biofilm. $\times 10,000$

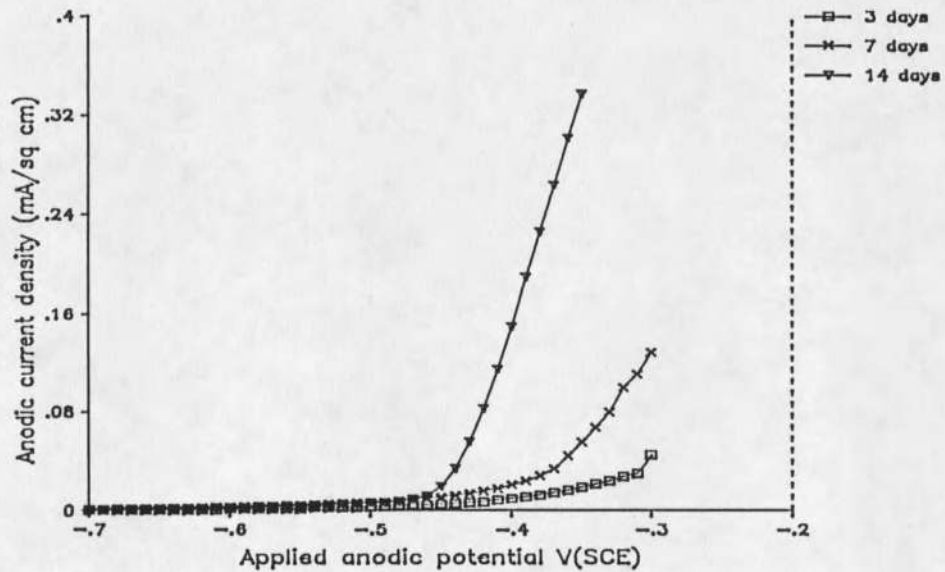


Figure 47. Anodic polarization curves of mild steel on a precoated iron sulfide film followed by biofilm accumulation at different exposed times.

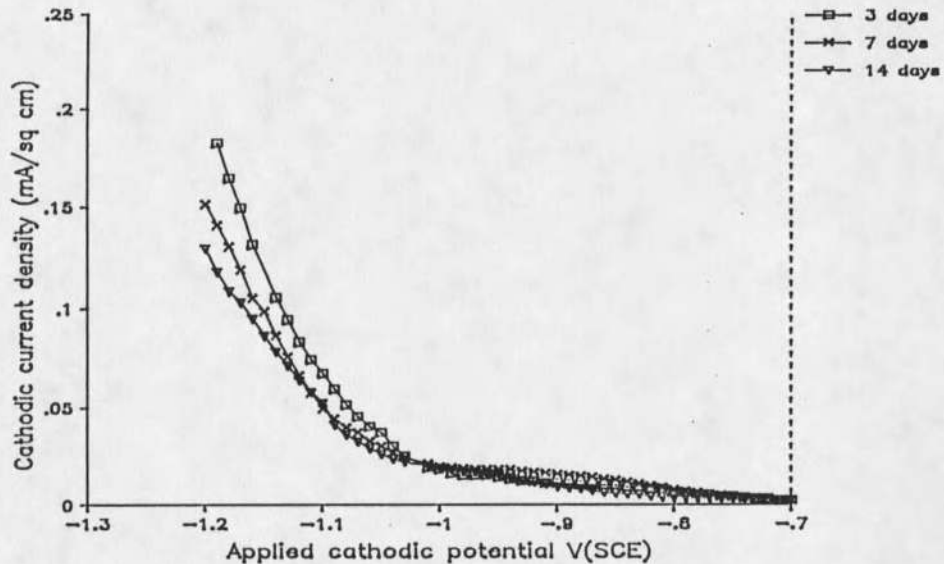


Figure 48. Cathodic polarization curves of mild steel on a pre-coated iron sulfide film followed by biofilm accumulation at different exposed times.

Anaerobic Corrosion under Abiotic Conditions

The sulfide concentration in the bulk liquid was maintained at 30 mg/L by continuous input of an abiotic sulfide solution which resulted in a similar redox potential to that under biotic conditions. pH was controlled at 8 as in the biotic experiments.

Weight loss measurements indicate significant corrosion during the 21 day experimental period (Figure 49). For the first 7 days, there was a linear increase in weight loss. After 7 days, the rate of corrosion decreased. Open circuit corrosion potential become more noble after four days (100 mV, Figure 50), but remain in the similar range till twenty-one

days, which indicates the precipitation of iron sulfide on the metal surface. A marked increase was noticed in the cathodic current (Figure 51) but no difference in the pitting potential (Figure 52).

Microscopic examination of the surface at 3 days indicates a coherent, featureless base layer with defects at some points (Figure 53). The "scratch" lines are still observed on the metal surface after the iron sulfide film was removed and inclusions were found (Figure 54). The entire surface area was covered with a loosely held precipitates after 7 days (Figure 55) and intergranular attack was evident over the entire surface (Figure 56). The amount of loosely held precipitated material reach a maximum at 21 days (Figure 57). Uniform intergranular attack was still evident after the iron sulfide film was removed (Figure 58). The bulk water was turbid and dark at the end of experiment indicating the detachment of iron sulfide from the metal surface.

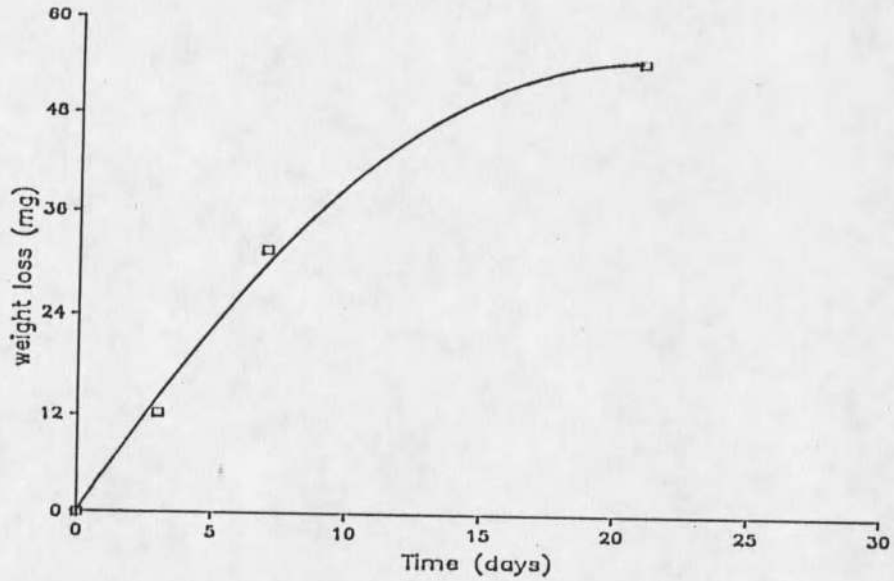


Figure 49. Weight loss vs. time curve in the abiotic conditions.

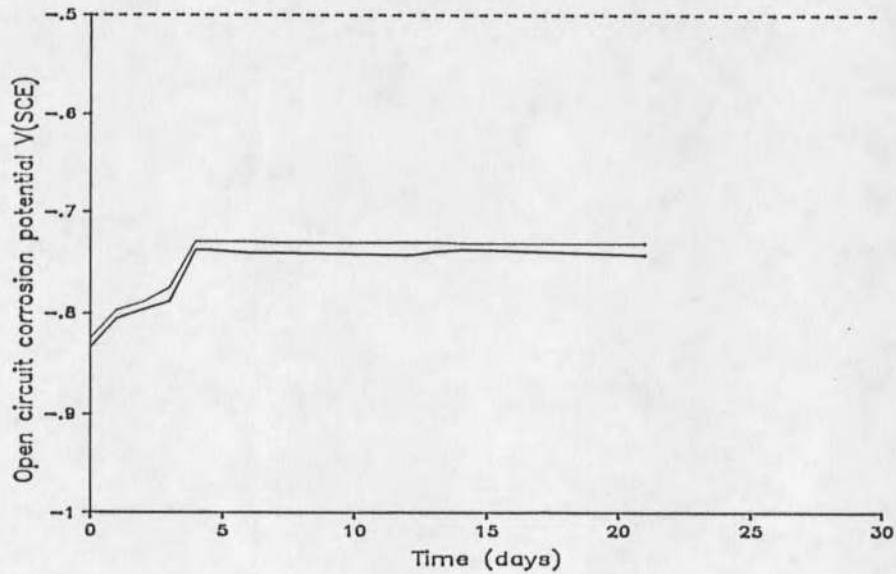


Figure 50. Open circuit corrosion potential vs. time curves in abiotic experimental conditions. Two curves indicate the scattering of twenty-four coupons.

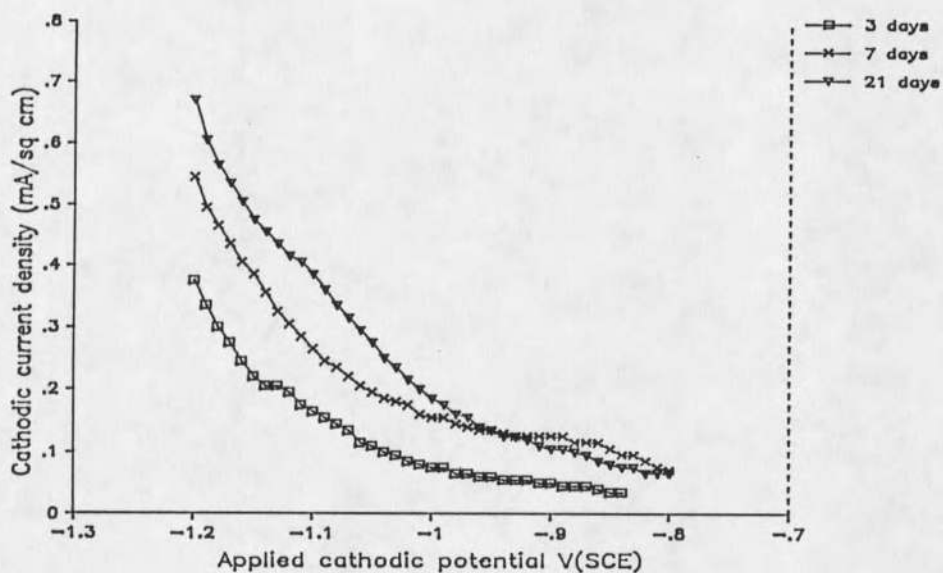


Figure 51. Cathodic polarization curves in the abiotic conditions at different exposed times.

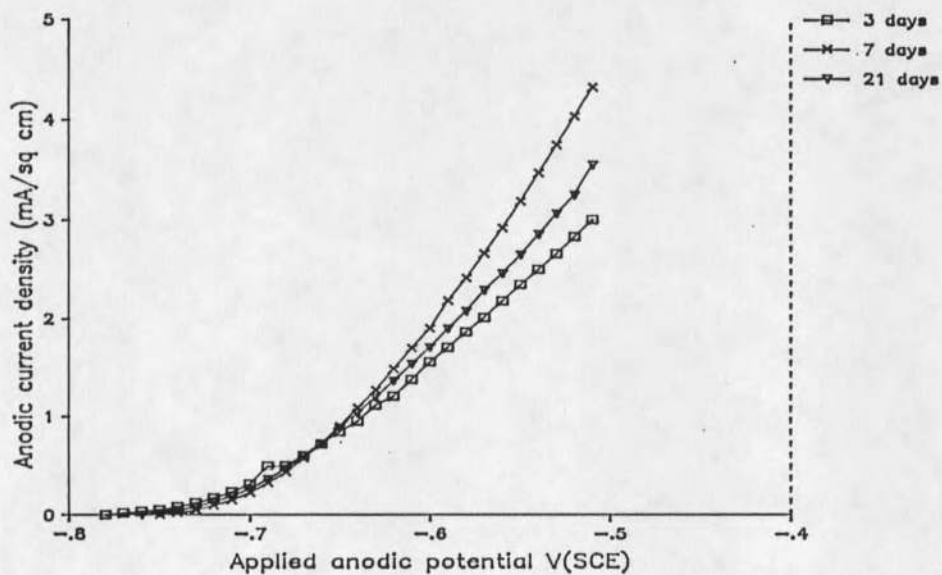


Figure 52. Anodic polarization curves in the abiotic conditions at different exposed times.

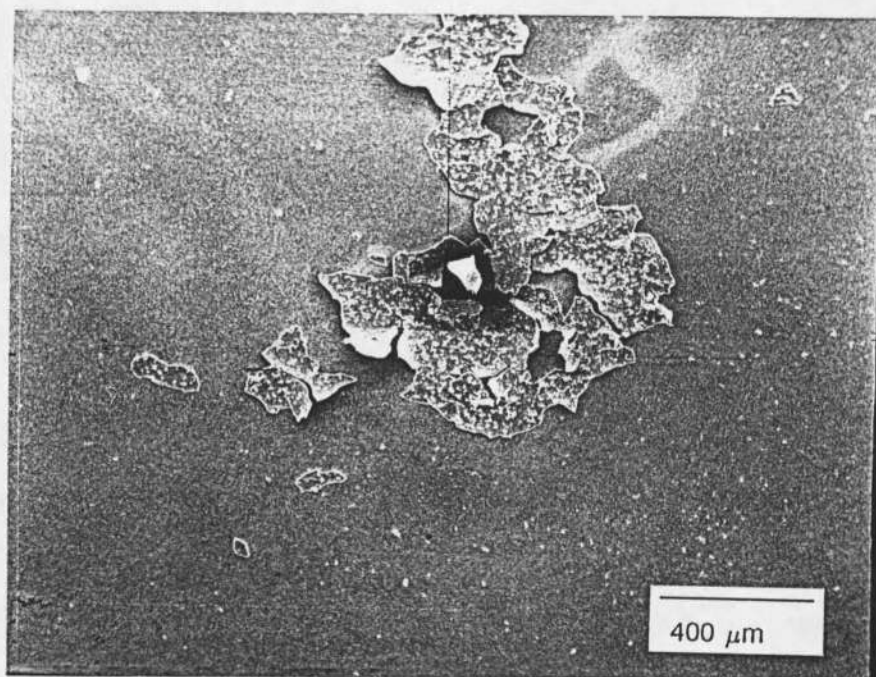


Figure 53. Scanning electron micrograph of iron sulfide film on mild steel in the abiotic conditions at 3 days. x50

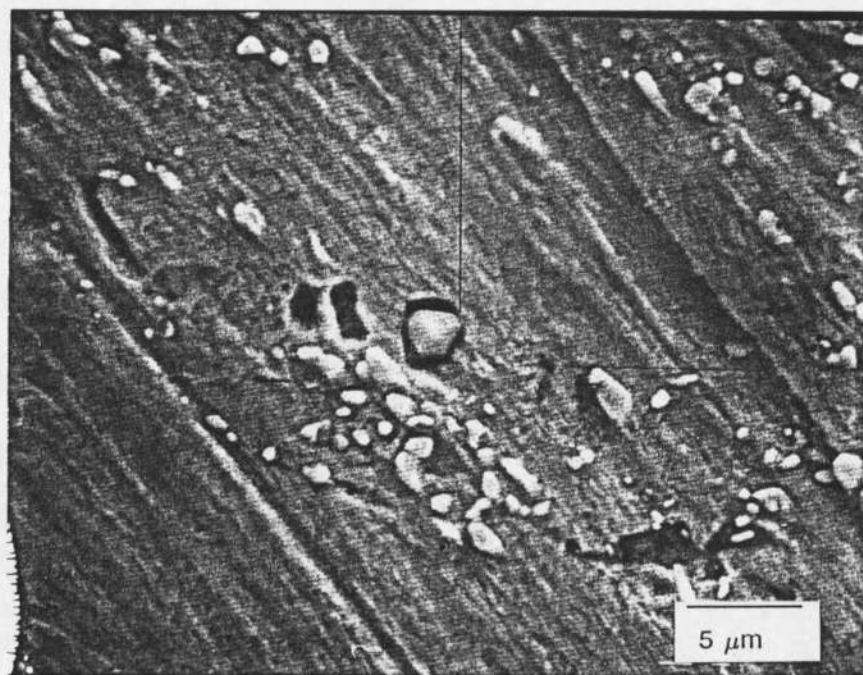


Figure 54. Scanning electron micrograph of a mild steel surface after iron sulfide film was removed in the abiotic conditions at 3 days. x 2,800

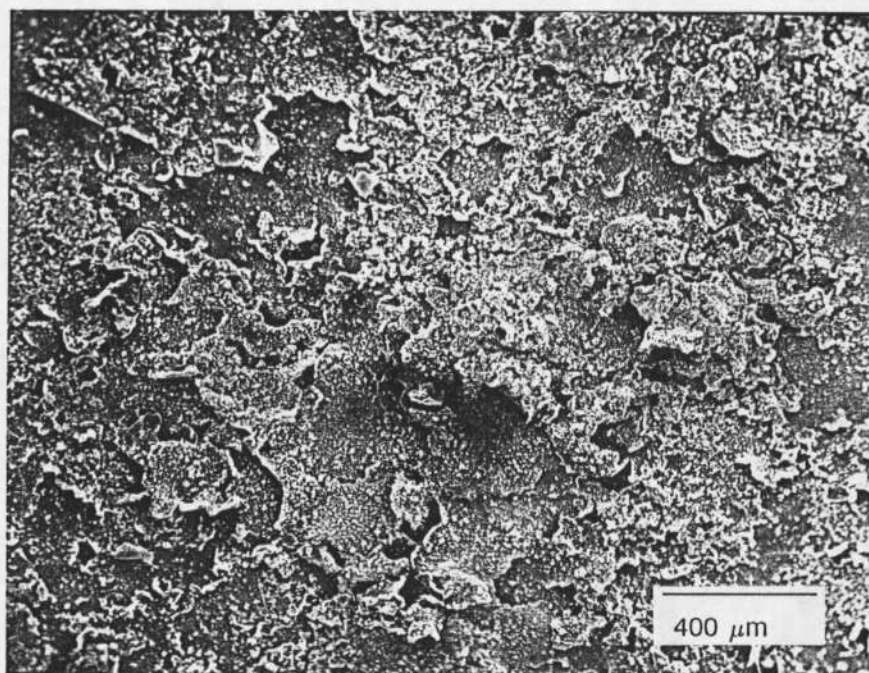


Figure 55. Scanning electron micrograph of iron sulfide film on mild steel in the abiotic conditions at 7 days. x50

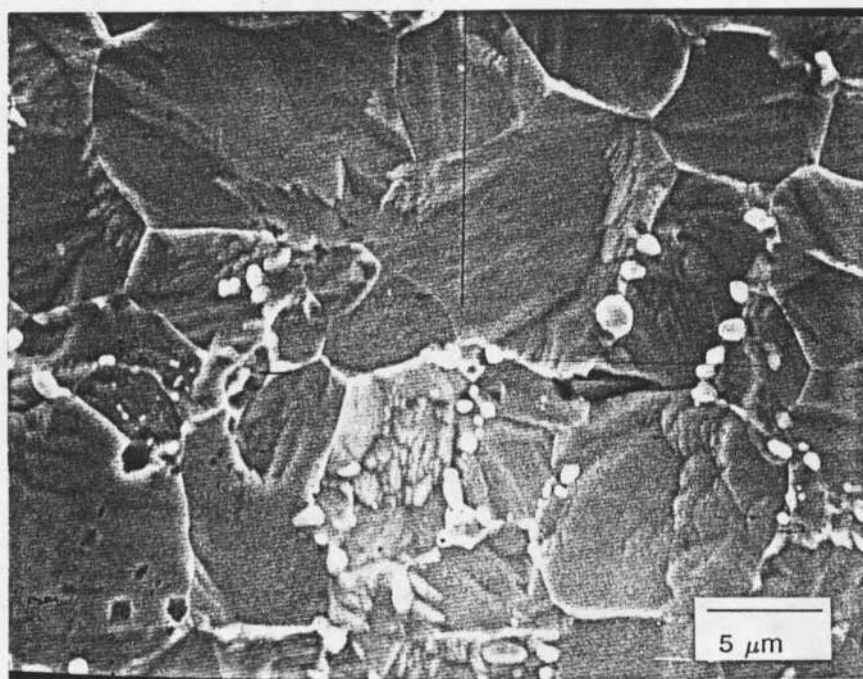


Figure 56. Scanning electron micrograph of a mild steel surface after iron sulfide film was removed in the abiotic conditions at 7 days. x 2,800

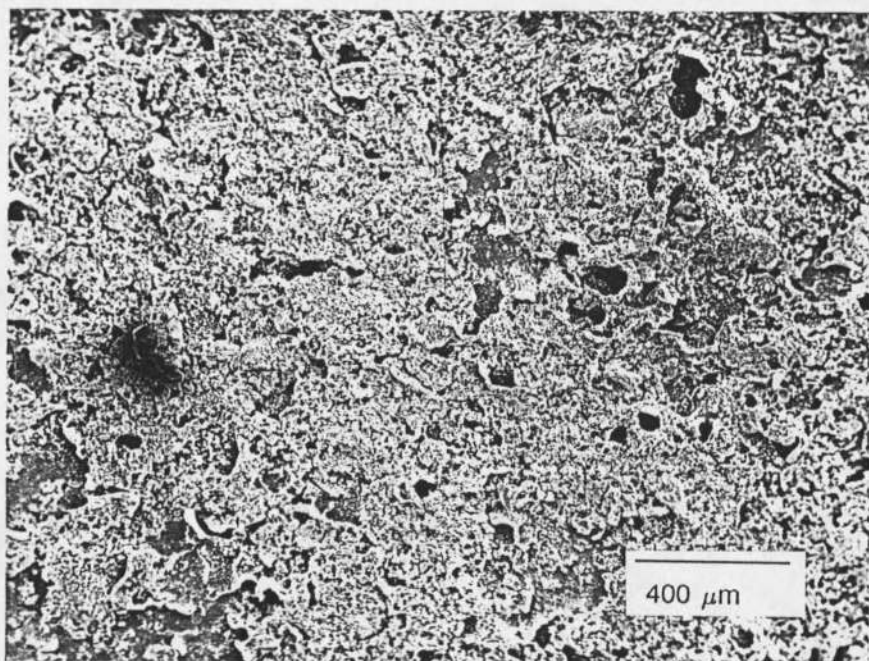


Figure 57. Scanning electron micrograph of iron sulfide film on mild steel in the abiotic conditions at 21 days. x50

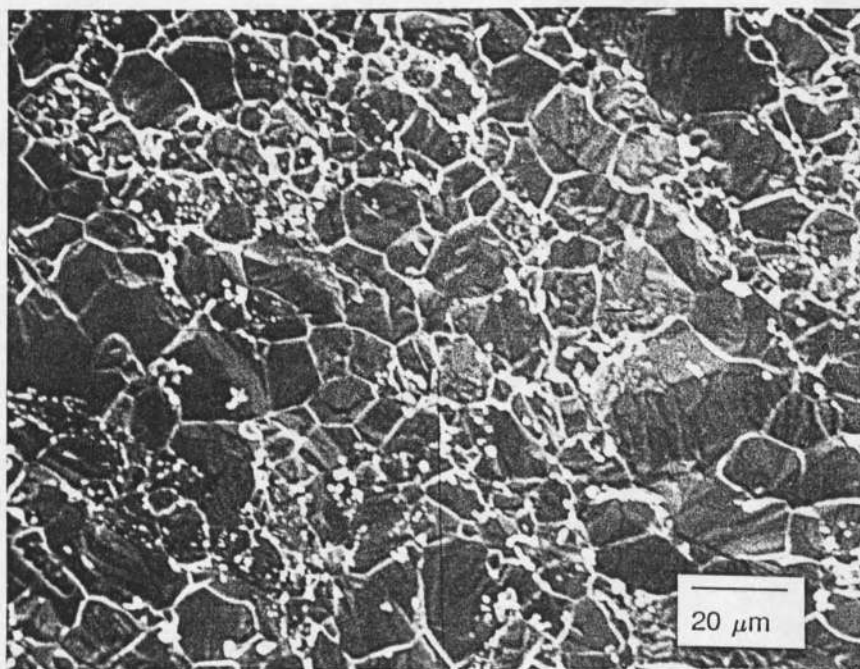


Figure 58. Scanning electron micrograph of a mild steel surface after iron sulfide film was removed in the abiotic conditions at 21 days. x 750

DISCUSSION

Effect of Substrate Loading Rates on the
Corrosion of Mild Steel

At low substrate loading rate, the ratio of SRB in the biofilm to that in bulk water is about 0.1 (Figure 13 and 15). However, at high substrate loading rate, the ratio of SRB in the biofilm to that in bulk water is about 100, which indicate that the increased substrate loading rate creates an environment more suitable for SRB biofilm accumulation.

Specific SRB activity in bulk water or within biofilm can be monitored indirectly by specific substrate removal rate (substrate removed per cell per unit time) or specific product formation rate (product produced per cell per time). The specific substrate removal rate for lactate is not a good indicator in a mixed culture experiment, neither the specific product formation rate for sulfide due to its volatile nature. However, the specific substrate removal rate for sulfate can indicate the specific SRB activity. Specific substrate removal rate is defined as following:

$$q_s = \frac{D(s_i - s)V}{X} \quad (17)$$

where

q_s	= specific substrate removal rate for sulfate	$(M_s M_x t^{-1})$
D	= dilution rate	(t^{-1})
s_i	= influent sulfate concentration	$(M_s L^{-3})$
s	= effluent sulfate concentration	$(M_s L^{-3})$
V	= bulk water volume in the reactor	(L^3)
X	= total cells in the biofilm or bulk liquid	(M_x)

The SRB activity can be obtained by following:

$$\text{SRB activity} = q_s X = D(s_i - s)V \quad (18)$$

According to equation (18), SRB activity is 21.6 mg/hr at low substrate loading rate while 338 mg/hr at high substrate loading rate at 21 days. The increased SRB activity did not enhance the corrosion of mild steel. There was no detectable difference in weight loss both in the two loading rates. This is further proved by the surface analysis and electrochemical measurements. The scratch lines on the coupon can be seen after 21 days under the biofilm and no iron sulfide film formed (Figure 17). An X-ray dot map (Figure 18) indicated no iron in the biofilm. No cathodic depolarization occurred either at low (Figure 19) or high (Figure 20) substrate loading rate in the absence of ferrous iron. At high substrate loading rate, the cathode was slightly polarized as a thick biofilm accumulated and was depolarized as the biofilm was removed (Figure 59). The difference is attributed to

polarization by the thick biofilm. Presumably, a diffusion barrier formed between the bulk water and the metal surface as a thick biofilm accumulated. The diffusion barrier prevented the diffusion of OH^- (cathodic reaction product) away from the metal surface during polarization and increased local pH on the metal surface compared to the bulk water. The same result was observed when a coupon was coated with a similar thickness of 1.5% agar instead of a SRB biofilm (Figure 60).

Salvarezza and Videla (1980) utilized potentiostatic polarization techniques and showed that SRB influence the metal in a similar manner to non-biogenic sulfide which shifts the pitting potential to a more active value. The pitting potential becomes more noble as biofilm become thicker both at low (Figure 21) and high (Figure 22) substrate loading rates, indicating that breakdown of passivity on mild steel becomes more difficult with time. Further evidence for increased passivity is the larger shift in pitting potential (150 mV) at higher loading rate as compared to the low loading rate (40 mV). There was no pitting or localized corrosion observed on the metal surface under open circuit conditions after 21 days. In summary, the passive surface on the mild steel does not break down even in the presence of a thick SRB biofilm. The probable role of biofilms in the protection of metal against corrosion in the SRB environment has been suggested by Gaylarde and Videla (1987). Our investigations

indicate that biofilm possibly reduces the adsorption of sulfide or chloride anions on the bare metal surface under the tested ionic conditions. The water chemistry in the biofilm phase and its effect on the corrosion behavior demands more study.

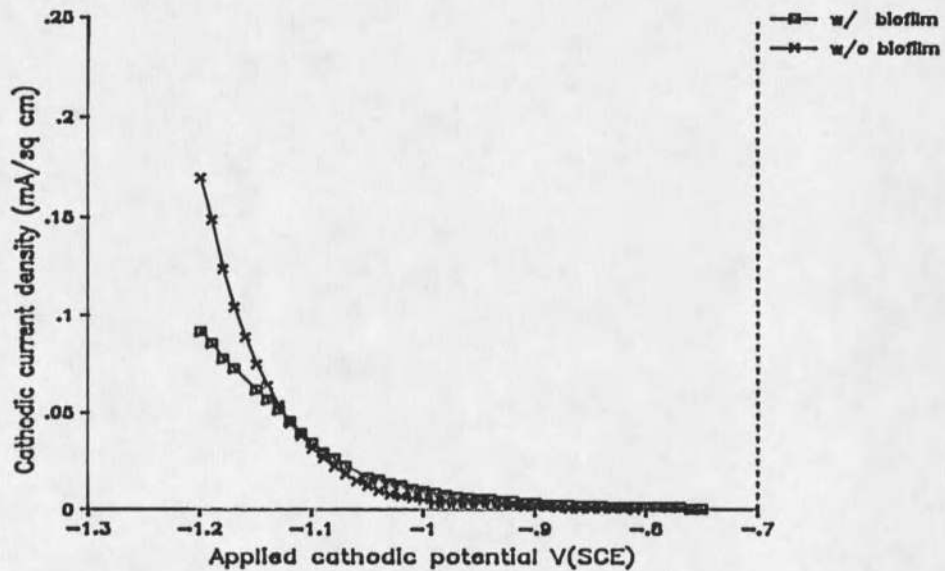


Figure 59. Cathodic polarization curves of a mild steel before and after biofilm has been removed.

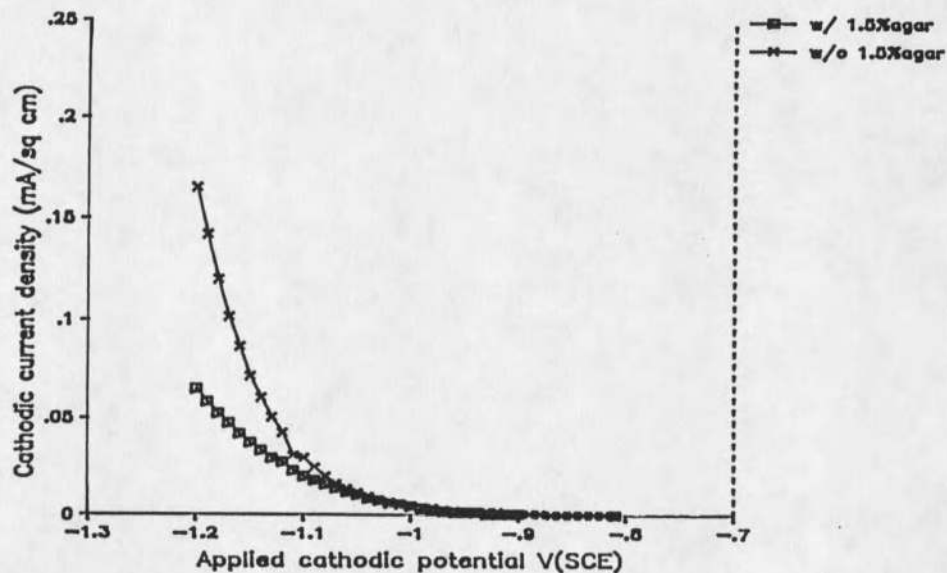


Figure 60. Cathodic polarization curves of a mild steel with and without 1.5% agar.

Effect of Ferrous Ion Concentrations on the Corrosion of Mild Steel with a Precoated Biofilm

There is no iron sulfide formed in the absence of ferrous ion during biofilm accumulation in the first week. This observation again supports the results in the first experiment conducted in the absence of ferrous ion. Iron sulfide film does not form when the medium contains low concentration of ferrous ions (1 and 10 mg/L) but the accumulation of iron sulfide particles in the biofilm increases. The corrosion is insignificant at ferrous iron concentrations up to 10 mg/L. The presence in the medium of sufficient ferrous ion (60 mg/L) to precipitate all the biogenic sulfide and to inhibit the protective iron sulfide film formation leads to a large

increase in corrosion rate.

The corrosion of mild steel under the anaerobic biofilm seems to be initiated by the precipitated iron sulfide particles when those particles contact the metal surface but not by the bacteria or dissolved sulfide. The initiation of corrosion is caused by the cathodic and anodic depolarization reactions (Figures 30 and 31).

Following the initiation of corrosion, the corrosion rate can be accelerated through two possible mechanisms:

(a) corrosion rate is accelerated by cathodic depolarization but is limited by diffusion of hydrogen sulfide through the corrosion product layer (concentration diffusion polarization) as observed in abiotic conditions (Martin et al, 1981).

(b) corrosion rate is accelerated due to cathodic depolarization but is not limited by concentration diffusion polarization. In this case, hydrogen sulfide production in the biofilm, which has accumulated in the loose iron sulfide, accelerates corrosion presumably by reducing the diffusion distance for the biogenic sulfide to reach the mild steel surface.

Gaylarde and Johnson (1980) report that biofilm (sessile) SRB on the metal surface result in higher corrosion rates as compared to the corrosion rate due to planktonic bacteria alone. Their observations support the second mechanism. However, the accelerated process may be reduced when sulfate or lactate diffusion within the biofilm limits the rate of

microbial activity.

The loose iron sulfide particles apparently play a more important role than the bacteria in the anaerobic corrosion process. The iron sulfide particles are cathodic to the mild steel but do not act as permanent cathodes unless dissolved sulfide or SRB (which produce dissolved sulfide) are present. The role of the mixed SRB biofilm on the anaerobic corrosion of mild steel is to continuously supply hydrogen sulfide to keep loose iron sulfide cathodically active. This interpretation of the experimental results is consistent with proposals of Miller (1981).

Corrosion Processes of Mild Steel on a Precoated Iron Sulfide Film Followed by Biofilm Accumulation

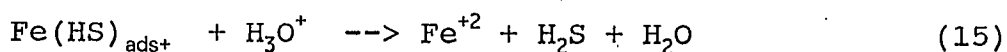
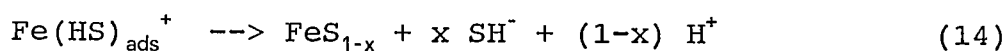
Localized corrosion is strongly related to the metallurgical heterogeneities in the metal matrix such as inclusions and grain boundary triple points (Figure 44). The metallurgical heterogeneities will affect the microstructure of iron sulfide film (Figure 43) and the subsequent corrosion behavior. In the reported experiments, we cannot distinguish between corrosion initiated by the breakdown of the iron sulfide film or by the heterogeneities in the metal matrix. However, some localized corrosion occurred underneath an iron sulfide film suggest that the latter case cannot escape easily. The iron sulfide film remains intact around the localized corrosion areas after 21 days experiment. At higher magnification, the grain sizes and growth orientation of iron

sulfide film underneath the biofilm are revealed which is highly orientated normal to the metal surface (Figure 46). The result is similar to the microstructure of iron sulfide growth on iron under hydrogen sulfide atmosphere at 700° C (McKee and Druschel, 1984). There is no spalling of the iron sulfide film in the presence of biofilm once corrosion is initiated. However, precipitation of iron sulfide particles within the localized corrosion area occurs. Under abiotic conditions, spalling of iron sulfide film is caused by the pressure inside the film. An osmotic pressure gradient develops such that the tendency to spall is enhanced wherever small cracks or imperfections form in the sulfide film (Hausler et al, 1972). Accumulation of biofilm on the iron sulfide film may prevent spalling of the iron sulfide film from the metal surface, thus, permitting a stable, coherent iron sulfide film to remain.

According to Iofa et al (1965), the stimulation of the anodic reaction by hydrogen sulfide is caused by chemisorption (Eq.12) and anodic discharge (Eq.13) reactions



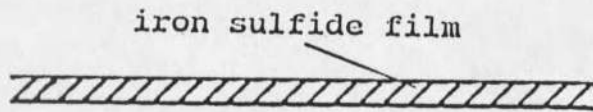
Subsequent to reaction (13), the $\text{Fe(HS)}_{\text{ads}^+}$ species may be incorporated directly into a growing layer of mackinawite (Eq.14), or may be hydrolyzed to yield a dissolved species (Eq.15)



Sulfide film formation occurred according to reaction (14) before biofilm accumulation. However, reaction (15) seems to dominate after biofilm accumulation occurs and leads to local supersaturation of ferrous ions at the alloy surface. Then, nucleation and growth of iron sulfide occurs. The accumulation of bacteria within the localized corrosion area may accelerate corrosion by enhancing the cathodic depolarization within the area and leads to incipient open pits or through-wall corrosion commonly found in industry and purportedly due to microbial processes. Accumulation of bacteria in the localized corrosion area also suggests breakdown of the iron sulfide film in the localized corrosion area.

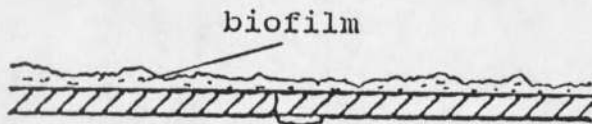
In general, biofilm accumulation appears to reduce the spalling iron sulfide film and decreases general corrosion

rate. However, the risk of localized corrosion is significant. It is suggested that cathodic hydrogen, an electron donor for sulphate-reducing bacteria and other microorganisms, is the initiation point at the metal surface (with respect to the microbial activity) of the anaerobic corrosion process (Ishverlal, 1988). However, our investigations indicate that the initiation of the localized corrosion process is strongly related to the heterogeneities in the metal matrix or in the iron sulfide film. Following the initiation of localized corrosion, localized corrosion is propagated through a dissolution-precipitation reaction. It is proposed that iron sulfide play a more important role than enzymatic activity (hydrogenase) in the anaerobic corrosion process. The hypothesized localized corrosion processes are illustrated schematically in Figure 61.



Formation of iron sulfide film on mild steel before biofilm accumulation.

1



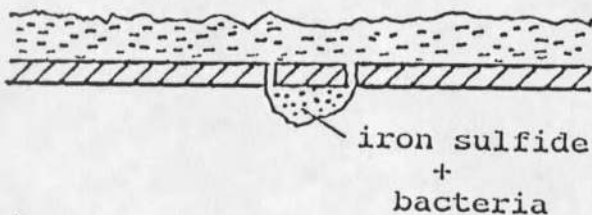
Initiation of corrosion at a heterogeneous site during biofilm accumulation.

2



Breakdown of iron sulfide film leads to the accumulation of bacteria within the localized corrosion area.

3



Extensive corrosion in the localized corrosion area due to the accumulated iron sulfide particles and bacteria.

4

Figure 61. Anaerobic corrosion process of mild steel on a precoated iron sulfide film followed by biofilm accumulation up to 21 days.

Anaerobic Corrosion under
Abiotic Conditions

The initial corrosion processes (about 3 days) under a saturated H₂S environment is film diffusion controlled and pH-dependent (Hausler et al, 1972). A low corrosion rate was observed due to formation of a thin, coherent iron sulfide film on the metal surface at pH 7. However, high corrosion rates were observed at pH 4 and resulted in a thick, noncoherent iron sulfide precipitate.

At low H₂S concentration (40-50 mg/L) and at pH 8, weight loss increased linearly in the first 7 days but became nonlinearly from 7 days to 21 days. The precipitated iron sulfide reach a maximum at 21 days. The formation of a coherent iron sulfide film on the mild steel surface was observed up to 3 days but the initiation of corrosion cannot be clearly demonstrated from the experimental data. There are some defect sites in the iron sulfide film at 3 days. Inclusions are generally found in the metal matrix after the iron sulfide film is removed (Figure 54). Thus, metallurgical heterogeneities are also responsible for the local dissolution of mild steel in abiotic conditions. There is no difference in the metal matrix at 3 days in biotic and abiotic environments. Spalling of the iron sulfide film and precipitation of iron sulfide lead to a noncoherent iron sulfide film at 7 days. The development of a porous iron sulfide deposit on the metal surface reduces the hydrogen

overvoltage and causes cathodic depolarization which enhances corrosion. However, the decrease in extent of the cathodic current and corrosion rate after 7 days suggest that the cathodic depolarization is limited by the loosely accumulated iron sulfide. As a result, concentration-diffusion polarization reduces corrosion rate. Thus, corrosion of mild steel under abiotic conditions at low concentration of iron sulfide and pH 8 is film diffusion-controlled. The abiotic corrosion processes are schematically illustrated in Figure 62.

A decrease in cathodic current but no change in anodic current is observed when the precipitated iron sulfide is removed (Figures 63 and 64). Thus, the corrosion of mild steel under the loose accumulation of iron sulfide under abiotic conditions is solely due to the cathodic-only acceleration if one assumes that hydrogen ion discharge and electron transfer were occurring on or through the accumulated particles (Figure 65).

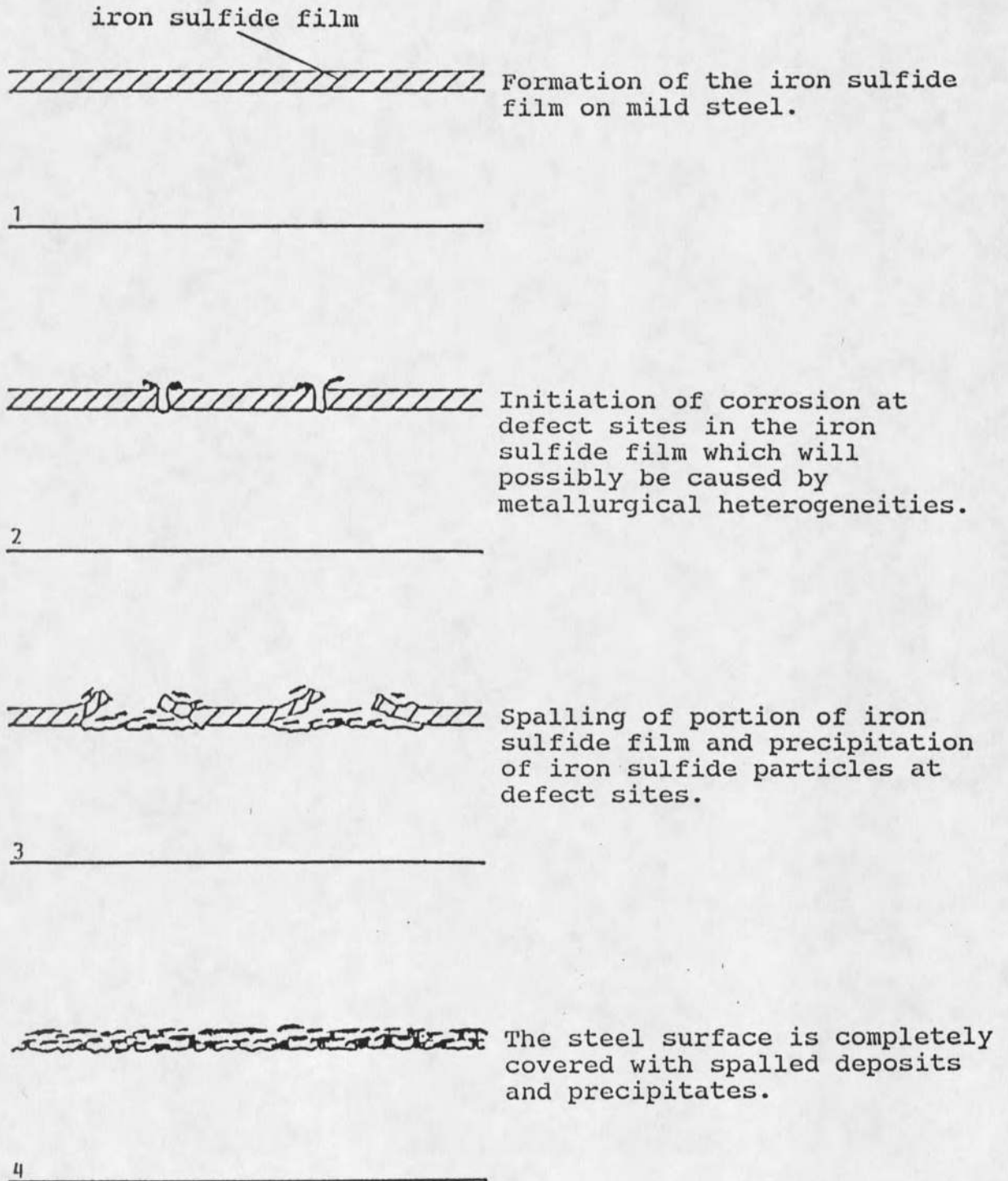


Figure 62. Anaerobic corrosion process of a mild steel in the abiotic conditions up to 21 days.

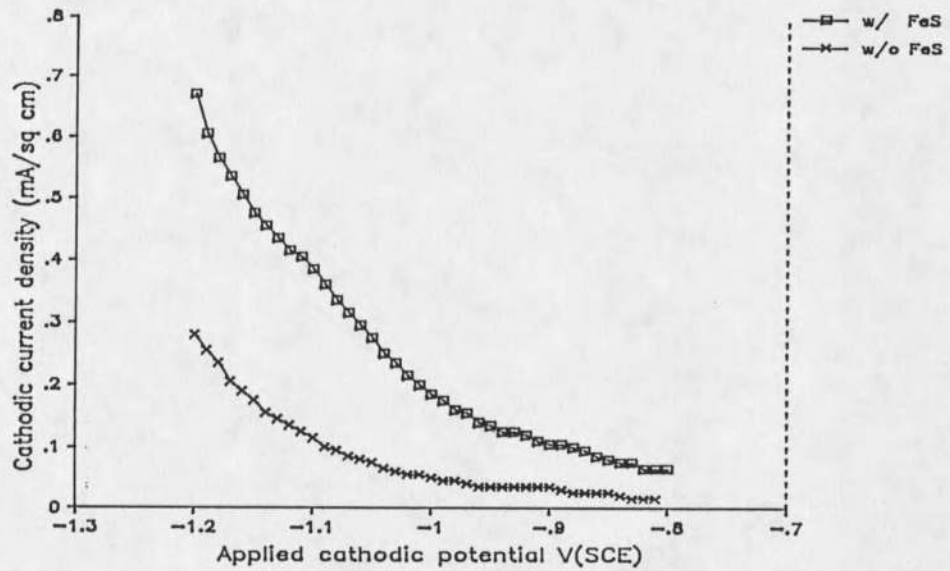


Figure 63. Cathodic polarization curves of a mild steel with and without noncoherent iron sulfide precipitation under abiotic conditions.

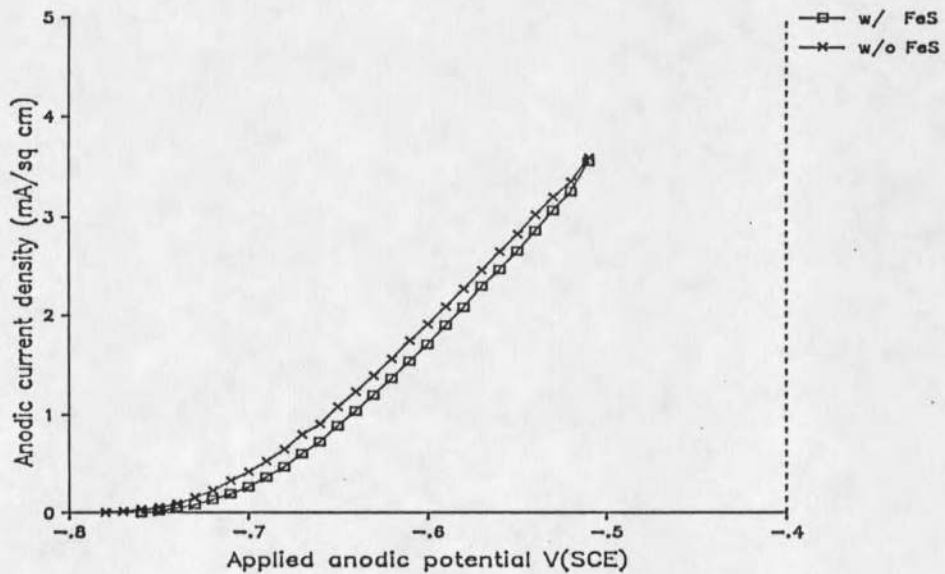
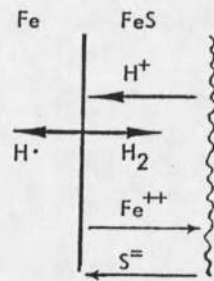


Figure 64. Anodic polarization curves for mild steel with and without noncoherent iron sulfide precipitates under abiotic conditions.

Ionic Conductivity



Electronic Conductivity

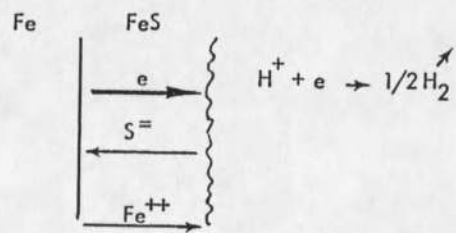


Figure 65. Mass and electron transfer through the loose iron sulfide film.

SUMMARY

The influence of microorganisms on anaerobic corrosion cannot be considered exclusively in terms of metabolic potential of the mixed microbial ecosystem on the metal surface. Metallurgical and chemical processes must be considered as well as biological processes.

This investigation provides strong evidence that the passive film (FeS) on mild steel does not break down in the presence of an active SRB biofilm. The biofilm may probably protect the metal against corrosion under suitable ionic conditions. However, the combination of an SRB biofilm with dissolved oxygen (Hardy and Brown, 1984), dissolved iron, and iron sulfide, can enhance corrosion. Hardy and Brown demonstrated that high corrosion rates and severe pitting attack on mild steel, sometimes observed in the field, occurs when oxygen is introduced into the system. Under completely anaerobic conditions, iron sulfide may play a similar key role in the corrosion process. The rate of corrosion is controlled by the physical properties of iron sulfide on the metal surface. Corrosion could be initiated where there is loose iron sulfide precipitation under the SRB biofilm. The accumulation of iron sulfide and SRB accelerates corrosion of mild steel and determines the type of corrosion (e.g. localized corrosion vs. uniformly corrosion). The rate and

extent of corrosion may be reduced when sulfate or lactate diffusion within the biofilm limits the microbial activity. Under such conditions, diffusion of hydrogen sulfide to the metal surface may become the rate-limiting step in the anaerobic corrosion process.

The coherent iron sulfide film may offer protection against the anaerobic corrosion process in the SRB environment. However, the risk of localized corrosion is significant when there are heterogeneities in the metal matrix such as inclusions or grain boundary triple points. Localized corrosion can be initiated and accelerated in those areas. Mild steel corrodes uniformly in an abiotic sulfide solution at pH 8 with the formation of a black iron sulfide precipitate. Most confirmed cases of microbial corrosion are characterized as localized corrosion, which is at least partially due to a patchy biofilm distribution on the metal surface. This study demonstrates that metal heterogeneities can also be an important parameter in the localized corrosion of mild steel.

CONCLUSIONS

The purpose of this study was to combine the biofilm process analysis with electrochemical measurements and surface analysis to observe the effect of anaerobic biofilm and other chemical parameters on the corrosion behavior of mild steel.

Based on mixed culture experiments, including SRB, the following conclusions are derived:

1. The passivity of mild steel remains stable under the anaerobic biofilm in the absence of ferrous ion regardless of substrate loading rate.
2. There is no cathodic depolarization and no correlation between corrosion and SRB activity in the absence of ferrous ion under continuous flow conditions at pH = 8.
3. Corrosion of mild steel in the presence of biofilm will be initiated by suspended iron sulfide once the iron sulfide particle contacts the metal surface.
4. Intergranular attack is always associated with loose iron sulfide deposition.
5. The SRB in a biofilm influence the anaerobic corrosion process by continuously supplying hydrogen sulfide to keep loose iron sulfide cathodically active and, thus accelerate corrosion.

6. Accumulation of biofilm on a precoated iron sulfide film can reduce spalling of the iron sulfide film but cannot eliminate localized corrosion.
7. The anaerobic corrosion process at low hydrogen sulfide concentration at pH 8 under continuous flow conditions is initiated at defect sites in iron sulfide film or metal matrix. Corrosion is propagated subsequent to film rupture and film spalling.
8. The loosely accumulated iron sulfide precipitates accelerate corrosion of mild steel due to cathodic-only depolarization, which is rate-limited by concentration-diffusion polarization.

REFERENCES

- Bolmer P. W. (1965), Polarization of Iron in H₂S-NaHS Buffers. *Corrosion*, 21, 3, p.65
- Booth G. H., P. M. Cooper, D. S. Wakerley (1966), Corrosion of Mild Steel by Actively Growing Cultures of Sulfate-Reducing Bacteria, the Influence of Ferrous Ions. *Br. Corrs. J.* 1, p.345.
- Booth G. H., J. A. Robb, D. S. Wakerley (1967), Effect of Iron(II) on the anaerobic Corrosion of Low-Carbon Steel as Determined by Actively Growing Cultures of Sulfate-Reducing Bacteria. *Third Int. Congress on Metallic Corrosion, Moscow*, 2, 5, p.542.
- Booth, G. H., L. Elford, and D. S. Warkerley (1968), Corrosion of Mild Steel by Sulfate-Reducing Bacteria: An Alternative Mechanism. *Br. Corrs. J.*, 3, p.242.
- Booth G. H. and A. K. Tiller (1962), Polarization Studies of Mild Steel in Cultures of Sulfate-Reducing Bacteria. Part 3, Halophilic Organisms, *Trans. Faraday Soc.*, 58, p.2510.
- Booth G. H., P. M. Shinn, and D. S. Wakerley (1964), *Congress International de la Corrosion Marine et des Salissures. Cannes. France.* p.363.
- Brown B. F. (1970), Concept of the Occluded Corrosion Cell. *Corrosion*, 26, p.249.
- Cappenberg T. A. (1975), A Study of Mixed Cultures of Sulfate-Reducing and Methane-Producing Bacteria. *Microbial Ecology*, 2, p.60.
- Cline J. D. (1969), Spectrophotometric Determination of Hydrogen Sulfide in Natural Water. *Limnol Oceanogr*, 14, p. 454.
- Costello J. A. (1974), Cathodic Depolarization by Sulfate-Reducing Bacteria. *South African Journal of Science*, 70, p,202.
- D'Alessandro P. L. Jr., W. G. Characklis, M. A. Kessick, and C. H. Ward (1974), Dissimilatory Sulfate Reduction in Anaerobic Systems. *Developments in Industrial Microbiology*, 15, American Ins. Biological Sciences. Washington, D. C.

- De Mele M. F. L., R. C. Salvarezza and H. A. Videla (1979), Microbial Contaminants Influencing the Electrochemical Behavior of Aluminum and Its Alloy in Fuel/Water Systems. *International Biodeterioration Bulletin*, 15, 2, p.39.
- Edyvean R. G. J., C. J. Thomas, R. Brook, I. M. Austen (1985), "The Use of Biologically Active Environments for Testing Corrosion Fatigue Properties of Offshore Structural Steels", *Proceedings of the International Conference on Biologically Induced Corrosion*, Gaithersburg, Maryland p.254.
- Gaylarde C. C. and J. M. Johnson (1980), *Microbial Adhesion to Surfaces*, Berkeley, R.C.W., Lynch, J.W., Rutter, P.R. and Vincent, B., Ellis Harwood, Ltd., Chichester, England. p. 511.
- Gaylarde C. and H. A. Videla (1987), Localized Corrosion Induced by a Marine Vibrio. *International Biodeterioration*, 23, 2, p.91.
- Gupta D. V. S. (1981), Corrosion Behavior of 1040 Carbon Steel, I. Effect of pH and Sulfide Ion Concentrations in Aqueous Neutral and Alkaline Solutions at Room Temperature. *Corrosion*, 37, 11, p.611.
- Gutzeit J. (1968), Corrosion of Steel by Sulfide and Cyanides in Refinery Condensate Water. *Material Protection*, 7, p.17.
- Hamilton W. A. and S. Maxwell (1985), Biological and Corrosion Activities of Sulfate-Reducing Bacteria Within Natural Biofilm, *Proceedings of the International Conference on Biologically Induced Corrosion*, June 10-12, 1985, Gaithersburg, Maryland.
- Hardy J. A., J. L. Brown (1984), The Corrosion of Mild Steel by Biogenic Sulfide Films Exposed to Air, *Corrosion*, 40, 12, p.650.
- Hausler R. H., L. A. Goeller, R. P. Zimmerman, and R. H. Rosenward (1972), Contribution to the "Filming Amine" Theory: An Interpretation of Experimental Results, *Corrosion*, 28, 1, p.7.
- Hedley R. F. (1943), The Influence of Sporovibrio Desulfuricans on the Current and Potential Behavior of Corroding Iron. *Natural Bureau of Standards Corrosion Conference*.
- Horvath J. (1960), Contributions to the Mechanism of Anaerobic Microbiological Corrosion. *Acta Chimica Hungarica*, 25, p.65.
- Hutchison C. B. and W. B. Hughes (1961), *Corrosion*, 17. p.514t.

Ingvorsen K. (1984), Kinetics of Sulfate and Acetate Uptake by Desulfovibrio Postgatei. Applied and Environmental Microbiology, 49, p.403.

Iofa Z. A., V. V. Batrakov, Cho-Ngok-Ba (1965), Influence of Anion Adsorption on the Action of Inhibitors on the Acid Corrosion of Fe and Co. Electrochim. Acta, 9, p.1645.

Ishverlal P. P (1988), Hydrogen Metabolism in Sulphate-Reducing Bacteria and Its Role in Anaerobic Corrosion. Biofouling, 1, p.27.

King R. H., J. D. A. Miller and J. S. Smith (1973), Corrosion of Mild Steel by Iron Sulfide. Br. Corrs. J., 8, p.137.

Lee W. (1986), AC Impedance and Microbial Corrosion, IPA Industrial Associates Report, Montana State University, Bozeman, p.2.

Mara D. A. and D. S. Williams (1972), Biod. of Materials, 2, A. H. Walters and E. H. Hueck van den plas (ed.), Applied Science, Barking, England.

Martin R. L. and R. R. Annand (1981), Accelerated Corrosion of Steel by Suspended Iron Sulfides in Brine. Corrosion, 36, 5, p.297.

McKee R. A. and R. E. Druschel (1984), The Microstructures and Growth Rates of FeS on Pure and Not-So-Pure Iron. J. Electrochem. Soc., 131, 4, p.853.

Meyer F. H., O. L. Riggs, R. L. Mcglasson, J. D. Sudbury (1958), Corrosion, 14,2, P.109t.

Miller, J.D.A. and Tiller, A.K. (1970), Microbial Aspects of Metallurgy. J.D.A. Miller (ed.), Elsevier, New York. p.61.

Miller J. D. A. (1981), Metals. In: Rose A. H. (ed), Microbial Biodeterioration, Academic press. New York, p.149.

Mond J. (1949), The Growth of Bacterial Cultures. Annual Review of Microbiology, 3, p.371.

Nielsen P. H. (1987), Biofilm Dynamics and Kinetics during High-Rate Sulfate Reduction under Anaerobic Conditions, Appl. Environ. Microbiol., 53, p.27.

Postgate J. R. (1984), The Sulfate-Reducing Bacteria, Cambridge U. Press, London.

Salvarezza R. C. and H. A. Videla (1980), Passivity breakdown of Steel in Seawater in the Presence of Sulfate-Reducing Bacteria. *Corrosion*, 36, p.550.

Salvarezza R. C., De Mele M. F. L. and H. A. Videla (1979), Use of Pitting Potential to Study Microbial Corrosion of 2024 Aluminum Alloy. *International Biodeterioration Bulletin*, 15, 4, p.125.

Sardisco T. B., W. B. Wright and E. C. Greco (1963), Corrosion of Fe in a $H_2S-CO_2-H_2O$ System- Corrosion Film Properties on Pure Fe. *Corrosion*, 19, 10, p.354t

Sardisco T. B. and R. E. Pitts. (1965), Composition and Protectiveness of the Sulfide Film as a Function of pH. *Corrosion*, 21, 11, p.350.

Shoesmith D. W., P. Taylor, M. G. Bailey, and D. G. Owen (1980), "The Formation of Ferrous Monosulfide Polymorphs during the Corrosion of Iron by Aqueous Hydrogen Sulfide at 21°C", *J. electrochem. Soc.* 127, 5, p.1007.

Smialowska Z. S. (1972), Influence of Inclusions on the Pitting Corrosion of Steel. *Corrosion*, 28, 10, p.388.

Smith J. S. and J. D. A. Miller (1975), Nature of Sulfides and their Corrosive Effect on Ferrous Metals: A Review, *Br. Corrs. J.* 10, 3, p,136.

Standard methods for the examination of water and waste water (1971), 13 th edition, Washington, American Public health Association.

Starkey R. L. (1985), Anaerobic Corrosion-Perspectives About Causes, Proceedings of the International Conference on Biologically Induced Corrosion, June 10-12, 1985, Gainthersburg, Maryland.

Tewari P. H. and A. B. Campell (1979), "Dissolution of Iron during the Initial Corrosion of Carbon Steel in Aqueous H_2S Solutions", *Can. J. Chem.*, 57, p.188.

Togano, H., Sasaki, H., Nakahara, T., Kanda, Y., and Osato, K. (1975), The Influence of Sulfate-Reducing Bacteria on the Corrosion of Mild Steel in Artificial Seawater, Proceedings of the 6th International Congress on Metallic Corrosion, Australian Corrosion Association, Victoria, p.1258.

Traore A. S., C. E. Hatchikian, L. G. Tean, and P. B. Tean (1982), Microcalorimetric Studies of the Growth of Sulfate-Reducing Bacteria: Comparison of the Growth Parameters of Same Desulfovibrio Species, *Journal of Bacteriology*, 149, 2. p.606.

Videla H. A. (1986), Mechanisms of MIC. Proceedings of Argentina-USA Workshop on Biodeterioration (CONICET-NSF), Videla, H.A. (ed.), Published by Aquatec Quimica S.A., Sao Paulo, Brasil, p.43.

Von Wolzogen Kühr and van der Vlugt (1934), Graphication of Cast Iron as an Electrochemical Process in Anaerobic Soils, Water (The Hague), 18, p.147.

Wanklin J. N. and C. P. Spruit (1952), Influence of Sulfate-Reducing Bacteria on the Corrosion Potential of Iron. Nature, London, 169, p.928.

APPENDIX

Table 10. MPN for GAB and SRB at different time periods in bulk water and biofilm at low substrate loading rate.

Time (days)	Bulk Water GAB	Log(Cell #) SRB	Biofilm GAB	Log(Cell #) SRB
3	11.85	8.35	10.07	7.07
7	---	---	---	---
21	12.61	8.19	11.93	6.93

Table 11. MPN for GAB and SRB at different time periods in bulk water and biofilm at high substrate loading rate.

Time (days)	Bulk Water GAB	Log(Cell #) SRB	Biofilm GAB	Log(Cell #) SRB
3	9.86	9.86	12.93	11.93
7	11.13	11.13	13.42	12.93
21	11.61	10.86	13.63	13.11

Table 12. MPN for GAB and SRB at different iron concentration in bulk water and biofilm at high substrate loading rate.

Fe ⁺² (mg/L)	Bulk Water GAB	Log(Cell #) SRB	Biofilm GAB	Log(Cell #) SRB
0	11.99	11.10	13.68	13.20
1	11.88	11.80	13.27	13.68
10	11.54	11.88	12.84	12.62
60	11.35	10.99	12.84	12.77

Table 13. MPN for GAB and SRB at different time periods in bulk water and biofilm when metal coupons are precoated with iron sulfide film.

Time (days)	Bulk Water GAB	Log(Cell #) SRB	Biofilm GAB	Log(Cell #) SRB
3	11.50	10.77	12.95	13.10
7	11.35	10.99	13.20	13.42
21	11.50	10.88	13.68	13.42

Table 14. Water chemistry analysis in the bulk water under batch culture conditions for stoichiometric study.

time (hr)	sulfate (ppm)	lactate (ppm)	sulfide (ppm)
0.5	2500	2658	31
4.5	2250	2210	49
11.75	1750	1080	310
22.5	1300	25	460
31.25	1300	14	350
72	1300	12.8	230

Table 15. Anodic polarization data at different time periods with low substrate loading rate in the absence of iron.

Potentials V(SCE)	3 days (mA/cm ²)	7 days (mA/cm ²)	21 days (mA/cm ²)
-0.54			
-0.55			
-0.56			
-0.57			
-0.58			1.05
-0.59			0.9225
-0.6			0.7925
-0.61			0.6735
-0.62			0.5565
-0.63			0.4475
-0.64		1.005	0.35
-0.65		0.8305	0.2645
-0.66		0.655	0.1925
-0.67		0.4975	0.1365
-0.68	1.095	0.3415	0.0985
-0.69	0.9225	0.219	0.068
-0.7	0.7345	0.1245	0.0375
-0.71	0.57	0.0595	0.0165
-0.72	0.3585	0.0165	0.0085
-0.73	0.1535	0.0065	0.0065
-0.74	0.0245	0.004	0.0045
-0.75	0.0095	0.0025	0.0035
-0.76	0.0065	0.0015	0.0025
-0.77	0.0045	0.001	0.0025
-0.78	0.0035	0.001	0.0015
-0.79	0.0025	0.0005	0.0015
-0.8	0.0015	0.0005	0.0015
-0.81	0.0015		0.0015
-0.82	0.0005		
-0.83	0.0005		
-0.84	0.0005		
-0.85			
-0.86			
-0.87			
-0.88			
-0.89			

Table 16. Cathodic polarization data at different time periods with low substrate loading rate in the absence of iron.

Potential V(SCE)	3 days (mA/cm ²)	7 days (mA/cm ²)	21 days (mA/cm ²)
-0.81			
-0.82			0.0005
-0.83		0.0005	0.0005
-0.84		0.0005	0.0005
-0.85	0.0005	0.0005	0.0015
-0.86	0.0005	0.0005	0.0015
-0.87	0.0005	0.001	0.0015
-0.88	0.0005	0.001	0.0015
-0.89	0.0005	0.001	0.0015
-0.9	0.0005	0.001	0.0015
-0.91	0.0005	0.0015	0.0015
-0.92	0.0005	0.0015	0.002
-0.93	0.0005	0.0015	0.0025
-0.94	0.0005	0.002	0.0025
-0.95	0.0015	0.0025	0.0025
-0.96	0.0015	0.0025	0.0025
-0.97	0.0015	0.0025	0.0035
-0.98	0.0015	0.0035	0.0035
-0.99	0.0015	0.0035	0.004
-1	0.0025	0.0045	0.0045
-1.01	0.0025	0.0055	0.005
-1.02	0.0025	0.006	0.0055
-1.03	0.0035	0.007	0.0065
-1.04	0.0045	0.0085	0.0075
-1.05	0.0055	0.0095	0.0085
-1.06	0.0065	0.011	0.0095
-1.07	0.0085	0.0135	0.0105
-1.08	0.0105	0.0155	0.0135
-1.09	0.0125	0.0185	0.0165
-1.1	0.0155	0.0215	0.0195
-1.11	0.0185		0.0225
-1.12	0.0235	0.0305	0.0265
-1.13	0.0295	0.0355	0.0315
-1.14	0.036	0.042	0.0375
-1.15	0.0445	0.0495	0.044
-1.16	0.055	0.057	0.0525
-1.17	0.0685	0.067	0.0615
-1.18	0.0805	0.075	0.0725
-1.19	0.0975	0.092	0.0835
-1.2	0.1135	0.102	

Table 17. Anodic polarization currents at different time periods at high substrate loading rate in the absence of iron.

Potentials V(SCE)	3 days (mA/cm ²)	7 days (mA/cm ²)	14 days (mA/cm ²)	21 days (mA/cm ²)
-0.41				
-0.42				
-0.43				
-0.44			1.845	1.485
-0.45			1.295	1.105
-0.46			0.7725	0.7635
-0.47			0.3845	0.496
-0.48			0.1935	0.325
-0.49		1.1	0.1145	0.2635
-0.50		0.7375	0.0805	0.2235
-0.51		0.2585	0.0615	0.1925
-0.52		0.0615	0.0475	0.1665
-0.53		0.0165	0.0375	0.1475
-0.54		0.0075	0.0305	0.1305
-0.55		0.0045	0.0255	0.1155
-0.56		0.0040	0.0215	0.1015
-0.57	1.4850	0.0035	0.019	0.0885
-0.58	1.1050	0.0025	0.0165	0.0785
-0.59	0.7635	0.0025	0.0145	0.0685
-0.6	0.5665	0.0025	0.0125	0.0595
-0.61	0.2215	0.0015	0.0105	0.0505
-0.62	0.0875	0.0015	0.0095	0.0425
-0.63	0.0355	0.0015	0.0075	0.0355
-0.64	0.0105	0.0015	0.0065	0.0295
-0.65	0.0025	0.0015	0.0055	0.024
-0.66	0.0005	0.0015	0.0045	0.0185
-0.67	0.0005	0.0015	0.0035	0.0145
-0.68	0.0005	0.0015	0.0025	0.0115
-0.69	0.0005	0.0015	0.0025	0.0085
-0.7	0.0005	0.0015	0.0015	0.0065
-0.71	0.0005	0.0015	0.0015	0.0045
-0.72	0.0005		0.0015	0.003
-0.73	0.0005		0.0005	0.0025
-0.74	0.0005			0.002
-0.75	0.0005			
-0.76				
-0.77				
-0.78				
-0.79				
-0.8				

Table 18. Cathodic polarization data at different time periods at high substrate loading rate in the absence of iron.

Potentials V(SCE)	3 days (mA/cm ²)	7 days (mA/cm ²)	14 days (mA/cm ²)	21 days (mA/cm ²)
-0.8		0.0005	0.0005	0.0015
-0.81		0.0005	0.0005	0.0015
-0.82		0.0005	0.0005	0.0015
-0.83		0.0005	0.0005	0.0015
-0.84		0.0005	0.001	0.002
-0.85		0.0005	0.0015	0.002
-0.86		0.0005	0.0015	0.002
-0.87		0.0005	0.0015	0.0025
-0.88		0.0005	0.0015	0.0025
-0.89	0.0005	0.0005	0.0015	0.0025
-0.9		0.001	0.002	0.0035
-0.91	0.0005	0.0015	0.0025	0.0035
-0.92	0.0005	0.0015	0.0025	0.0045
-0.93	0.0005	0.0015	0.003	0.0045
-0.94	0.0005	0.002	0.003	0.0055
-0.95	0.001	0.0025	0.0035	0.0055
-0.96	0.0015	0.0025	0.0035	0.006
-0.97	0.0015	0.0035	0.004	0.0065
-0.98	0.0015	0.0035	0.0045	0.0075
-0.99	0.0025	0.0045	0.0055	0.0085
-1	0.0025	0.0055	0.007	0.0095
-1.01	0.0035	0.0065	0.0095	0.0105
-1.02	0.0045	0.0075	0.0105	0.0125
-1.03	0.0055	0.0095	0.0125	0.0135
-1.04	0.0075	0.0105	0.0145	0.0155
-1.05	0.0095	0.0135	0.0165	0.0165
-1.06	0.0105	0.0155	0.0195	
-1.07	0.0155	0.0165	0.0235	0.0225
-1.08	0.0195	0.0225	0.0275	0.0265
-1.09	0.0235	0.0265	0.0315	0.0295
-1.1	0.0295	0.0305	0.0365	0.0345
-1.11	0.0365	0.035		0.0395
-1.12	0.0455	0.0405	0.0485	0.0455
-1.13	0.0535	0.0455	0.0535	0.0515
-1.14	0.0655	0.0515	0.0595	0.0565
-1.15	0.0795	0.0585	0.0645	0.0615
-1.16	0.0975	0.0635	0.0695	
-1.17	0.1175	0.0705		0.0725
-1.18	0.1395	0.0755	0.0825	0.0775
-1.19	0.1645	0.0825		0.0855
-1.2	0.19	0.0895		0.0915

Table 19. Anodic polarization data for different ferrous ion concentrations at high substrate loading rate.

potential V(SCE)	0 ppm (mA/cm ²)	1 ppm (mA/cm ²)	10 ppm (mA/cm ²)	60 ppm (mA/cm ²)
-0.38				3.66
-0.39	1.245			3.55
-0.4	0.9055			3.45
-0.41	1.245			3.32
-0.42	0.9055			3.21
-0.43	0.6365			3.09
-0.44	0.4195	1.3		2.975
-0.45	0.2775	1.055		2.84
-0.46	0.1835	0.795	1.345	2.72
-0.47	0.1215	0.5345	0.9315	2.64
-0.48	0.008	0.2615	0.5515	2.49
-0.49	0.0535	0.1075	0.266	2.35
-0.5	0.0355	0.0605	0.1025	2.24
-0.51	0.0235	0.0395	0.051	2.14
-0.52	0.016	0.0285		2.01
-0.53	0.0115	0.0225	0.03	1.9
-0.54	0.0085	0.0185	0.0255	1.78
-0.55	0.0075	0.016	0.0215	1.665
-0.56	0.0065	0.0145	0.0185	1.58
-0.57	0.0055	0.0125	0.0165	1.46
-0.58	0.0055	0.0115	0.0145	1.36
-0.59	0.0045	0.0095	0.0115	1.26
-0.6	0.004	0.0085	0.0095	1.15
-0.61	0.0035	0.0075	0.0085	1.05
-0.62	0.0035	0.0065	0.0075	0.98
-0.63	0.0025	0.0055	0.0065	0.885
-0.64	0.0025	0.0045	0.0055	0.79
-0.65	0.002	0.004	0.0045	0.71
-0.66	0.0015	0.0035	0.004	0.625
-0.67	0.0015	0.003	0.003	0.55
-0.68	0.0015	0.0025	0.0025	0.48
-0.69	0.001	0.0025	0.002	0.405
-0.7	0.0005	0.0015	0.0015	0.34
-0.71	0.0005	0.0015	0.001	0.27
-0.72	0.0005	0.0005	0.0005	0.19
-0.73	0.0005	0.0005	0.0005	0.1
-0.74	0.0005	0.0005		
-0.75		0.0005		
-0.76		0.0005		
-0.77		0.0005		
-0.78		0.0005		
-0.79		0.0005		
-0.8				

Table 20. Cathodic polarization data for different ion concentrations at high substrate loading rate.

potentials V(SCE)	0 ppm (mA/cm ²)	1 ppm (mA/cm ²)	10 ppm (mA/cm ²)	60 ppm (mA/cm ²)
-0.79				0.695
-0.8		0.0005	0.0005	0.725
-0.81		0.0005	0.0005	0.76
-0.82	0.0005	0.0005	0.0005	0.795
-0.83	0.0005	0.0005	0.0005	0.84
-0.84	0.0005	0.0005	0.0005	0.86
-0.85	0.0005	0.0005	0.0005	0.895
-0.86	0.0005	0.0005	0.0005	0.945
-0.87	0.0005	0.0005	0.0005	0.995
-0.88	0.0005	0.0005	0.001	1.015
-0.89	0.0005	0.0005	0.0015	1.065
-0.9	0.0005	0.0005	0.0015	1.115
-0.91	0.001	0.0015	0.0015	1.165
-0.92	0.0015	0.0015	0.002	1.215
-0.93	0.0015	0.0015	0.0025	1.28
-0.94	0.0015	0.0015	0.0035	1.36
-0.95	0.0015	0.0015	0.0045	1.43
-0.96	0.002	0.0025	0.0045	1.505
-0.97	0.0025	0.0025	0.0045	1.56
-0.98	0.0025	0.0025	0.0055	1.64
-0.99	0.0035	0.0035	0.0055	1.7
-1	0.004	0.0035	0.0055	1.75
-1.01	0.0045	0.0035	0.006	1.795
-1.02	0.0055	0.004	0.0075	1.83
-1.03	0.0065	0.0045	0.009	1.87
-1.04	0.008	0.0055	0.0105	1.89
-1.05	0.0095	0.0075	0.0125	1.935
-1.06	0.0105	0.0085	0.016	1.97
-1.07	0.0125	0.01	0.0195	1.99
-1.08	0.0145	0.012	0.024	2.035
-1.09	0.0175	0.0145	0.0285	2.075
-1.1	0.0195	0.0175	0.0335	2.13
-1.11	0.023	0.0205	0.04	2.18
-1.12	0.0265	0.0245	0.046	2.25
-1.13	0.0305	0.0285	0.054	2.325
-1.14	0.0355	0.0335	0.062	2.4
-1.15	0.04	0.0385	0.072	2.475
-1.16	0.0405	0.0445	0.082	2.585
-1.17	0.0515	0.0515	0.095	2.655
-1.18	0.0575	0.0585	0.108	2.78
-1.19	0.0635	0.0665	0.123	2.87
-1.2	0.0705	0.0745	0.1395	3

Table 21. Anodic polarization data at different time periods on a precoated iron sulfide film at high substrate loading rate.

potentials V(SCE)	3 days (mA/cm ²)	7 days (mA/cm ²)	14 days (mA/cm ²)
-0.3	0.045	0.1285	
-0.31	0.03	0.1105	
-0.32	0.0275	0.0995	
-0.33	0.024	0.0795	
-0.34	0.0215	0.067	
-0.35	0.019	0.055	0.3375
-0.36	0.0165	0.044	0.3015
-0.37	0.0145	0.0335	0.2635
-0.38	0.0125	0.028	0.226
-0.39	0.011	0.0235	0.19
-0.4	0.0095	0.0205	0.1495
-0.41	0.0085	0.0175	0.1145
-0.42	0.007	0.0155	0.0825
-0.43	0.0065	0.0135	0.0555
-0.44	0.0055	0.012	0.034
-0.45	0.005	0.0105	0.0195
-0.46	0.0045	0.0095	0.012
-0.47	0.0045	0.0085	0.0095
-0.48	0.004	0.0075	0.0075
-0.49	0.0035	0.0065	0.0065
-0.5	0.003	0.006	0.0065
-0.51	0.0025	0.006	0.0055
-0.52	0.0025	0.0055	0.0055
-0.53	0.0025	0.005	0.0045
-0.54	0.0025	0.0045	0.0045
-0.55	0.0015	0.004	0.004
-0.56	0.0015	0.004	0.004
-0.57	0.0015	0.0035	0.0035
-0.58	0.0015	0.003	0.0035
-0.59	0.0015	0.003	0.0025
-0.6	0.0015	0.0025	0.0025
-0.61	0.0005	0.0025	0.0025
-0.62	0.0005	0.002	0.002
-0.63	0.0005	0.0015	0.002
-0.64	0.0005	0.0015	0.002
-0.65	0.0005	0.0015	0.0015
-0.66	0.0005	0.001	0.0015
-0.67	0.0005	0.0005	0.0015
-0.68	0.0005	0.0005	0.0015
-0.69	0.0005	0.0005	0.0005
-0.7	0.0005	0.0005	0.0005

Table 22. Cathodic polarization data at different time periods on a precoated iron sulfide film at high substrate loading rate.

potentials V(SCE)	3 days (mA/cm ²)	7 days (mA/cm ²)	14 days (mA/cm ²)
-0.78	0.0055	0.0065	0.0035
-0.79	0.0065	0.007	0.0035
-0.8	0.0065	0.008	0.0035
-0.81	0.0085	0.009	0.004
-0.82	0.0085	0.01	0.0045
-0.83	0.0095	0.011	0.0055
-0.84	0.0095	0.012	0.0055
-0.85	0.0105	0.013	0.006
-0.86	0.0105	0.0135	0.0065
-0.87	0.0105	0.0145	0.0075
-0.88	0.0105	0.015	0.0085
-0.89	0.011	0.0155	0.009
-0.9	0.0115	0.016	0.0095
-0.91	0.0115	0.0165	0.011
-0.92	0.0125	0.017	0.012
-0.93	0.0125	0.0175	0.013
-0.94	0.0135	0.0185	0.0145
-0.95	0.0145	0.0185	0.016
-0.96	0.0155	0.0185	0.0165
-0.97	0.0155	0.0185	0.0175
-0.98	0.0155	0.019	0.0175
-0.99	0.0165	0.0195	0.0185
-1	0.0185	0.02	0.0195
-1.01	0.0195	0.0215	0.0205
-1.03	0.0255	0.0245	0.0225
-1.04	0.0305	0.027	0.024
-1.05	0.0375	0.0305	0.0265
-1.06	0.0405	0.033	0.0295
-1.07	0.0455	0.0375	0.033
-1.08	0.0515	0.04	0.0365
-1.09	0.0595	0.0445	0.0415
-1.1	0.0675	0.0495	0.0525
-1.11	0.0745	0.0575	0.058
-1.12	0.0835	0.0665	0.064
-1.13	0.0945	0.076	0.0715
-1.14	0.1055	0.0865	0.0785
-1.15		0.0985	0.0865
-1.16	0.1315	0.105	0.095
-1.17	0.1495	0.119	0.103
-1.18	0.1645	0.1305	0.1085
-1.19	0.1825	0.141	0.118
-1.2		0.1515	0.1295

Table 23. Anodic polarization data at different time periods in the abiotic conditions.

potentials V(SCE)	3 days (mA/cm ²)	7 days (mA/cm ²)	21 days (mA/cm ²)
-0.8			
-0.79			
-0.78	0.005		
-0.77	0.025		
-0.76	0.04		0.005
-0.75	0.055	0.005	0.025
-0.74	0.085	0.025	0.055
-0.73	0.125	0.05	0.085
-0.72	0.175	0.095	0.135
-0.71	0.235	0.15	0.195
-0.7	0.315	0.225	0.265
-0.69	0.495	0.325	0.365
-0.68	0.5	0.435	0.47
-0.67	0.6	0.575	0.605
-0.66	0.72	0.725	0.725
-0.65	0.845	0.895	0.885
-0.64	0.95	1.085	1.035
-0.63	1.115	1.265	1.195
-0.62	1.205	1.48	1.36
-0.61	1.375	1.695	1.535
-0.6	1.555	1.9	1.705
-0.59	1.705	2.185	1.9
-0.58	1.865	2.415	2.08
-0.57	2.015	2.665	2.295
-0.56	2.185	2.92	2.465
-0.55	2.35	3.185	2.655
-0.54	2.505	3.465	2.86
-0.53	2.665	3.745	3.065
-0.52	2.835	4.035	3.25
-0.51	3.005	4.325	3.55
-0.5			

Table 24. Cathodic polarization data at different time periods in the abiotic conditions.

potentials V(SCE)	3 days (mA/cm ²)	7 days (mA/cm ²)	21 days (mA/cm ²)
-0.8		0.07	0.065
-0.81		0.075	0.065
-0.82	0.005	0.085	0.065
-0.83	0.025	0.095	0.075
-0.84	0.035	0.095	0.075
-0.85	0.035	0.105	0.08
-0.86	0.04	0.115	0.085
-0.87	0.045	0.115	0.095
-0.88	0.045	0.115	0.1
-0.89	0.045	0.125	0.105
-0.9	0.05	0.125	0.105
-0.91	0.05	0.125	0.11
-0.92	0.055	0.125	0.12
-0.93	0.055	0.125	0.125
-0.94	0.055	0.13	0.125
-0.95	0.06	0.135	0.135
-0.96	0.06	0.135	0.14
-0.97	0.065	0.14	0.155
-0.98	0.065	0.145	0.16
-0.99	0.075	0.155	0.175
-1	0.075	0.155	0.185
-1.01	0.08	0.16	0.2
-1.02	0.085	0.175	0.215
-1.03	0.095	0.18	0.235
-1.04	0.1	0.185	0.25
-1.05	0.11	0.195	0.275
-1.06	0.115	0.205	0.295
-1.07	0.135	0.22	0.315
-1.08	0.145	0.235	0.335
-1.09	0.155	0.245	0.36
-1.1	0.165	0.265	0.385
-1.11	0.175	0.285	0.405
-1.12	0.195	0.305	0.415
-1.13	0.205	0.325	0.435
-1.14	0.205	0.355	0.455
-1.15	0.22	0.385	0.475
-1.16	0.245	0.405	0.505
-1.17	0.275	0.435	0.535
-1.18	0.3	0.465	0.565
-1.19	0.335	0.495	0.605
-1.2	0.375	0.545	0.67



MONTANA STATE UNIVERSITY LIBRARIES



3 1762 10071959 8

